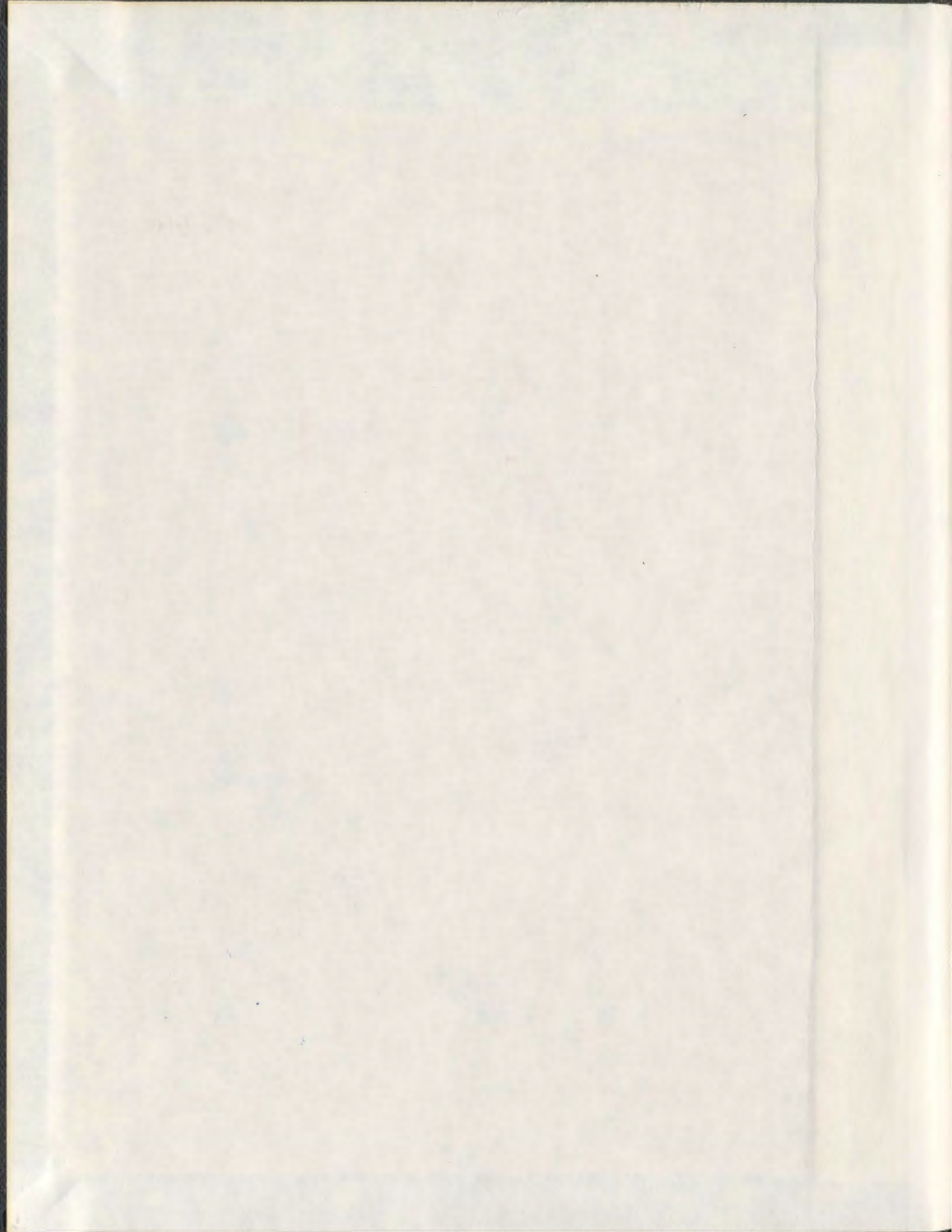


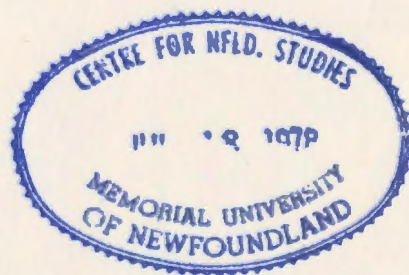
SUPERCONDUCTIVITY IN THE HEAVY FERMION

SYSTEM $\text{PrOs}_4\text{Sb}_{12}$

TAYSEER RAFE' ABU ALRUB



001311



Superconductivity in the heavy fermion system $\text{PrO}_{0.4}\text{Sb}_{1.2}$

by

© Tayseer Rafe' Abu Alrub

M. Sc. (Yarmouk University, Irbid, Jordan) 2003

B. Sc. (Yarmouk University, Irbid, Jordan) 1998

A thesis submitted to the
School of Graduate Studies
in partial fulfillment of the
requirements for the degree of
Doctor of Philosophy.

Department of Physics and Physical Oceanography
Memorial University of Newfoundland

August 28, 2008

ST. JOHN'S

NEWFOUNDLAND

Contents

Abstract	v
Acknowledgements	vi
<i>To my parents</i>	<i>vii</i>
List of Tables	viii
List of Figures	x
1 Introduction	1
1.1 Overview	1
1.2 Gap functions and gap equations	6
1.3 Group theory approach	12
1.4 Conventional superconductivity	18
1.5 Nodal superconductors	23
1.6 Superconductors in a magnetic field	26
1.7 The heavy fermion superconductor $\text{PrOs}_4\text{Sb}_{12}$	28
2 Symmetry properties of the nodal superconductor $\text{PrOs}_4\text{Sb}_{12}$	31
2.1 Abstract	31

2.2	Introduction	31
2.3	The Superconducting Gap Function	34
2.4	Density of states	40
2.4.1	A-phase	40
2.4.2	B-Phase	41
2.5	Specific heat and nuclear spin relaxation rate	43
2.6	Domains	44
2.7	Conclusions	45
2.8	Appendix A: Proof of the existence of nodes in the $D_2(E)$ phase in the triplet channel	46
3	Impurity induced density of states and residual transport in nonunitary superconductors	49
3.1	Abstract	49
3.2	Introduction	50
3.3	Mean Field Results	52
3.4	Density of states	55
3.5	Electrical conductivity	55
3.6	Thermal conductivity	58
3.7	Application to $\text{PrOs}_4\text{Sb}_{12}$	63
3.7.1	Density of states	65
3.7.2	Electrical and thermal conductivities	67
3.7.3	Discussion	68
3.8	Summary and Conclusions	69
3.9	Appendix: Derivation of Green's functions for a nonunitary superconducting state	71

4	Field angle-dependent thermal conductivity in nodal superconductors	76
4.1	Abstract	76
4.2	Introduction	77
4.3	Density of States and thermal conductivity for superconductors with line nodes	80
4.3.1	Density of States	82
4.3.2	Thermal conductivity	84
4.4	Density of states and thermal conductivity for a point node superconductor	85
4.4.1	Density of states	89
4.4.2	Thermal Conductivity	90
4.5	Discussion	94
4.6	Summary and conclusions	96
5	Concluding remarks	98

Abstract

Superconductivity was observed in the Pr-filled skutterudite heavy fermion system $\text{PrOs}_4\text{Sb}_{12}$ in 2002. Symmetry considerations, based on the Landau theory of second order phase transitions, were used to derive all possible superconducting states in this material. It was found that a three-component order parameter that belongs to the T_u irreducible representation of the tetrahedral point group T_h best describes superconductivity in $\text{PrOs}_4\text{Sb}_{12}$. Two different superconducting phases have been observed in $\text{PrOs}_4\text{Sb}_{12}$; the lower temperature B phase occupies the bulk of the phase diagram, while the higher temperature A phase is found in a narrow region below H_{c2} , and possibly does not exist at all. The proposed gap function in the A phase is unitary and has two point nodes in the $[00 \pm 1]$ directions. In the B phase, the proposed gap function is nonunitary and the lower branch has four point nodes in the $[\pm\alpha, 0, \pm\beta]$ directions. Hence, thermodynamic and transport properties of a nonunitary superconducting state are analyzed. It is shown that the conductivity tensor has inequivalent diagonal components due to the off-axis nodal positions of the B phase. Moreover, nonuniversal conductivities (impurity scattering dependent) have been obtained. A semi-classical approach based on the Doppler shift of the quasiparticle energy is used to calculate the oscillatory part of the magnetic field-angle dependent density of states and thermal conductivity. All possible point node configurations for superconducting phases of a tetrahedral superconductor are considered.

Acknowledgements

I would like to acknowledge all people who have accompanied me in this journey, and shared with me their knowledge, friendship, kindness and love. First of all, I am very grateful to my supervisor Stephanie Curnoe for her unlimited support throughout my program. Guided by her broad knowledge, experience, and her gifted intuition, I have learned so many things, but most importantly, I have learned how a successful research can be made. I would like to thank also my committee members, Guy Quirion and John Whitehead, for their help and review of my thesis; and my professors, Jolanta Lagowski, John Lewis and Martin Plumer for their valuable courses. Moreover, I want to express my deep gratitude and love to my parents, brothers and sisters for their patience and support during my study. Last but not least, I am very thankful to all my friends, officemates and roommates who have shared with me those great and excitful moments of my life.

To my parents

List of Tables

1.1	Character table for the tetrahedral point group T_h , $\omega = e^{i\frac{2\pi}{3}}$ [11]. . . .	14
1.2	The superconducting phases and their symmetries for each irreducible representation in T_h point group symmetry. The nodes and their locations on the Fermi surface are also listed. α and β are parameters indicating the position of nodes away from the principal axes [12, 15].	17
2.1	Order parameter (OP) components and symmetry group elements for the proposed normal \rightarrow A \rightarrow B second order phase transition sequence. Note that the A-phase can be skipped, since the B-phase is also accessible from the normal phase by a second order phase transition. . . .	36
4.1	Oscillatory contributions to the thermal conductivity with a field rotating in the xy plane for various nodal configurations. 's' stands for $\sin 2\epsilon$, 'c' stands for $\cos 2\epsilon$, '1' stands for no oscillations and '0' means that the component vanishes. ϵ is the angle of the field with respect to the x axis.	95

List of Figures

1.1	Superconducting phase transitions within the superconducting phases of the three dimensional irreducible representation T of the T_h group symmetry [12].	18
1.2	The BCS density of states $N'(\omega') = N(\omega')/N(0)$ vs. $\omega' = \omega/\Delta_0$	19
1.3	Electrical conductivity in BCS superconductors vs. $\Omega' = \Omega/\Delta_0$	21
1.4	Fully dressed fermion-bubble which represents the current-current correlation function. The upper and lower lines (bold) represent the dressed propagators, and dressed vertices are represented by the shaded areas.	25
1.5	Bare bubble diagram, no interactions between the dressed propagators, which is represented by the bare vertices (no shaded areas).	25
1.6	A unit cell of $\text{PrOs}_4\text{Sb}_{12}$, the Pr ions occupy the center and the corners. The Sb ions are at the octahedron corners with Os ions inside [27]. . . .	29

- 2.1 The gap function $\Delta_{\pm}(\mathbf{k})$ drawn over a spherical Fermi surface (bold) in the k_x - k_z plane. In a) the gap function (red) is unitary and degenerate. In b)-e) it is non-unitary and non-degenerate. The lower branch $\Delta_{-}(\mathbf{k})$ (red) and the upper branch $\Delta_{+}(\mathbf{k})$ (blue) are both shown. a) A-phase, $\eta_2 = 0$. b) B-phase, $|\eta_2|a = 0.1|\eta_1|b$. c) B-phase, $|\eta_2|a = 0.5|\eta_1|b$. d) B-phase, $|\eta_2|a = 0.9|\eta_1|b$. e) B-phase, $|\eta_2|a = |\eta_1|b$ 38
- 2.2 The gap function drawn over a spherical Fermi surface for the a) A-phase and b) B-phase. In a) the gap function is unitary and degenerate. In b) it is non-unitary and non-degenerate. Only the lower branch of the gap function $\Delta_{-}(\mathbf{k})$ is shown. 39
- 3.1 Gap function for the B phase of $\text{PrOs}_4\text{Sb}_{12}$ drawn in the k_x - k_z plane over a spherical Fermi surface (bold black). Left: the '+' branch is shown in blue (dashed) and the '-' branch in red (solid). Right: the '1' branch is shown in blue (dashed) and the '2' branch in red (solid). . . 64

Chapter 1

Introduction

1.1 Overview

It has been almost a century since the discovery of superconductivity. In 1911, Kamerlingh Onnes observed this state in mercury as the resistivity suddenly disappeared at 4.2 K. After that, superconductivity was found in other metals and alloys and many theories were proposed.

One of the major theories that was introduced in the last century, and had a strong impact in the understanding of superconductivity, is the Ginzburg-Landau theory of superconductivity. In 1950, Ginzburg and Landau proposed a theory for superconductivity based on Landau's theory of second order phase transitions. The theory is macroscopic and is applicable at temperatures close to the superconducting transition temperature. It is particularly useful when the superconducting state is spatially inhomogeneous, which results from, for example, applying a strong magnetic field to type II superconductors. Ginzburg-Landau theory is phenomenological with no microscopic origin or derivation. It was not until 1957 that a microscopic theory of superconductivity was formulated, which is commonly known as BCS theory [1],

named after Bardeen, Cooper and Schrieffer. This theory is based on the weak interaction of electrons with lattice vibrations (*Fröhlich interaction*) [2], which is usually called *weak coupling*. BCS theory was the first successful microscopic theory that best explained most of the observed superconducting properties of that time. Shortly after that, the universality of some formulas in BCS theory was broken by the discovery of new kinds of superconducting materials. In these new superconductors, the electron-phonon interaction is not weak (*strong coupling*), so some predictions of BCS theory do not apply. Consequently, this led to the formulation of the strong coupling theory of superconductivity in 1960 [3].

In BCS theory, the electron-phonon interaction leads to the condensation of pairs of electrons (*Cooper pairs*) below the superconducting transition temperature T_c . As the temperature is lowered, the density of Cooper pairs increases while the free electron density decreases. At zero temperature, all electrons are paired, and the ground state energy becomes less than the Fermi energy. An energy cost equal to the pair binding energy (*energy gap*) is needed to break up a Cooper pair, and create a single excitation from the superconducting condensate (*Bogoliubov quasiparticles*). The opening of the energy gap in the excitation spectrum manifests itself in all thermodynamic and transport measurements, such that they decay exponentially down to zero at low temperatures.

Superconductivity was believed to be a low temperature phenomenon. This is because the transition temperature that was predicted by BCS theory was low, which was consistent with experiment. However, this belief changed when relatively higher transition temperatures were observed in strong coupling superconductors. Consequently, the dream of high transition temperature superconductivity inspired much work on these materials, but the highest transition temperature observed was still low, *e.g.* $T_c = 23$ K in Nb_3Ge . Surprisingly, in 1986, a high transition temperature was

found in a completely different material. Bednorz and Müller [4] discovered superconductivity in the oxide ($\text{Ba}_x\text{La}_{5-x}\text{Cu}_5\text{O}_{5(3-y)}$), which is an insulator in the normal state. The superconducting transition temperature for this material is relatively high, $T_c = 35$ K. But after that, the transition temperature was raised many times, and the highest temperature achieved so far is $T_c = 133$ K in $\text{HgBa}_2\text{Ca}_2\text{Cu}_3\text{O}_{8+\delta}$.

Beside high T_c superconductors, superconductivity was found also in other materials, including heavy fermion materials, layered organic compounds and strontium ruthenate. However, the mechanism that is responsible for superconductivity in these materials is still obscure. For example, in high T_c superconductors, spin fluctuations, rather than electron-phonon interactions, are thought to be responsible for superconductivity. Usually, the term “*unconventional*” is used to describe those superconductors, and “*conventional*” refers to superconductors for which the BCS theory is applicable. In conventional superconductors, the energy gap is isotropic around the Fermi surface, while it is anisotropic or vanishes at lines or points (*nodes*) in unconventional superconductors. For example, in the high T_c cuprates, where the pairing symmetry is widely believed to be *d*-wave, the energy gap has four line nodes.

The heavy fermion superconductor $\text{PrOs}_4\text{Sb}_{12}$ is another example where unconventional superconductivity occurs [25, 29–36]. Since its discovery in 2002 [29] and up to date, little has been known about the symmetry of the order parameter or the origin of the attractive interaction in the superconducting state. Nevertheless, broken time reversal symmetry [41] and spin triplet pairing symmetry [36] were recently observed. Two superconducting phase transitions were shown by some thermodynamic and transport measurements [30–32, 41–46], but more recent works have suggested only one superconducting phase transition [47–50]. Moreover, while point nodes in the gap function were observed in low temperature thermodynamic and transport measurements [29, 30, 32, 35, 37], other experiments have shown that the gap function is

nodeless [38–40]. Furthermore, it has been suggested that the attractive interaction in this superconductor is unconventional; namely, electric quadrupole fluctuations [24].

Some theoretical work that has been done on the superconductor $\text{PrOs}_4\text{Sb}_{12}$ is phenomenological [51–54], in which order parameters have been introduced, and extensively used to predict various thermodynamic and transport properties. Other theoretical works have studied unconventional pairing mechanisms [55, 56]. In this thesis we will not introduce a microscopic theory for superconductivity in $\text{PrOs}_4\text{Sb}_{12}$. Instead, we will use group theory and Landau theory of second order phase transitions to find the symmetry of the superconducting state that best describes experiments on $\text{PrOs}_4\text{Sb}_{12}$. Also, we will present two possible scenarios for the superconducting phase transitions in $\text{PrOs}_4\text{Sb}_{12}$, and compare our results with experiment.

A valuable tool for identifying the symmetry of the order parameter in unconventional superconductors is the measurement of low energy, low temperature thermodynamic and transport properties. Since, in these materials, the energy gap vanishes at lines or points (nodes) on the Fermi surface, quasiparticles will remain conducting heat and electricity at very low temperature. For this reason, many techniques have been used, including measurements of microwave conductivity, heat conductivity, specific heat, nuclear spin lattice relaxation rate, ultra sound attenuation, etc. In addition, field angle-dependent thermal conductivity and specific heat measurements have also been performed to determine the locations of nodes at the Fermi surface. This method is based on Volovik's theory for the density of states in superconductors with line nodes in a magnetic field [5]. According to this theory, the density of states will be minimum when the magnetic field is parallel to the nodes, and maximum when it is pointed in the antinodal direction. As a result, there are field angle-dependent oscillations in thermodynamic and transport measurements. Consequently, locations of nodes at the Fermi surface can be determined.

For this reason, we will calculate the low energy, low temperature thermodynamic and transport properties associated with our symmetry-derived superconducting state in $\text{PrOs}_4\text{Sb}_{12}$. In particular, we will study the impurity induced density of states and transport coefficients in the Born and unitary scattering limits, and compare our results to experiments. Furthermore, we will calculate the magnetic field angle-dependent density of states and thermal conductivity using our proposed superconducting state in $\text{PrOs}_4\text{Sb}_{12}$, and compare the results to superconductors with lines of nodes. In our calculations, we will consider two limits, the clean and dirty limits in which the impurity scattering rate is much smaller or larger than the magnetic energy, respectively. Finally, the outcome of our calculations will be compared to experiment.

This thesis is a collection of published and submitted articles. Chapters 2 and 3 are articles which appear in Physical Review B [66,117] while Chapter 4 is a submitted article [13]. In this thesis, superconductivity in the heavy fermion material $\text{PrOs}_4\text{Sb}_{12}$ has been investigated. The outline of this study is the following: in the remaining sections of Chapter 1, background and introductory materials are presented. In Chapter 2, we use the Landau theory of phase transitions and symmetry arguments to predict the possible superconducting states and their symmetry in $\text{PrOs}_4\text{Sb}_{12}$. Furthermore, we predict the possible superconducting phase transitions that could occur within the superconducting phases, and we compare our results to experiment [66]. In Chapter 3 we calculate the impurity induced density of states and transport in a nonunitary superconducting state in general, and then we apply our results to $\text{PrOs}_4\text{Sb}_{12}$ [117]. In Chapter 4 we calculate the field angle-dependent density of states and thermal conductivity for point node superconductors. In our calculation, we consider two limiting cases; the clean and the dirty limits, in which the magnetic energy is much larger (smaller) than the impurity scattering rate, respectively. The results were applied to

$\text{PrOs}_4\text{Sb}_{12}$ and compared with experiment [13].

1.2 Gap functions and gap equations

The order parameter for a given superconducting state is characterized by the *gap function*. The gap function is a mean field potential which has the symmetry of a Cooper pair in \mathbf{k} space. Accordingly, information about the gap function should be introduced before any further study of a given superconducting state. In this section, we define the gap function for the two possible spin pairing configurations; which are spin singlet and spin triplet. Then, the *gap equation*, which is a self consistent equation for the gap function, is derived for each case. A full treatment can be found in the literature [6, 7]; here, only major steps are highlighted.

We start by constructing the Hamiltonian for a pair of electrons interacting at the Fermi surface. Let the pair potential be

$$V_{s_1 s_2 s_3 s_4}(\mathbf{k}, \mathbf{k}') = \langle -\mathbf{k}, s_1; \mathbf{k}, s_2 | \hat{V} | -\mathbf{k}', s_4; \mathbf{k}', s_3 \rangle \quad (1.1)$$

where the operator \hat{V} is a general interaction potential between a pair of electrons, which is attractive at regions close to the Fermi surface. Then, the Hamiltonian for this system can be written in second quantization form as

$$H = \sum_{\mathbf{k}, s} \varepsilon(\mathbf{k}) c_{\mathbf{k}, s}^\dagger c_{\mathbf{k}, s} + \frac{1}{2} \sum_{\mathbf{k}, \mathbf{k}', s_1, s_2, s_3, s_4} V_{s_1 s_2 s_3 s_4}(\mathbf{k}, \mathbf{k}') c_{-\mathbf{k}, s_1}^\dagger c_{\mathbf{k}, s_2}^\dagger c_{\mathbf{k}', s_3} c_{-\mathbf{k}', s_4} \quad (1.2)$$

where,

$$\begin{aligned} \Delta_{s s'}(\mathbf{k}) &= - \sum_{\mathbf{k}', s_3, s_4} V_{s' s s_3 s_4}(\mathbf{k}, \mathbf{k}') \langle c_{\mathbf{k}', s_3} c_{-\mathbf{k}', s_4} \rangle \\ \Delta_{s s'}^*(-\mathbf{k}) &= \sum_{\mathbf{k}' s_1 s_2} V_{s_1 s_2 s' s}(\mathbf{k}', \mathbf{k}) \langle c_{-\mathbf{k}', s_1}^\dagger c_{\mathbf{k}', s_2}^\dagger \rangle \end{aligned}$$

are the mean fields or the gap functions, and c^\dagger and c are fermion creation and annihilation operators, respectively. The short-hand notation $f_{\mathbf{k}} = f(\mathbf{k})$ has been

used and interchanged throughout this thesis. Using mean field theory (see Sec. 3.9), Eq. 1.2 can be written as

$$H_{MF} = \sum_{\mathbf{k},s} \varepsilon(\mathbf{k}) c_{\mathbf{k},s}^\dagger c_{\mathbf{k},s} + \frac{1}{2} \sum_{\mathbf{k},s_1,s_2} [\Delta_{s_1 s_2}(\mathbf{k}) c_{\mathbf{k},s_1}^\dagger c_{-\mathbf{k},s_2}^\dagger - \Delta_{s_1 s_2}^*(-\mathbf{k}) c_{-\mathbf{k},s_1} c_{\mathbf{k},s_2}]. \quad (1.3)$$

The energy eigenvalues can be found by diagonalizing the above Hamiltonian, which is nontrivial. This problem is solved by using the following *Bogoliubov transformation*,

$$c_{\mathbf{k},s} = \sum_{s'} [u_{\mathbf{k},s,s'} \gamma_{\mathbf{k},s'} + v_{\mathbf{k},s,s'} \gamma_{-\mathbf{k},s'}^\dagger] \quad (1.4)$$

where γ^\dagger and γ are new creation and annihilation fermion's operators, it acts on the excitations from the superconducting state (or Bogoliubov quasiparticles). Eq. 1.4 can be written in matrix form as

$$\tilde{c}_{\mathbf{k}} = \tilde{U}_{\mathbf{k}} \tilde{\gamma}_{\mathbf{k}}, \quad \tilde{U}_{\mathbf{k}} \tilde{U}_{\mathbf{k}}^\dagger = \tilde{1} \quad (1.5)$$

where

$$\tilde{c}_{\mathbf{k}} = \begin{pmatrix} c_{\mathbf{k}\uparrow} & c_{\mathbf{k}\downarrow} & c_{-\mathbf{k}\uparrow} & c_{-\mathbf{k}\downarrow} \end{pmatrix}, \quad \tilde{U}_{\mathbf{k}} = \begin{pmatrix} \tilde{u}_{\mathbf{k}} & \tilde{v}_{\mathbf{k}} \\ \tilde{v}_{-\mathbf{k}}^* & \tilde{u}_{-\mathbf{k}}^* \end{pmatrix}, \quad \tilde{\gamma}_{\mathbf{k}} = \begin{pmatrix} \gamma_{\mathbf{k}\uparrow} \\ \gamma_{\mathbf{k}\downarrow} \\ \gamma_{-\mathbf{k}\uparrow}^\dagger \\ \gamma_{-\mathbf{k}\downarrow}^\dagger \end{pmatrix} \quad (1.6)$$

where $\tilde{u}_{\mathbf{k}}$ and $\tilde{v}_{\mathbf{k}}$ are 2×2 matrices in spin space. The anticommutation relations for the fermion operators c and c^\dagger should also be satisfied by the new operators γ and γ^\dagger . So, the following relations hold [6],

$$\begin{aligned} \tilde{u}_{\mathbf{k}}^T &= \tilde{u}_{-\mathbf{k}}, & \tilde{v}_{\mathbf{k}}^T &= -\tilde{v}_{-\mathbf{k}} \\ \tilde{u}_{\mathbf{k}} \tilde{u}_{\mathbf{k}}^\dagger + \tilde{v}_{\mathbf{k}} \tilde{v}_{\mathbf{k}}^\dagger &= 1, & \tilde{u}_{\mathbf{k}} \tilde{v}_{\mathbf{k}} - \tilde{v}_{\mathbf{k}} \tilde{u}_{\mathbf{k}} &= 0 \end{aligned} \quad (1.7)$$

Using 1.5 and 1.7, the energy eigenvalues will be

$$\tilde{E}_{\mathbf{k}} = \tilde{U}_{\mathbf{k}}^\dagger \tilde{\varepsilon}_{\mathbf{k}} \tilde{U}_{\mathbf{k}} \quad (1.8)$$

where

$$\tilde{\varepsilon}_{\mathbf{k}} = \begin{pmatrix} \varepsilon_{\mathbf{k}}\sigma_0 & \tilde{\Delta}_{\mathbf{k}} \\ -\tilde{\Delta}_{-\mathbf{k}}^* & -\varepsilon_{\mathbf{k}}\sigma_0 \end{pmatrix} \quad (1.9)$$

and

$$\tilde{E}_{\mathbf{k}} = \begin{pmatrix} E_{\mathbf{k}+} & 0 & 0 & 0 \\ 0 & E_{\mathbf{k}-} & 0 & 0 \\ 0 & 0 & -E_{-\mathbf{k}+} & 0 \\ 0 & 0 & 0 & -E_{-\mathbf{k}-} \end{pmatrix} \quad (1.10)$$

where $E_{\mathbf{k}+} = E_{\mathbf{k}\uparrow}$ and $E_{\mathbf{k}-} = E_{\mathbf{k}\downarrow}$. The solution for Eq. 1.8 will be different for the two kinds of pairing symmetries, spin singlet and triplet. Consequently, we should define the gap function for each case.

The gap function can be written in a matrix form as

$$\tilde{\Delta}_{\mathbf{k}} = \begin{pmatrix} \Delta_{\mathbf{k}\uparrow\uparrow} & \Delta_{\mathbf{k}\uparrow\downarrow} \\ \Delta_{\mathbf{k}\downarrow\uparrow} & \Delta_{\mathbf{k}\downarrow\downarrow} \end{pmatrix} \quad (1.11)$$

which lists all the possible spin configurations for electrons paired state. Hence, it should satisfy the symmetry of a Cooper pair wavefunction as

$$\tilde{\Delta}(\mathbf{k}) = -\tilde{\Delta}^T(-\mathbf{k}). \quad (1.12)$$

For spin singlet state, the diagonal components are zero, so the gap function is

$$\tilde{\Delta}(\mathbf{k}) = \begin{pmatrix} 0 & \psi(\mathbf{k}) \\ -\psi(\mathbf{k}) & 0 \end{pmatrix} = i\sigma_y\psi(\mathbf{k}) \quad (1.13)$$

where $\psi(\mathbf{k})$ is an even function of \mathbf{k} and $\boldsymbol{\sigma} = (\sigma_x, \sigma_y, \sigma_z)$ are the Pauli matrices. On the other hand, for spin triplet state we get

$$\tilde{\Delta}(\mathbf{k}) = \begin{pmatrix} -d_x(\mathbf{k}) + id_y(\mathbf{k}) & d_z(\mathbf{k}) \\ d_z(\mathbf{k}) & d_x(\mathbf{k}) + id_y(\mathbf{k}) \end{pmatrix} = i(\mathbf{d}(\mathbf{k}) \cdot \boldsymbol{\sigma})\sigma_y \quad (1.14)$$

where $\mathbf{d}(\mathbf{k})$ is a complex vector and an odd function of \mathbf{k} , see Ref. [8] for a review and for information about the development of this notation. If $\tilde{\Delta}(\mathbf{k})\tilde{\Delta}^\dagger(\mathbf{k}) \propto \sigma_0$ then the gap function $\tilde{\Delta}(\mathbf{k})$ is called *unitary*, otherwise it is called *nonunitary*. Spin singlet pairing is always unitary, $\tilde{\Delta}(\mathbf{k})\tilde{\Delta}^\dagger(\mathbf{k}) = |\psi(\mathbf{k})|^2\sigma_0$, while it could be nonunitary for spin triplet pairing, $\tilde{\Delta}(\mathbf{k})\tilde{\Delta}^\dagger(\mathbf{k}) = |\mathbf{d}(\mathbf{k})|^2\sigma_0 + \mathbf{q}(\mathbf{k}) \cdot \boldsymbol{\sigma}$, where $\mathbf{q}(\mathbf{k}) = i \mathbf{d}(\mathbf{k}) \times \mathbf{d}^*(\mathbf{k})$.

Now, substituting the gap functions for spin singlet and spin triplet into Eq. 1.8, after mathematical manipulations, we get the energy eigenvalues for spin singlet and spin triplet pairing. Also, we get solutions for the Bogoliubov transformation matrices in each case. So, the energy eigenvalues (or the excitation spectrum) for spin singlet pairing will be

$$E(\mathbf{k}) = \sqrt{\varepsilon^2(\mathbf{k}) + |\psi(\mathbf{k})|^2} \quad (1.15)$$

which is degenerate for spin-up and spin-down quasiparticles, the energy gap is equal to $|\psi(\mathbf{k})|$. On the other hand, the excitation energy for spin triplet state will be

$$E_{\pm}(\mathbf{k}) = \sqrt{\varepsilon^2(\mathbf{k}) + |\mathbf{d}(\mathbf{k})|^2 \pm |\mathbf{q}(\mathbf{k})|}. \quad (1.16)$$

which is non-degenerate for non-vanishing $\mathbf{q}(\mathbf{k})$. In this case, there are two energy gaps corresponding to the two different spin orientations,

$$\Delta_{\pm}(\mathbf{k}) = (|\mathbf{d}(\mathbf{k})|^2 \pm |\mathbf{q}(\mathbf{k})|)^{1/2}. \quad (1.17)$$

As we have mentioned before, this state is called nonunitary. As we will see in later chapter, the lower gap in a nonunitary state may have nodes, while the upper gap is usually nodeless although it may be anisotropic.

The solutions for the Bogoliubov transformation matrices have similar form for spin singlet and unitary spin triplet states as follows

$$\tilde{u}_{\mathbf{k}} = \left[\frac{\varepsilon_{\mathbf{k}} + E_{\mathbf{k}}}{2E_{\mathbf{k}}} \right]^{1/2} \sigma_0, \quad \tilde{v}_{\mathbf{k}} = -\frac{\tilde{\Delta}_{\mathbf{k}}}{\sqrt{2[\varepsilon_{\mathbf{k}} + E_{\mathbf{k}}]E_{\mathbf{k}}}} \quad (1.18)$$

but it has a more complicated form for nonunitary spin triplet state, see Ref. [7]. Once the excitation spectrums and the Bogoliubov transformation matrices are known, the gap equation can be derived for each type of pairing.

Using the Bogoliubov transformations in 1.5, the transformation matrices in 1.18 and the energy of excitations in 1.15, this leads to the following result for the gap equation in a spin singlet or unitary spin triplet state,

$$\Delta_{s,s'}(\mathbf{k}) = - \sum_{\mathbf{k}', s_3, s_4} V_{s's_3s_4}(\mathbf{k}, \mathbf{k}') \frac{\Delta_{s_3s_4}(\mathbf{k}')}{2E_{\mathbf{k}'}} \tanh \left(\frac{E_{\mathbf{k}'}}{2k_B T} \right). \quad (1.19)$$

Similarly, the gap equation for a nonunitary spin triplet state can be derived and is found to be

$$\Delta_{s,s'}(\mathbf{k}) = - \sum_{\mathbf{k}', s_3, s_4} V_{s's_3s_4}(\mathbf{k}, \mathbf{k}') h_{s_3s_4}(\mathbf{k}', T) \quad (1.20)$$

where

$$\begin{aligned} \tilde{h}(\mathbf{k}, T) = & \left[\frac{1}{2E_{\mathbf{k}+}} \left[\mathbf{d}_{\mathbf{k}} + \frac{\mathbf{q}_{\mathbf{k}} \times \mathbf{d}_{\mathbf{k}}}{|\mathbf{q}_{\mathbf{k}}|} \right] \tanh \left(\frac{E_{\mathbf{k}+}}{2k_B T} \right) \right. \\ & \left. + \frac{1}{2E_{\mathbf{k}-}} \left[\mathbf{d}_{\mathbf{k}} - \frac{\mathbf{q}_{\mathbf{k}} \times \mathbf{d}_{\mathbf{k}}}{|\mathbf{q}_{\mathbf{k}}|} \right] \tanh \left(\frac{E_{\mathbf{k}-}}{2k_B T} \right) \right] \cdot i\sigma\sigma_y. \end{aligned} \quad (1.21)$$

The above gap equations should be solved self-consistently, once a knowledge of the interaction potential has been established. For example, in BCS theory, it is assumed that the interaction potential is constant (*s*-wave) and attractive on a small range around the Fermi surface. Also, it is assumed that the interaction leaves the spin invariant. So

$$\begin{aligned} V(\mathbf{k}, \mathbf{k}') = & -V_0, & |\varepsilon_{\mathbf{k}}| < \varepsilon_c \ll \varepsilon_F \\ & 0, & \text{Otherwise.} \end{aligned} \quad (1.22)$$

Substituting this in 1.19, one obtains the following BCS self consistent gap equation as a function of temperature,

$$\Delta(T) = V_0 \sum_{\mathbf{k}'} \frac{\Delta(T)}{2E_{\mathbf{k}'}} \tanh\left(\frac{E_{\mathbf{k}'}}{2k_B T}\right). \quad (1.23)$$

where the sum is over a momentum shell around the Fermi surface. Transforming the summation into integration at the Fermi surface as

$$1 = N_F V_0 \int_0^{\varepsilon_c} d\varepsilon \frac{1}{2\sqrt{\varepsilon^2 + \Delta^2(T)}} \tanh\left(\frac{\sqrt{\varepsilon^2 + \Delta^2(T)}}{2k_B T}\right), \quad (1.24)$$

where variations of the density of states with energies close to the Fermi surface are assumed to be negligible. At zero temperature, this gives

$$\Delta(0) = \frac{\varepsilon_c}{\sinh(1/N(0)V_0)} \quad (1.25)$$

$$\approx 2\varepsilon_c e^{-N_F V_0}, \quad N_F V_0 \ll 1 \quad (1.26)$$

where the limit $N_F V_0 \ll 1$ is usually called the weak coupling limit. Also, setting $T = T_c$ in 1.24, noting that $\Delta(T_c) = 0$, we get the following expression for the superconducting transition temperature,

$$T_c = 1.13 \varepsilon_c e^{-1/N_F V_0}. \quad (1.27)$$

At temperatures far from zero and close to T_c , Eq. 1.24 can be solved numerically and we get

$$\Delta(T) \approx 1.74 \Delta(0) \left[1 - \frac{T}{T_c}\right]^{1/2}. \quad (1.28)$$

Further details and treatment of the BCS gap equation can be found in many textbooks, see *e. g.* Ref. [9].

The above example, in which the pairing of electrons is spin singlet and *s*-wave, represents conventional superconductivity that was mentioned before. This problem

is well explained and described by BCS theory. On the other hand, in unconventional superconductors the pairing symmetry is different from s -wave or it is not spin singlet. In almost all conventional superconductors, the exchange of phonons between each pair of electrons gives the attractive potential responsible for superconductivity, while for unconventional superconductors, the origin of the attractive interaction could be due to other mechanisms, like magnetic or quadrupole fluctuations. However, details about the origin of the interaction potential are not crucial, although the fact that it is attractive is a cornerstone for any theory of superconductivity. Using group theory, one can obtain much information without any specific knowledge of the source of the attractive interaction.

1.3 Group theory approach

Superconductivity is a state of broken symmetry. While the the normal state has the symmetry group $G \times U \times \mathcal{K}$, where G is the crystal space group, $U(1)$ is the gauge (or phase) symmetry and \mathcal{K} is the time reversal symmetry. $U(1)$ and possibly other symmetry elements of this group are absent in the superconducting phase. In conventional pairing, superconductivity breaks only the gauge symmetry, while more symmetries are broken in the case of unconventional superconductivity.

The group theory approach, *e. g.* see Ref. [10], is a powerful tool for studying superconductivity in the absence of microscopic theory. In this approach, a knowledge of the crystal point group symmetry for a given superconductor reveals much information about its superconductivity. For example, all the possible superconducting states, their symmetries, and the superconducting phase transitions within these states can be worked out. As an example, the tetrahedral point group T_h , which is the point group of $\text{PrOs}_4\text{Sb}_{12}$, has been used throughout this discussion.

A symmetry group, in general, can be divided into different classes of the symmetry group elements. Each element in the group can be represented by a matrix in which the trace (which is usually called *character*) is the same for all elements in a class. When the matrix is reducible to a block form, the representation is called *reducible*, otherwise it is called *irreducible*. All classes, irreducible representations and their characters of a given symmetry group can be written in one table, which is called *character table*. In a character table, there are columns labeled by the classes, preceded by the number of elements in each class, and rows labeled by the irreducible representations. The entries of a character table are just the characters of each irreducible representation. Further information about character tables can be found in many classic books, *e. g.* see Ref. [11].

In our example, the tetrahedral point group T_h is a *subgroup* of the octahedral group O_h , where h refers to inversion symmetry. The group T has four classes: three two-fold rotations, two classes with four three-fold rotations (where each class corresponds to different direction of rotation) and the identity. The character table of the T_h group is shown in Table 1.1. The subscripts g and u refer to even parity and odd parity, respectively. The dimensionality of the irreducible representation is indicated in the first column in the character table. So, the tetrahedral point group T_h has one dimensional, two-dimensional and three-dimensional irreducible representations in each parity (even and odd).

An order parameter, whether structural, magnetic or superconducting belongs to one of the irreducible representations of the point group. The dimensionality of the representation gives the number of components in the order parameter. For superconductors, anti-symmetrisation of the electronic wavefunction requires that spin singlet states (which are odd) correspond to an even representation while spin triplet states belong to odd representations.

T_h	E	$3C_2$	$4C_3$	$4C'_3$	i	$3\sigma_h$	$4S_6$	$4S'_6$
A_{1g}	1	1	1	1	1	1	1	1
E_g	1	1	ω	ω^2	1	1	ω	ω^2
	1	1	ω^2	ω	1	1	ω^2	ω
T_g	3	-1	0	0	3	-1	0	0
A_{1u}	1	1	1	1	-1	-1	-1	-1
E_u	1	1	ω	ω^2	-1	-1	$-\omega$	$-\omega^2$
	1	1	ω^2	ω	-1	-1	$-\omega^2$	ω
T_u	3	-1	0	0	-3	1	0	0

Table 1.1: Character table for the tetrahedral point group T_h , $\omega = e^{i\frac{2\pi}{3}}$ [11].

The gap function can be expressed in terms of the basis functions for each irreducible representation as

$$\psi(\mathbf{k}) = \sum_{i=1}^l \eta_i \psi_i(\mathbf{k}) \quad (1.29)$$

for even parity (spin singlet), and

$$\mathbf{d}(\mathbf{k}) = \sum_{i=1}^l \eta_i \mathbf{d}_i(\mathbf{k}) \quad (1.30)$$

for odd parity (spin triplet) in the limit of strong spin-orbit coupling, where η_i are the components of the superconducting order parameter, and l is the dimensionality of the irreducible representation. In the T_h point group there are one-component, two-component, and three-component order parameters in each channel; spin singlet and spin triplet.

To find the possible superconducting states for each irreducible representation, we must construct a Landau functional $F(\eta_i)$ that is invariant under the normal phase group symmetry $G \times U \times \mathcal{K}$ and find its minima. For example, the irreducible

representations $E_{g,u}$ in the T_h point group are two dimensional, so the order parameter has two components (η_1, η_2) . The Landau free energy that is invariant under the symmetry operations of the group $T_h \times U \times \mathcal{K}$ of the normal phase is [12]

$$\begin{aligned} F(\eta_1, \eta_2) = & \alpha(|\eta_1|^2 + |\eta_2|^2) + \beta_1(|\eta_1|^4 + |\eta_2|^4) + 2\beta_2|\eta_1|^2|\eta_2|^2 \\ & + \gamma_1(\eta_1^3\eta_2^{*3} + \eta_2^3\eta_1^{*3}) + i\gamma_2(\eta_1^3\eta_2^{*3} - \eta_2^3\eta_1^{*3}) \end{aligned} \quad (1.31)$$

Three possible superconducting states can be obtained by including additional higher order terms to the above Landau free energy,

$$(1, 0), (\phi_1, \phi_2), \text{ and } (\eta_1, \eta_2) \quad (1.32)$$

where, in the (ϕ_1, ϕ_2) state, the two components of the order parameter have the same amplitude but different phases, in (η_1, η_2) the amplitudes as well as the phases are different, and in $(1,0)$ only the first component is non-zero.

The symmetry group for any superconducting state is a subgroup of the normal phase group, $G \times U \times \mathcal{K}$. For example, the superconducting phases in (1.32) have $T(D_2)$, $D_2 \times \mathcal{K}$, and D_2 symmetry groups; respectively, and they are subgroups of the normal phase group $T_h \times U \times \mathcal{K}$. Notation like $T(D_2)$ means a combined group, in which the elements of this group are a combination from both the tetrahedral (T) and the dihedral (D_2) group-elements.

Another important and more relevant example is the three dimensional irreducible representation T . This representation has three-component order parameter and the corresponding Landau free energy, expanded to sixth-order terms, is [12]

$$\begin{aligned} F(\eta_1, \eta_2, \eta_3) = & \alpha I_1 + \beta_1 I_1^2 + \beta_2 I_2 + \beta_3 I_3 + \gamma_1 I_1^3 + \gamma_2 I_1 I_2 + \gamma_3 I_1 I_3 + \gamma_4 I_4 \\ & + \gamma_5 I_5 + \gamma_6 I_6 + \gamma_7 I_7 \end{aligned} \quad (1.33)$$

where

$$\begin{aligned}
 I_1 &= |\eta_1|^2 + |\eta_2|^2 + |\eta_3|^2, \quad I_2 = |\eta_1|^4 + |\eta_2|^4 + |\eta_3|^4, \quad I_3 = \eta_1^2 \eta_2^{*2} + \eta_2^2 \eta_3^{*2} + \eta_3^2 \eta_1^{*2} + c.c \\
 I_4 &= |\eta_1|^6 + |\eta_2|^6 + |\eta_3|^6, \quad I_5 = |\eta_1|^4 (|\eta_2|^2 - |\eta_3|^2) + |\eta_2|^4 (|\eta_3|^2 - |\eta_1|^2) \\
 &\quad + |\eta_3|^4 (|\eta_1|^2 - |\eta_2|^2), \quad I_{6,7} = |\eta_1^4 \eta_2^{*2} + \eta_2^4 \eta_3^{*2} + \eta_3^4 \eta_1^{*2} \pm (\eta_2^4 \eta_1^{*2} + \eta_3^4 \eta_2^{*2} + \eta_1^4 \eta_3^{*2})| + c.c
 \end{aligned} \tag{1.34}$$

Additional higher order terms are required to obtain all possible superconducting phases. There are nine possible superconducting phases:

$$\begin{aligned}
 &(1, 0, 0), (1, 1, 1), (1, \varepsilon, \varepsilon^2), (|\eta_1|, i|\eta_2|, 0), (|\eta_1|, |\eta_2|, 0), \\
 &(\eta_1, \eta_2, 0), (|\eta_1|, i|\eta_2|, |\eta_3|), (|\eta_1|, |\eta_2|, |\eta_3|), (\eta_1, \eta_2, \eta_3).
 \end{aligned} \tag{1.35}$$

All the possible superconducting phases and their symmetries in a T_h point group symmetry are summarized in Table 1.2. The combined groups that appear in this table are

$$T(D_2) = \{D_2, 4U(4\pi/3)C_3, 4U(2\pi/3)C_3^2\} \tag{1.36}$$

$$D_2(C_2) = \{E, C_2^x, U(\pi)C_2^y, U(\pi)C_2^z\} \tag{1.37}$$

$$C_3(E) = \{E, U(4\pi/3)C_3, U(2\pi/3)C_3^2\} \tag{1.38}$$

$$C_2(E) = \{E, U_1(\pi)C_2^z\} \tag{1.39}$$

$$C_2'(E) = \{E, U_1(\pi)C_2^y \mathcal{K}\} \tag{1.40}$$

Furthermore, all the possible second order phase transitions that may occur within the superconducting states can be determined. These transitions can only occur between states which are connected by group-subgroup relations. If some states are connected to more than one other superconducting state, an effective Landau functional with an effective order parameter can be constructed. The effective Landau free energy can specify the states that have additional superconducting phase transitions.

S. C. State	Symmetry	Irred. Rep.	Nodes	Irred. Rep.	Nodes
(1)	$T \times \mathcal{K}$	A_g	none	A_u	none
(1, 0)	$T(D_2)$	E_g	8 points (111)	E_u	8 points (111)
(ϕ_1, ϕ_2)	$D_2 \times \mathcal{K}$		8 points (111)		none
(η_1, η_2)	D_2		8 points (111)		none
(1, 0, 0)	$D_2(C_2) \times \mathcal{K}$	T_g	2 lines $k_y = 0, k_z = 0$	T_u	2 points [100]
(1, 1, 1)	$C_3 \times \mathcal{K}$		6 points (001)		none
$(1, \varepsilon, \varepsilon^2)$	$C_3(E)$		6 points (001), 2 points [111]		2 points [100]
$(\eta_1 , i \eta_2 , 0)$	$D_2(E)$		1 line $k_x = 0, 2$ points [001]		4 points $[\pm\alpha, \pm\beta, 0]$
$(\eta_1 , \eta_2 , 0)$	$C_2(E) \times \mathcal{K}$		1 line $k_x = 0, 2$ points [001]		2 points [111]
$(\eta_1, \eta_2, 0)$	$C_2(E)$		1 line $k_x = 0, 2$ points [001]		none
$(\eta_1 , i \eta_2 , \eta_3)$	$C_2'(E)$		6 points (001)		none
$(\eta_1 , \eta_2 , \eta_3)$	\mathcal{K}		6 points (001)		none
(η_1, η_2, η_3)	E		6 points (001)		none

Table 1.2: The superconducting phases and their symmetries for each irreducible representation in T_h point group symmetry. The nodes and their locations on the Fermi surface are also listed. α and β are parameters indicating the position of nodes away from the principal axes [12, 15].

For example, the two-component order parameter (η_1, η_2) for the E irreducible representation has D_2 symmetry. The latter is a subgroup of other superconducting phases of E , $(1, 0)$ and (ϕ_1, ϕ_2) , and have $T(D_2)$ and $D_2 \times \mathcal{K}$ symmetries, respectively. The effective order parameter that describes the superconducting phase transition between the superconducting states $(1, 0)$ and (η_1, η_2) is η_2 , and between (ϕ_1, ϕ_2) and (η_1, η_2) is $|\eta_1| - |\eta_2|$. Since the effective Landau free energy must be invariant under the symmetry operations of the $(1, 0)$ phase, a second order phase transition between the states $(1, 0)$ and (η_1, η_2) cannot happen. This is because the effective free energy $F_{\text{eff}}(\eta_2)$ has third-order terms which rules out the possibility of 2nd-order phase transition [12]. In contrary, the effective free energy for the transition between (ϕ_1, ϕ_2) and (η_1, η_2) , $F_{\text{eff}}(|\eta_1| - |\eta_2|)$ has no third-order terms and the transition may be second order.

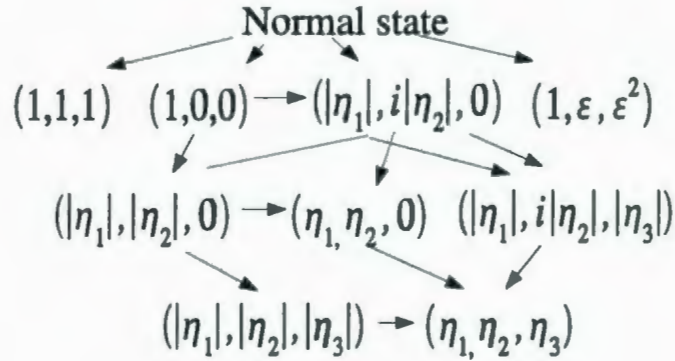


Figure 1.1: Superconducting phase transitions within the superconducting phases of the three dimensional irreducible representation T of the T_h group symmetry [12].

Similarly, all possible 2nd-order superconducting phase transitions within the superconducting states of the irreducible representation T can be calculated. The results are shown in Fig. 1.1.

Following this procedure, one can predict all possible superconducting phase transitions which may occur within the superconducting states of an irreducible representation. The results of this approach should be matched with experiment.

1.4 Conventional superconductivity

Here, we present the main conclusions of BCS theory regarding the behavior of thermodynamic and transport properties in a superconducting state. As mentioned above, BCS theory gives the description of conventional superconductivity on a microscopic

scale. The pairing has *s*-wave orbital symmetry, so the gap function is isotropic in \mathbf{k} -space. Hence, excitations from the superconducting condensate require a minimum energy equal to the energy gap. Recalling Eq. 1.15, the quasiparticle energy for spin singlet pairing is

$$E(\mathbf{k}) = \sqrt{\varepsilon^2(\mathbf{k}) + \Delta^2(\mathbf{k})}$$

where $\varepsilon(\mathbf{k}) = k^2/2m^* - \varepsilon_F$. The energy gap, $\Delta(\mathbf{k}) = |\psi(\mathbf{k})|$, is isotropic everywhere in BCS superconductor, $\Delta(\mathbf{k}) = \Delta$. So, the quasiparticles density of states, which is given by the following equation

$$\begin{aligned} N(\omega) &= N(0) \frac{|\omega|}{\sqrt{\omega^2 - \Delta_0^2}}, & |\omega| > \Delta_0 \\ &= 0 & |\omega| < \Delta_0 \end{aligned} \quad (1.41)$$

and is shown in Fig. 1.2, is zero for energies less than the gap maximum Δ_0 , and is singular at the edge of the gap. $N(0)$ refers to the density of states at the Fermi surface and Δ_0 is the energy gap at zero temperature.

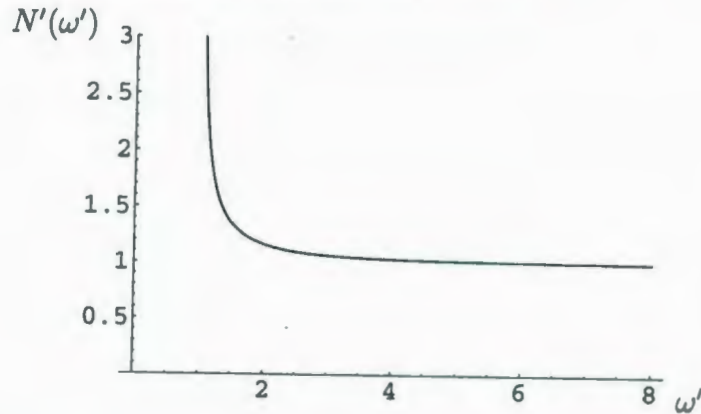


Figure 1.2: The BCS density of states $N'(\omega') = N(\omega')/N(0)$ vs. $\omega' = \omega/\Delta_0$.

Other thermodynamic properties, like specific heat, will decay exponentially at low temperature,

$$\frac{C_e^s(T)}{C_e^n(T_c)} \sim \frac{\Delta_0}{T_c} \left[\frac{\Delta_0}{T} \right]^{3/2} e^{-\frac{\Delta_0}{T}} \quad (1.42)$$

but, it usually shows a peculiar behavior for temperatures just below the superconducting transition temperature. For example, the nuclear spin-lattice relaxation rate rises abruptly, showing what is commonly known as the Hebel-Slichter peak [16].

Similarly, the transport properties will be significantly affected by the transition to the superconducting state. In fact, superconductivity was first discovered by the observation of infinite d.c. electrical conductivity at low temperatures. However, while the *superflow* (Cooper pairs current) electrical conductivity is infinite, its thermal conduction is zero. This is due to the fact that Cooper pairs have zero entropy, and consequently they cannot conduct heat.

In general, the electrical conductivity can be written as a complex function of electromagnetic frequency, $\sigma(\Omega) = \sigma_1(\Omega) - i\sigma_2(\Omega)$. At zero temperature, the real and imaginary parts for a given superconductor can be calculated and the results are given by the following expressions [9]

$$\frac{\sigma_{1s}}{\sigma_n} = \left[1 + \frac{\Delta_0}{\Omega}\right] E(\alpha) - \frac{2\Delta_0}{\Omega} K(\alpha), \quad \Omega > \Delta_0 \quad (1.43)$$

$$\frac{\sigma_{2s}}{\sigma_n} = \frac{1}{2} \left[1 + \frac{\Delta_0}{\Omega}\right] E(\alpha') - \frac{1}{2} \left[1 - \frac{\Delta_0}{\Omega}\right] K(\alpha') \quad (1.44)$$

$$\alpha = \frac{\Omega - \Delta_0}{\Omega + \Delta_0} \quad (1.45)$$

$$\alpha' = \sqrt{1 - \alpha^2} \quad (1.46)$$

where K and E are the complete elliptic integrals of the first and second kinds respectively,

$$K(\alpha) = \int_0^{\frac{\pi}{2}} \frac{d\theta}{\sqrt{1 - \alpha^2 \sin^2 \theta}} \quad (1.47)$$

$$E(\alpha) = \int_0^{\frac{\pi}{2}} d\theta \sqrt{1 - \alpha^2 \sin^2 \theta} \quad (1.48)$$

and σ_n is the normal state conductivity. The behaviors of the real and imaginary parts with an applied electromagnetic field are shown in Fig. 1.3. The imaginary

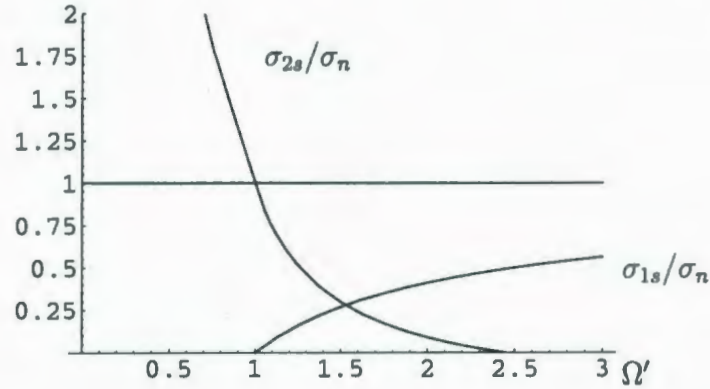


Figure 1.3: Electrical conductivity in BCS superconductors vs. $\Omega' = \Omega/\Delta_0$.

part of the conductivity rises sharply below $\Omega = \Delta_0$ and behaves like $1/\Omega$ at low frequencies, which is the d.c. limit. This behavior can be directly deduced from London's first equation of electromagnetic waves in superconductor, which is

$$\mathbf{E}(t) = \frac{m}{n_s e^2} \frac{\partial}{\partial t} \mathbf{J}_s(t) \quad (1.49)$$

Fourier transforming in time, this gives the following expression for the imaginary part of the electrical conductivity,

$$\sigma(\Omega) = \frac{n_s e^2}{m \Omega} \quad (1.50)$$

which is infinite at zero frequency. The real part of the conductivity has a delta function at $\omega = 0$ which represents the supercurrent response to the applied electromagnetic field. Then the real part of the conductivity, which vanishes for frequencies less than Δ_0 , must be due to excitations from the superconducting condensate. This is why measurements of the real part of electrical conductivity were used before to probe the energy gap and estimate its magnitude [17]. If the gap function has zeros, the real part will not vanish at the edge of the gap; instead, the conduction will be finite down to zero energy. Hence, measurements of the real part of the conductivity have been also performed to study the excitations in nodal superconductors. So,

whenever the electrical conductivity is mentioned in this thesis, we refer to the real part.

One of the most popular measurements in superconductors nowadays is the measurement of thermal conduction. This is because it may precisely determine the symmetry of the order parameter in unconventional superconductors. In general, thermal conduction has two major contributions: one is pure electronic and the other is due to phonons. In the normal state of a superconducting material, thermal conductivity is dominated by the electronic part which is, $\kappa_e^{-1} = aT^2 + (b/T)$, where a and b are constants [18]. In the superconducting state, each contribution behaves differently: while the phonon conduction rises exponentially, the electronic part decreases exponentially. This is due to the fact that the main scatterers of phonons are electrons. When the temperature drops below the superconducting transition temperature, the density of electrons will reduce by Cooper pairing. Hence, the thermal resistance will decrease considerably, and an abrupt rise in the phonon's thermal conductivity appears. This is, of course, accompanied by a decrease in the electronic thermal conductivity. At low temperatures, the phonon thermal conductivity will decrease because of several scattering mechanisms, like crystal boundaries. So, a maximum will appear in the phonons thermal conduction in the superconducting phase.

If the energy gap has nodes, the electronic part of the thermal conductivity will decrease as a power law at low temperatures. This slowing-down depression of the thermal conductivity, compared to the case of conventional superconductors, is due to the low energy excitations at the nodes.

1.5 Nodal superconductors

In almost all unconventional superconductors, the energy gap has nodes at the Fermi surface. At low energy and temperature, quasiparticles can be easily excited at the position of nodes. Consequently, the density of states and all thermodynamic and transport properties will be dominated by those nodal quasiparticles. For this reason, it is a good approximation to consider only the regions in \mathbf{k} -space close to the gap nodes for calculating various quantities at low temperature. This is usually done by changing the summation to integration over separate regions around each node and adding after that the contributions from all nodes. Also, it is convenient to set a new coordinate system in momentum space defined at the position of node. The position of the nodes can be found by setting the gap function equal to zero. A Taylor expansion at the position of nodes is crucial, since this determines how the gap function vanishes on the Fermi surface. For example, we get totally different results between a gap vanishing linearly (cusp nodes) and a gap vanishing with higher powers.

In superconductors with lines of nodes, the density of states and related quantities will be different from superconductors with an isotropic gap. As an example, in high T_c superconductors the order parameter has d -wave pairing symmetry characterized by four cusp line nodes on the Fermi surface. For a pure sample, the density of states will be linear in energy

$$N(\omega) = \frac{|\omega|}{\pi v_F v_g} \quad (1.51)$$

where v_g is the slope of the energy gap at the node (the gap velocity) and v_F is the Fermi velocity. Consequently, the electronic specific heat behaves as T^2 at low temperature. Also, nuclear spin lattice relaxation rate does not show a Hebel-Slichter peak below T_c and at low temperatures it goes like T^3 .

If the sample contains nonmagnetic impurities, the above expression for the density of states will be significantly modified and become more complicated [19]. At zero energy, the density of states will be finite and proportional to the impurity scattering rate Γ_0 ,

$$N(\omega = 0) = \frac{2\Gamma_0}{\pi^2 v_F v_g} \ln \frac{p_0}{\Gamma_0}. \quad (1.52)$$

where p_0 is a cutoff in energy. As a result, nonmagnetic impurities will act as pair breakers for the superconducting condensate in addition to scattering off quasiparticles. Those impurity-induced quasiparticles can be easily detected in low energy, low temperature measurements like electrical and thermal conductivities.

Calculations of the impurity-induced transport coefficients in d -wave superconductors, using the Kubo formula [22] have been done recently [19]. *Universal* conductivities (independent of impurity scattering rate) have been predicted for isotropic impurity scattering potential (*bare bubble approximation*). On the other hand, when the impurity scattering potential is anisotropic (*vertex corrections*), electrical conductivity becomes nonuniversal but thermal conductivity remain universal. In other words, the results are

$$\sigma_0 = \frac{e^2 v_F}{\pi^2 v_g} \beta_{vc} \quad (1.53)$$

for electrical conductivity, where β_{vc} is the vertex correction factor which is equal one in the bare bubble limit, and

$$\frac{\kappa_0}{T} = \frac{k_B^2}{3} \left[\frac{v_F}{v_g} + \frac{v_g}{v_F} \right]. \quad (1.54)$$

for thermal conductivity. In each case (isotropic and anisotropic scattering), the Wiedemann-Franz law $\frac{\kappa}{\sigma T} = \frac{\pi^2 k_B^2}{3e^2}$ is violated, although the deviations are very small [19]. In addition to vertex corrections, which appear in electrical conductivity but not

in thermal conductivity, violation of Wiedemann-Franz law also arises while deriving the transport currents using the mean field Hamiltonian. The expression for the heat current has a term proportional to the gap velocity which is absent in the electrical current. In this thesis, this term is assumed to be very small and has been neglected right from the beginning.

Usually, the current-current correlation function $\tilde{\Pi}_{ret}(\Omega)$, which appears in the Kubo formulas [23], is diagrammatically represented by a fermion-bubble, as shown in Fig. 1.4. The upper and lower lines are in bold, indicating a fully dressed (self

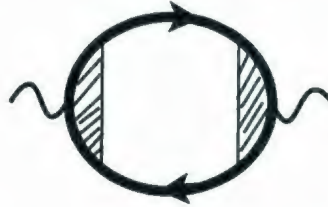


Figure 1.4: Fully dressed fermion-bubble which represents the current-current correlation function. The upper and lower lines (bold) represent the dressed propagators, and dressed vertices are represented by the shaded areas.

energy is included) propagators (Green's functions), and the shaded (dressed) vertices represent the interactions between the dressed propagators. When the interactions between the propagators vanishes (bare vertices), the fermion-bubble is called the bare bubble, as shown in Fig. 1.5.

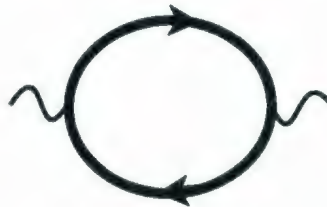


Figure 1.5: Bare bubble diagram, no interactions between the dressed propagators, which is represented by the bare vertices (no shaded areas).

Detailed calculations will appear in Chapter 3, where the same formalism has been used to derive the transport properties for a nonunitary superconducting state with point nodes in the lower gap. However, since the impurity potential is assumed to be isotropic in \mathbf{k} space, by assumption, only the bare bubble diagram is considered.

1.6 Superconductors in a magnetic field

In general, superconductors can be categorized into two classes according to their behavior in an applied magnetic field. The two classes are usually called *type I* and *type II*. At low magnetic fields, both types are perfect diamagnetic; *i. e.* the magnetic field cannot penetrate the sample and will be strongly expelled. This phenomenon is called *Meissner effect*. However, at relatively high magnetic fields, superconductivity will be destroyed in type I, while a different superconducting state will arise in type II. While type I is characterized by a Ginzburg-Landau factor $\kappa \sim \delta_L/\xi_0 < 1/\sqrt{2}$, in type II it is greater than $1/\sqrt{2}$. This means that the magnetic field penetration depth δ_L is less than the coherence length ξ_0 in type I, while the opposite is true in type II.

In type II superconductors, raising the magnetic field above a critical value H_{c1} , causes the sample to go into a state called *vortex state* (or *mixed state*). In this state, the magnetic field partially penetrates the sample in the form of vortex lines. The superconducting electrons will circulate around each vortex by the effect of Lorentz force, speed up close to vortex lines and destroy superconductivity at vortex cores. Hence, this creates a normal regions in the sample while it is still in the superconducting state. At magnetic fields close to H_{c2} , the vortices form a triangular lattice which is usually called Abrikosov lattice (referring to Abrikosov [20] after his discovery of the vortex state); see Ref. [21] for derivation. When the magnetic field is

raised above the critical value H_{c1} , vortex lines will approach each other until the field reaches another critical value H_{c2} , where at this value, superconductivity will be completely destroyed. The fields H_{c1} and H_{c2} are called the lower and upper critical fields; respectively, and they are temperature dependent.

In the vortex state, each vortex line carries a *magnetic flux quantum* $\Phi_0 = (hc/2e)$, where h is the Planck constant, e is the electron charge, and c is the speed of light. This comes from the fact that the magnetic flux through a region enclosed by a circulating superflow is quantized as $\Phi = N\Phi_0$, $N = 1, 2, \dots$.

In conventional superconductors, when a low magnetic field is applied such that $H_{c1} \leq H \ll H_{c2}$, the density of states will be nonzero at zero energy, and determined by the localized quasiparticles inside the vortex cores. Hence, the density of states will be linearly dependent on the magnetic field H . However, this is not the case for nodal superconductors (as will be discussed in more detail in Chapter 4). For example, in superconductors with lines of nodes in the energy gap, the density of states is dominated by the delocalized quasiparticles generated at the nodes.

The energy of these nodal quasiparticles will be Doppler shifted by the flow of the superfluid around each vortex as $\omega \rightarrow \omega - \mathbf{v}_s \cdot \mathbf{k}_n$ [5], where $\mathbf{v}_s = (\hbar/2m\mathbf{r})\hat{\beta}$, is the superfluid velocity around each vortex, \mathbf{r} is the radial distance from the center of the vortex core and β is the vortex winding angle. This expression for \mathbf{v}_s is valid only outside the vortex at a distance equal to the coherence length ξ_0 up to a cutoff of order the intervortex spacing $R = \sqrt{(\Phi_0/a^2\pi H)}$, where a is a geometrical vortex lattice constant of order one and $\Phi_0 = 2\pi\xi_0^2 H_{c2}$ is the magnetic flux quantum. In the limit of zero energy $\omega = 0$, we get an expression for the density of states in terms of the Doppler shifted energy. This expression is finally averaged over the vortex unit

cell as

$$N_{\text{ave.}}(H) = \frac{1}{\pi R^2} \int_{\xi_0}^R dr r \int_0^{2\pi} d\beta N(0, r, \beta) \quad (1.55)$$

where we assume a circular vortex unit cell instead of hexagonal. As a result, the density of states will be proportional to \sqrt{H} and oscillates with a period that reflects the symmetry of the order parameter in a superconductor with lines of nodes. Similarly, other field-dependent thermodynamic and transport properties can be calculated, and the location of nodes can be accurately determined by analyzing the observed oscillations.

Although the above treatment has been widely accepted for superconductors with lines of nodes, in Chapter 4 it is argued that this may not be completely valid for superconductors with point nodes. For example, Figs. 2 and 4 of Ref. [30] show the field-angle dependent thermal conductivity measurement in the superconductor $\text{PrOs}_4\text{Sb}_{12}$. The four-fold oscillations were ascribed to four point-nodes in the A phase at the [100] and [010] directions, and the two-fold oscillations to two point-nodes in the B phase at the [010] direction. However, it has been shown in Chapter 4 that these oscillations are not related at all to the number of point nodes or their locations on the Fermi surface.

1.7 The heavy fermion superconductor $\text{PrOs}_4\text{Sb}_{12}$

The subject of this thesis is superconductivity in $\text{PrOs}_4\text{Sb}_{12}$ (Pr=praseodymium, Os=osmium, and Sb=antimony). This system has a bcc structure (body center cubic) with space group $Im\bar{3}$ and T_h (tetrahedral) point group symmetry [26]. The bcc unit cell is shown in Fig. 1.6. It has three Fermi surfaces; two closed surfaces and one multiply connected surface upon which the heavy electrons ($m^* = 8m_e$) reside [28].

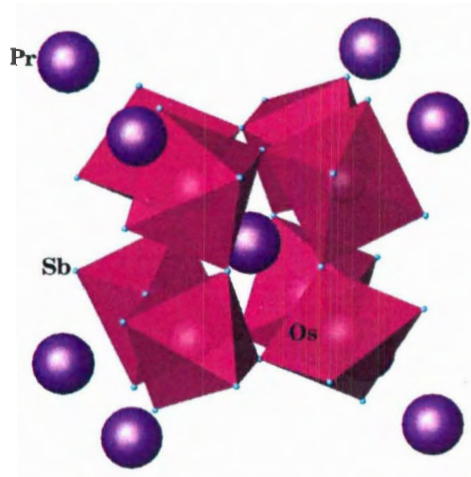


Figure 1.6: A unit cell of $\text{PrOs}_4\text{Sb}_{12}$, the Pr ions occupy the center and the corners. The Sb ions are at the octahedron corners with Os ions inside [27].

Superconductivity in $\text{PrOs}_4\text{Sb}_{12}$ has many features that have attracted much interest since its discovery in 2002 by Bauer *et al.* [29]. For example, it is unconventional and it is the first Pr-based heavy fermion system that become superconducting. Also, it is the first heavy fermion superconductor among the rare-earth filled skutterudite family RT_4X_{12} (R -rare earth; T=Fe, Ru or Os; X=P, As or Sb). Microscopically, it has been claimed that superconductivity could be due to quadrupole exchange instead of phonons or spin fluctuations [24]. In addition, two superconducting phase transitions with $T_{c1} \sim 1.89$ K and $T_{c2} \sim 1.72$ K are observed in some experiments. For example, specific heat shows two jumps in Fig. 2 of Ref. [42], which is a signature of two 2nd-order superconducting phase transitions. Moreover, the superconducting state

breaks time reversal symmetry [31] and the electrons have spin triplet pairing [36]. Furthermore, points of nodes in the gap function were observed as power law behavior in thermodynamic and transport measurements [29, 30, 32, 35, 37].

Hence, superconductivity in $\text{PrOs}_4\text{Sb}_{12}$ is rich in many peculiar and somewhat obscure properties which distinguish it from other superconducting materials.

Nevertheless the experimental results regarding superconductivity in this material are still contradictory and subject to extensive debate (as will be discussed in the next chapters). In this thesis, it will be argued that the superconducting pairing symmetry is well described by a three component order parameter which belongs to the irreducible representation T_u of the point group T_h with components $(|\eta_1|, i|\eta_2|, 0)$. That is, the pairing symmetry is spin triplet. This state can be reached directly from the normal phase or via an intermediate phase $(|\eta_1|, 0, 0)$, as shown in Fig. 1.1. The state $(|\eta_1|, 0, 0)$ is unitary and it is denoted as the A-phase, on the other hand, $(|\eta_1|, i|\eta_2|, 0)$ is nonunitary and it is denoted as the B-phase. The gap function in the A-phase is degenerate and has two linear point nodes in the $[00\pm 1]$ directions, whereas it is non-degenerate in the B-phase with four linear point nodes in the lower gap and a nodeless upper gap. The nodes in the lower gap are located at the directions $[\pm\alpha, \pm\beta, 0]$. More details will be presented in Chapter 2, where a full study of the symmetry of the order parameter in $\text{PrOs}_4\text{Sb}_{12}$ can be found.

Chapter 2

Symmetry properties of the nodal superconductor $\text{PrOs}_4\text{Sb}_{12}$

2.1 Abstract

We present a theoretical study of the superconducting gap function in $\text{PrOs}_4\text{Sb}_{12}$ using a symmetry-based approach. A three-component order parameter in the triplet channel best describes superconductivity. The gap function is non-degenerate and the lower branch has four cusp nodes at unusual points of the Fermi surface, which lead to power law behaviours in the density of states, specific heat and nuclear spin relaxation rate.

2.2 Introduction

By most accounts, $\text{PrOs}_4\text{Sb}_{12}$ is an unconventional superconductor [25, 29–36]. The superconducting phase breaks time-reversal symmetry [31] and the paired electrons are in a spin triplet configuration [36]. The existence of point nodes in the super-

conducting gap function is indicated by power law behaviour in the temperature dependencies of specific heat [29, 35], penetration depth [32], thermal conductivity [30], and Sb-NQR (Sb nuclear quadrupole resonance) [37]; however other experiments find the gap function to be nodeless [38–40]. Two distinct features in the specific heat [31, 41, 42] and other measurements [30, 32, 43–46] were initially interpreted as two phase transitions involving a change in symmetry of the superconducting order parameter, but recently these results have been ascribed to sample inhomogeneity or two-band superconductivity [47–50]. On the theoretical side, several phenomenological unconventional order parameters have been proposed [51–54] and unconventional pairing mechanisms have been studied [55, 56]. In light of all these intriguing and somewhat contradictory findings, it is not surprising that the only consensus on the symmetry of the superconducting order parameter is that it is probably unconventional.

In this study, we will consider the results of a strict analysis of symmetry and symmetry-breaking described by Landau theory [7, 10, 12]. According to this approach, the order parameter which describes the normal to superconducting phase transition must belong to one of the irreducible representations of the crystallographic point group. Each irreducible representation yields a limited number of superconducting phases. The most convenient and accurate way to label the various phases is by their symmetry groups. All of the superconducting symmetry groups are subgroups of the normal phase symmetry $G \times U \times \mathcal{K}$, where G is the point group of the crystal, U is $U(1)$ gauge (phase) symmetry and \mathcal{K} is time-reversal. Some of the subgroups include elements which are non-trivial combinations of phases, time reversal and point group elements. As described by Sigrist and Ueda [7] and Volovik and Gor'kov [10], strong spin-orbit coupling is assumed in this classification scheme.

The point group symmetry of $\text{PrOs}_4\text{Sb}_{12}$ is T_h (tetrahedral), which has a one-

dimensional representation $A_{g,u}$, a two-dimensional representation $E_{g,u}$ and a three-dimensional representation $T_{g,u}$, in each of the singlet (subscripted by g) and triplet (subscripted by u) channels. The A_g order parameter describes a “conventional” or “s-wave” superconductor. It is associated with a single, fully gapped superconducting phase. The A_u order parameter describes triplet superconductivity, also with a single, fully gapped superconducting phase. The $A_{g,u}$ phases have symmetry $T \times \mathcal{K}$, where T is the tetrahedral point group. The $E_{g,u}$ and $T_{g,u}$ order parameters are each associated with more than one superconducting phases, corresponding to different symmetries. The $E_{g,u}$ order parameters describe three different superconducting phases, of which two are accessible from the normal state via a second order phase transition, while the $T_{g,u}$ order parameters describe nine different superconducting phases, of which four are accessible from the normal state. The symmetry properties of all of these states and their corresponding gap nodes are given in Table 1.2.

The order parameter which best describes experiments is T_u , the three component order parameter in the triplet channel. Broken time reversal symmetry rules out the $A_{g,u}$ order parameters. The $E_{g,u}$ phase that is accessible from the normal phase and that breaks time reversal symmetry is $T(D_2)$, which has point nodes in the $\langle 111 \rangle$ directions which are not indicated in any experiment. The T_g phases which are accessible from the normal state have either time reversal symmetry, line nodes, or nodes in the $\langle 111 \rangle$ directions, leaving T_u as the only possibility. There are two T_u phases accessible from the normal phase that break time reversal symmetry: $C_3(E)$ and $D_2(E)$; the former has nodes in the $\langle 111 \rangle$ directions, leaving the phase $D_2(E)$ as the most likely candidate. The elements of the symmetry group $D_2(E)$ are $\{E, C_2^x \mathcal{K}, U_1(\pi) C_2^y \mathcal{K}, U_1(\pi) C_2^z\}$, where E is the identity, $U_1(\pi)$ are phases, C_2^i are rotations of π about the i -axis, and \mathcal{K} is time reversal. The triplet $D_2(E)$ phase has four point nodes in the $[\pm\alpha, \pm\beta, 0]$ directions. The proof that $D_2(E)$ has nodes in

the triplet channel is given in the Appendix.

The issue of whether there are two different superconducting phases (as suggested by specific heat and thermal conductivity experiments [30, 31, 41–44]) or only one (according to the two-band superconductivity scenario [47–50]) is to some extent by-passed by a fluke of Landau theory: the $D_2(E)$ phase is accessible via second order phase transitions both directly from the normal phase and via an intermediate phase $D_2(C_2) \times \mathcal{K}$. Thus it is a viable candidate for either situation. Therefore, we identify $D_2(C_2) \times \mathcal{K}$ as the ‘A-phase’ and $D_2(E)$ as the ‘B-phase’, and we will consider both the case when the A-phase is present and the case when the A-phase is absent on the phase diagram. Note that the elements of the group $D_2(C_2) \times \mathcal{K}$ are $\{E, C_2^x, U(\pi)C_2^y, U(\pi)C_2^z\} \times \mathcal{K}$ and that $D_2(E)$ is a subgroup of $D_2(C_2) \times \mathcal{K}$.

Recently, microscopic weak coupling theory has been applied to tetrahedral superconductors [57, 58], and it was shown that the phase $D_2(C_2) \times \mathcal{K}$ is stable, while $D_2(E)$ is not [58]. This is apparently in disagreement with the observation of broken time reversal symmetry, which means either that $\text{PrOs}_4\text{Sb}_{12}$ is a strong coupling superconductor, as claimed in Refs. [40, 42, 46, 49] or that the B-phase is better described as a $D_2(C_2) \times \mathcal{K}$ phase. We shall not pursue this possibility here, apart from noting that there are still issues whose resolution may change the conclusions of this work.

2.3 The Superconducting Gap Function

The superconducting gap function is a 2×2 matrix in pseudospin space,

$$\tilde{\Delta}(\mathbf{k}) = i\sigma_y \psi(\mathbf{k}) = \begin{pmatrix} 0 & \psi(\mathbf{k}) \\ -\psi(\mathbf{k}) & 0 \end{pmatrix} \quad (2.1)$$

in the singlet channel, and

$$\tilde{\Delta}(\mathbf{k}) = i[\boldsymbol{\sigma} \cdot \mathbf{d}(\mathbf{k})]\sigma_y = \begin{pmatrix} -d_x(\mathbf{k}) + id_y(\mathbf{k}) & d_z(\mathbf{k}) \\ d_z(\mathbf{k}) & d_x(\mathbf{k}) + id_y(\mathbf{k}) \end{pmatrix} \quad (2.2)$$

in the triplet channel, where $\psi(\mathbf{k})$ and $\mathbf{d}(\mathbf{k})$ are even and odd functions of \mathbf{k} , respectively. For singlet pairing, the gap function is given by

$$\Delta(\mathbf{k}) = |\psi(\mathbf{k})|, \quad (2.3)$$

while for triplet pairing the gap function may be non-degenerate,

$$\Delta_{\pm}(\mathbf{k}) = [|\mathbf{d}(\mathbf{k})|^2 \pm |\mathbf{q}(\mathbf{k})|]^{1/2}, \quad (2.4)$$

where $\mathbf{q}(\mathbf{k}) = i\mathbf{d}(\mathbf{k}) \times \mathbf{d}^*(\mathbf{k})$. When $\mathbf{d}(\mathbf{k})$ is real $\mathbf{q}(\mathbf{k})$ vanishes and the gaps are degenerate and unitary. Otherwise, the gap is non-degenerate and the lowest energy branch has a cusp where the two branches meet.

The gap function may be expanded in terms of the basis functions for a single representation of the point group,

$$\psi(\mathbf{k}) = \sum_i \eta_i \psi_i(\mathbf{k}) \quad (2.5)$$

$$\mathbf{d}(\mathbf{k}) = \sum_i \eta_i \mathbf{d}_i(\mathbf{k}) \quad (2.6)$$

where $\psi_i(\mathbf{k})$ and $\mathbf{d}_i(\mathbf{k})$ are basis functions for even (spin-singlet) and odd (spin-triplet) representations of the point group, respectively, and η_i are components of the order parameter. For the remainder of this work we will limit our discussion to the three component order parameter in the triplet channel T_u . An appropriate set of basis functions for this representation are [12]

$$\begin{aligned} \mathbf{d}_1 &\sim ak_y \hat{z} + bk_z \hat{y}, \\ \mathbf{d}_2 &\sim ak_z \hat{x} + bk_x \hat{z}, \\ \mathbf{d}_3 &\sim ak_x \hat{y} + bk_y \hat{x}. \end{aligned} \quad (2.7)$$

where a and b are arbitrary real numbers. More general forms, which include higher orders in \mathbf{k} , are considered in the Appendix.

The phases associated with each representation are minima of the Landau potential, which is expanded in terms of the order parameter. The transformation properties of the basis functions (2.7) get transferred to the order parameter, and the Landau potential is constructed to be invariant under all operations of the space group, gauge transformations and time reversal. The Landau potential also determines which phases are connected by second order phase transitions. A complete analysis of the Landau potentials for the tetrahedral point group T is given in Ref. [12]. The three component order parameter (η_1, η_2, η_3) , defined by (2.6) and (2.7), has four phases which are accessible from the normal state by a second order phase transition, $(0, 0, 1)$, $(1, 1, 1)$, $(1, e^{2\pi i/3}, e^{-2\pi i/3})$ and $(0, i|\eta_2|, |\eta_1|)$, with symmetries $D_2(C_2) \times \mathcal{K}$, $C_3 \times \mathcal{K}$, $C_3(E)$ and $D_2(E)$ respectively. Thus the components of the order parameter in the A-phase are $(0, 0, 1)$ (or, more precisely, $(0, 0, |\eta_1|)$) and in the B-phase are $(0, i|\eta_2|, |\eta_1|)$. These statements are summarised in Table 2.1. Different domains of each phase are obtained by permuting the components; the analysis below uses this particular choice of domain. A discussion of domains appears in Section 2.6.

phase	normal	→	A	→	B
OP components	$(0, 0, 0)$	→	$(0, 0, \eta_1)$	→	$(0, i \eta_2 , \eta_1)$
symmetry group	$T_h \times U \times \mathcal{K}$	→	$D_2(C_2) \times \mathcal{K}$	→	$D_2(E)$

Table 2.1: Order parameter (OP) components and symmetry group elements for the proposed normal→A→B second order phase transition sequence. Note that the A-phase can be skipped, since the B-phase is also accessible from the normal phase by a second order phase transition.

The gap function (2.4) in the A-phase,

$$\Delta_{\pm}(\mathbf{k}) = |\eta_1| [a^2 k_y^2 + b^2 k_x^2]^{1/2}, \quad (2.8)$$

is unitary (degenerate) and has cusp point nodes in the [001] directions, as shown in Fig. 2.1a. In the B-phase, the gap function is

$$\Delta_{\pm}(\mathbf{k}) = \left[(|\eta_1|^2 b^2 + |\eta_2|^2 a^2) k_x^2 + |\eta_1|^2 a^2 k_y^2 + |\eta_2|^2 b^2 k_z^2 \pm 2|\eta_1||\eta_2||k_x| \sqrt{a^2 b^2 k_x^2 + a^4 k_y^2 + b^4 k_z^2} \right]^{1/2}. \quad (2.9)$$

In this case the gap function is non-unitary and degenerate only where $\mathbf{d}(\mathbf{k}) \times \mathbf{d}^*(\mathbf{k}) = 0$, that is, along the line $k_x = 0$. The gap has four nodes which are solutions to $\Delta_{-}(\mathbf{k}) = 0$. When $|\eta_1|^2 b^2 > |\eta_2|^2 a^2$ the nodes are found at $k_y = 0$ and $\sqrt{|\eta_1|^2 b^2 - |\eta_2|^2 a^2} k_x = \pm |\eta_2| b k_z$, shown in Figs. 2.1b)-2.1d), and when $|\eta_1|^2 b^2 < |\eta_2|^2 a^2$ they are found at $k_z = 0$ and $\sqrt{|\eta_2|^2 a^2 - |\eta_1|^2 b^2} k_x = \pm |\eta_2| b k_y$. A three dimensional rendering of the lower branch of the gap function is shown in Fig. 2.2.

As discussed in the Introduction, the B-phase may evolve either from the A-phase, with $|\eta_2| \ll |\eta_1|$, or directly from the normal phase, in which case $|\eta_2| \approx |\eta_1|$. We now discuss these two scenarios in detail.

The order parameter of the A→B transition is η_2 , which increases continuously from zero at the phase transition. The two degenerate cusp nodes in the [001] directions in the A-phase (Fig. 2.1a) split into four non-degenerate cusp nodes in the B-phase at the phase transition (Fig. 2.1b).

The order parameter of the normal→B transition is $|\eta_1| = |\eta_2|$. In this case, the B-phase resembles the $D_4(E)$ phase of octahedral systems corresponding to the three-dimensional representations with components $(0, i, 1)$. In the Landau potential, the difference between octahedral and tetrahedral appears only in sixth order and

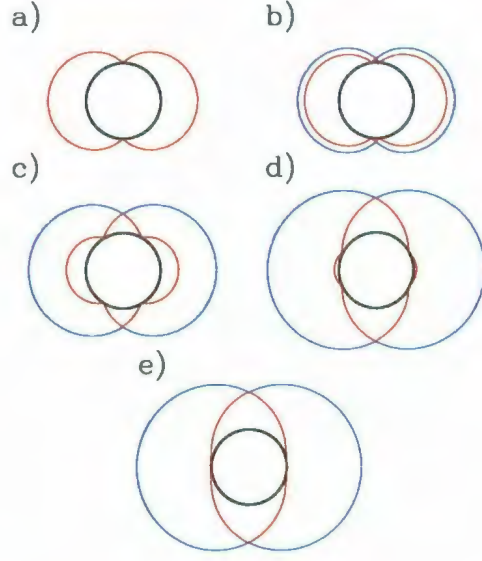


Figure 2.1: The gap function $\Delta_{\pm}(\mathbf{k})$ drawn over a spherical Fermi surface (bold) in the k_x - k_z plane. In a) the gap function (red) is unitary and degenerate. In b)-e) it is non-unitary and non-degenerate. The lower branch $\Delta_{-}(\mathbf{k})$ (red) and the upper branch $\Delta_{+}(\mathbf{k})$ (blue) are both shown. a) A-phase, $\eta_2 = 0$. b) B-phase, $|\eta_2|a = 0.1|\eta_1|b$. c) B-phase, $|\eta_2|a = 0.5|\eta_1|b$. d) B-phase, $|\eta_2|a = 0.9|\eta_1|b$. e) B-phase, $|\eta_2|a = |\eta_1|b$.

higher terms in the order parameter [12]. Near the normal-to-superconducting phase transition, when all components of the order parameter are small, the growth of the order parameter is governed by fourth order terms in the Landau potential, which are identical for octahedral and tetrahedral systems, so $|\eta_2| = |\eta_1|$ at the phase transition in both cases. The difference between the gap functions of octahedral and tetrahedral systems with 3D order parameter components $(0, i, 1)$ is due to a difference in the basis functions (2.7): $|a| = |b|$ in octahedral systems. Thus the octahedral phase $(0, i, 1)$ has two non-degenerate smooth nodes in the $[100]$ directions shown in Fig. 2.1e), while the tetrahedral system has four cusp nodes (Figs. 2.1b-2.1d).

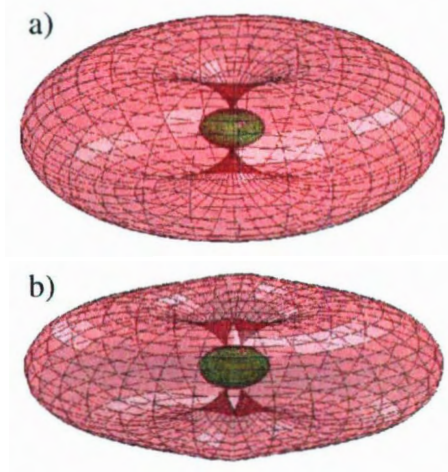


Figure 2.2: The gap function drawn over a spherical Fermi surface for the a) A-phase and b) B-phase. In a) the gap function is unitary and degenerate. In b) it is non-unitary and non-degenerate. Only the lower branch of the gap function $\Delta(\mathbf{k})$ is shown.

Thus the main difference between the two possible scenarios is the positioning of the nodes at the onset of the B-phase. In the normal $\rightarrow A \rightarrow B$ scenario, the nodes will always be found in pairs near the $[001]$ directions (Fig. 2.1b), while in the normal $\rightarrow B$ scenario, the positions of the four nodes are arbitrary (Fig. 2.1b-2.1d) and depend on the parameters a and b .

2.4 Density of states

The low temperature form of the density of states (DOS) in superconductors is governed by the presence of nodes [7, 59, 60]. In general, cusp-like point nodes give rise to a quadratic dependence on energy.

The DOS is given by [7]

$$N(\omega) = \frac{1}{(2\pi)^3} \int d^3k \sum_{\pm} \delta(\omega - E_{\pm}(\mathbf{k})), \quad (2.10)$$

where $E_{\pm}(\mathbf{k}) = \sqrt{\varepsilon^2(\mathbf{k}) + \Delta_{\pm}^2(\mathbf{k})}$ and $\varepsilon(\mathbf{k}) = \frac{k^2}{2m} - E_F$ is the free particle energy.

2.4.1 A-phase

The gap function of the A-phase (3.69) is unitary and non-degenerate (Fig. 2.1a). Since the main contributions to the integral come from the vicinity of the nodes, the integral over \mathbf{k} can be split into two separate regions centred over each node, which are cut off such that the total integrated region in k -space equals the Brillouin zone [19]. The nodes are degenerate and the contributions from each node are equal,

$$N(\omega) = \frac{4v^2}{ab|\eta_1|^2(2\pi)^3} \int_0^{2\pi} d\phi \int_0^{\infty} dk_{\parallel} k_{\parallel} \int_{-\infty}^{\infty} dk_{\perp} \delta(\omega - E(k_{\parallel}, k_{\perp})) \quad (2.11)$$

where k_{\parallel} and k_{\perp} are the momenta parallel and perpendicular to the Fermi surface at the node, $v^2 k_{\parallel}^2 = |\eta_1|^2 (a^2 k_y^2 + b^2 k_x^2)$, $k_{\perp} = k_z - k_F$ and $E(k_{\parallel}, k_{\perp}) \approx \sqrt{k_{\perp}^2 v_F^2 + k_{\parallel}^2 v^2}$. Changing variables again and using $p_1 = v_F k_{\perp} = p \cos \theta$, $p_2 = v k_{\parallel} = p \sin \theta$, we find

$$N(\omega) = \frac{4}{ab|\eta_1|^2(2\pi)^2 v_F} \int_0^{\infty} dp_2 p_2 \int_{-\infty}^{\infty} dp_1 \delta(\omega - E(p_1, p_2)) \quad (2.12)$$

$$= \frac{4}{ab|\eta_1|^2(2\pi)^2 v_F} \int_0^{\pi} \sin \theta d\theta \int_0^{p_0} dp p^2 \delta(\omega - p) \quad (2.13)$$

$$= \frac{2\omega^2}{ab|\eta_1|^2 \pi^2 v_F}$$

where the cutoff p_0 is finally introduced in the last equation. This result is equivalent to the usual result for a degenerate cusp node, $N(\omega) = \omega^2/\pi^2 v_F v_g^2$ [60], apart from a factor of two because there are two degenerate nodes in our calculation. In our case, the gap velocity, defined by $v_g = \nabla_{\mathbf{k}} \Delta(\mathbf{k})$ is not the same in all directions since the node is not rotationally symmetric, and so the geometric average $\bar{v}_g = |\eta_1|(ab)^{1/2}$ appears.

Eq. 2.13 is the density of states of the phase $(0, 0, 1)$ ($D_2(C_2) \times \mathcal{K}$) at low temperatures. However, according to the considerations outlined in Section 2.2, this phase is identified as the A-phase, which is only found in a narrow region of phase space just below H_{c2} . Therefore, Eq. 2.13 is not expected to be observed in $\text{PrOs}_4\text{Sb}_{12}$.

2.4.2 B-Phase

In triplet, non-unitary phases in general, the gap function is non-degenerate, except along some lines on the Fermi surface. If all nodes are found in the lower energy branch of the gap function Δ_- , the higher energy branch Δ_+ is usually neglected. However, if the nodes are found near the line where the gaps are degenerate then both gaps should be taken into account.

To find the density of states in the B-phase, we should consider the two different scenarios, normal \rightarrow A-phase \rightarrow B-phase or normal \rightarrow B-phase, separately. In the former scenario, $|\eta_2| \ll |\eta_1|$, and pairs of nodes are found on opposite sides of the Fermi surface. The partners in each pair are very close to each other and close to the gap degeneracy line, as shown in Fig. 2.1b). In this case, the higher energy gap should not be neglected. In the normal \rightarrow B-phase scenario, the positions of the nodes depend on the parameters a and b which are arbitrary.

normal→**A-phase**→**B-phase**

At the onset of the B-phase $|\eta_2| \ll |\eta_1|$, and we will assume that $|\eta_1|^2 b^2 > |\eta_2|^2 a^2$. Then the pairs of nodes are found in the vicinity of [001] in the plane $k_y = 0$, as shown in Fig. 2.1b). The integration over k -space is divided into four regions, which overlap for nodes within a pair.

The gap function in the vicinity of the nodes for the case when $|\eta_1|^2 b^2 > |\eta_2|^2 a^2$ can be approximated by

$$\Delta(\mathbf{k}) \approx \sqrt{|\eta_1|^2 b^2 - |\eta_2|^2 a^2} \sqrt{k_{\parallel}^2 + k_y^2} \quad (2.14)$$

where $k_y' = \frac{a}{b} k_y$ and

$$k_{\parallel}' = \frac{\sqrt{|\eta_1|^2 b^2 - |\eta_2|^2 a^2}}{|\eta_1| b} k_x \pm \frac{|\eta_2| a}{|\eta_1| b} k_z. \quad (2.15)$$

With this approximation, the ‘-’ branch of the gap function continues smoothly to the ‘+’ branch of the gap function at the line where the gap function is degenerate. Then two difficulties are overcome at once: both branches of the gap function are taken into account, and the contributions from each integration region are distinct, even though the regions overlap. Each region yields the same contribution to the density of states,

$$N(\omega) = \frac{4}{(2\pi)^3} \frac{b}{a} \frac{v^2}{|\eta_1|^2 b^2 - |\eta_2|^2 a^2} \int_0^{2\pi} d\phi \int_0^{\infty} dk_{\parallel} k_{\parallel} \int_{-\infty}^{\infty} dk_{\perp} \delta(\omega - E(k_{\parallel}, k_{\perp})) \quad (2.16)$$

where $v^2 k_{\parallel}^2 = (|\eta_1|^2 b^2 - |\eta_2|^2 a^2)(k_{\parallel}'^2 + k_y'^2)$, $k_{\perp} = \frac{\sqrt{|\eta_1|^2 b^2 - |\eta_2|^2 a^2}}{|\eta_1| b} k_x \mp \frac{|\eta_2| a}{|\eta_1| b} k_z$ and $E(k_{\parallel}, k_{\perp}) \approx \sqrt{k_{\perp}^2 v_F^2 + k_{\parallel}^2 v^2}$ as before. Then performing the same change of variables as in the A-phase calculation, we find

$$N(\omega) = \frac{b}{a} \frac{2\omega^2}{\pi^2 v_F (|\eta_1|^2 b^2 - |\eta_2|^2 a^2)} \quad (2.17)$$

Note that in the limit $|\eta_2| \rightarrow 0$ we recover the A-phase result, as expected.

normal \rightarrow B-phase

In this situation, near the phase transition we have $|\eta_1| \approx |\eta_2|$, however the positions of the nodes depend on the parameters a and b , which are completely undetermined. Then there are three possibilities to consider. The first is shown in Fig. 2.1b), where the nodes appear in pairs such that the pairs are close to the gap degeneracy line (if $|a| \ll |b|$ or $|b| \ll |a|$); in this case the above calculation is valid and the result (2.17) is obtained for $|\eta_1| \approx |\eta_2|$,

$$N(\omega) = \frac{b}{a} \frac{2\omega^2}{\pi^2 v_F |\eta_1|^2 (b^2 - a^2)}. \quad (2.18)$$

Second, when all four nodes are spaced far apart as shown in Fig. 2.1c), then the above calculations are again valid and the result (2.18) is obtained.

Finally, the nodes may appear in pairs which are far away from the gap degeneracy line, as shown in Fig. 2.1d). In this case the above treatment is invalid. Here we have a crossover between $N(\omega) \sim \omega^2$ and $N(\omega) \sim |\omega|$, which is the behaviour of the limiting case shown in Fig. 2.1e), *i.e.*, the octahedral phase $(0, i, 1)$, with smooth (quadratic) nodes. Such behaviour is not observed in experiments, which could mean that either the components of the order parameter are unequal (normal \rightarrow A-phase \rightarrow B-phase scenario) or $a \neq b$.

2.5 Specific heat and nuclear spin relaxation rate

The specific heat at low temperatures is given by [7]

$$C(T) = \frac{2}{T} \int_0^\infty d\omega \omega^2 N(\omega) \left[-\frac{\partial f}{\partial \omega} \right] \quad (2.19)$$

Eqs. 2.13 and 2.17 yield

$$C(T) = \frac{14 \pi^2}{15 v_F a b |\eta_1|^2} T^3 \quad (2.20)$$

for the A-phase, and

$$C(T) = \frac{b}{a} \frac{14 \pi^2}{15 v_F (|\eta_1|^2 b^2 - |\eta_2|^2 a^2)} T^3 \quad (2.21)$$

for the B-phase.

The longitudinal nuclear spin-lattice relaxation rate is given by [7]

$$\frac{(1/T_1)_T}{(1/T_1)_{T_c}} = 2 \frac{T}{T_c} \int_0^\infty d\omega N(\omega) N(\omega - \omega_0) \left[-\frac{\partial f}{\partial \omega} \right]. \quad (2.22)$$

In the limit of small nuclear resonance frequency ω_0 , one finds

$$\frac{(1/T_1)_T}{(1/T_1)_{T_c}} = \frac{28}{15 \pi^4 v_F^2 a^2 b^2 |\eta_1|^4} \frac{T^5}{T_c} \quad (2.23)$$

in the A-phase, while in the B-phase it is

$$\frac{(1/T_1)_T}{(1/T_1)_{T_c}} = \frac{b^2}{a^2} \frac{28}{15 \pi^4 v_F^2 (|\eta_1|^2 b^2 - |\eta_2|^2 a^2)^2} \frac{T^5}{T_c}. \quad (2.24)$$

These expressions give the low temperature behaviour of the specific heat and nuclear relaxation rate in terms of the tetrahedral parameters a and b and the order parameter components η_1 and η_2 .

2.6 Domains

Directional dependent measurements are the ideal way to observe the anisotropy of the gap function. However, such measurements may be confounded by the presence of domains, different regions in space where the components of the order parameter are interchanged. In this section we offer a brief discussion of domains for the A-phase and the B-phase.

The A-phase has three different domains $(1, 0, 0)$, $(0, 1, 0)$ and $(0, 0, 1)$, which, in the absence of unusual crystal shape or external fields, are all expected to be present,

and will lead to the observation of the full tetrahedral symmetry. Six (degenerate) nodes will be observed in the directions $\langle 00 \pm 1 \rangle$. Now let us suppose that there is some kind of external effect along the z -axis which effectively lowers the symmetry from T_h to D_{2h} . In an octahedral system, either the single domain $(0, 0, 1)$, with nodes in the $[00 \pm 1]$ directions will be favoured, *or* the other two domains, $(1, 0, 0)$ and $(0, 1, 0)$ will be favoured. In the latter case, four nodes would be observed in the directions $[\pm 100]$ and $[0 \pm 10]$. However, because the crystal symmetry of $\text{PrOs}_4\text{Sb}_{12}$ is tetrahedral to begin with, any axial perturbation will lift the degeneracy of all three domains, any of which could be favoured. Therefore, in the A-phase, if all domains are present then tetrahedral symmetry with six nodes will be observed. Otherwise, only one domain is present, the symmetry will be $D_2(C_2)$, with two nodes. It is not likely that two out of three domains would be present in the A-phase, but could be possible if they were very close in energy.

The same arguments also hold for the more complicated B-phase. Three domains are possible [61], with twelve non-degenerate nodes. If there is a single domain, then the symmetry is $D_2(E)$, and four nodes will be present.

2.7 Conclusions

In this study, we have attempted to give a physical description and comparison of the sequences of phase transitions $\text{normal} \rightarrow D_2(C_2) \times \mathcal{K} \rightarrow D_2(E)$ and $\text{normal} \rightarrow D_2(E)$, which we identify with the phase transitions seen in experiments, $\text{normal} \rightarrow \text{A} \rightarrow \text{B}$ or $\text{normal} \rightarrow \text{B}$, respectively. Although this description is derived entirely from basic considerations of symmetry, a complicated gap structure emerges with several unusual features. First, the positions of the nodes in the B-phase are not located on any symmetry axes. Although this is allowed by symmetry to occur in crystals with other

point groups, such a feature has never before been considered. Second, because the B-phase is triplet and non-unitary, there are two non-degenerate gaps. The only known example of this is Sr_2RuO_4 , but in that case the two gaps remain close in energy [8]. In $\text{PrOs}_4\text{Sb}_{12}$, for a direct normal \rightarrow B transition, the energy difference is not necessarily small. Finally, the proposed A \rightarrow B transition, which is characterised by the splitting into two of the degenerate nodes of the the A-phase, is highly unusual.

In summary, we have proposed phase transition sequences in accordance with experimental evidence available to date and studied its basic properties. Superconductivity is best-described by a three component order parameter in the triplet channel. The superconducting phase has $D_2(E)$ symmetry, is non-unitary, and has four cusp nodes at unusual points on the Fermi surface. The presence of nodes leads to a quadratic dependence on energy in the density of states, and power law behaviour in the specific heat and nuclear spin relaxation rate. There is also a second, higher energy, nodeless gap which may be experimentally accessible.

Acknowledgements

We thank Ivan Sergienko for assistance with the proof in the Appendix and Ilya Vekhter for helpful discussions.

2.8 Appendix A: Proof of the existence of nodes in the $D_2(E)$ phase in the triplet channel

In Section 2.3, we found the gap function using basis functions given by (2.7), and order parameter components $(0, i|\eta_2|, |\eta_1|)$. The gap function takes the form (3.70), which vanishes either in the plane $k_y = 0$ at the points defined by $\sqrt{|\eta_1|^2 b^2 - |\eta_2|^2 a^2} k_x =$

$\pm|\eta_2|bk_z$ when $|\eta_1|^2b^2 > |\eta_2|^2a^2$, or in the plane $k_z = 0$ at the points $\sqrt{|\eta_2|^2a^2 - |\eta_1|^2b^2}k_x = \pm|\eta_2|bk_y$ when $|\eta_1|^2b^2 < |\eta_2|^2a^2$. In Section 2.3, only p-wave pairing (basis functions linear in \mathbf{k}) was considered. In order to rigorously demonstrate the existence of nodes all possible higher order pairings must be included in the basis functions. We now consider this most general case.

The most general form for the basis functions of the representation T in T_h is

$$d_1 = (f(k_x, k_y, k_z), g(k_x, k_y, k_z), h(k_x, k_y, k_z)) \quad (2.25)$$

$$\begin{aligned} d_2 &= (h(k_y, k_z, k_x), f(k_y, k_z, k_x), g(k_y, k_z, k_x)) \quad (2.26) \\ &= (h', f', g') \end{aligned}$$

$$\begin{aligned} d_3 &= (g(k_z, k_x, k_y), h(k_z, k_x, k_y), f(k_z, k_x, k_y)) \quad (2.27) \\ &= (g'', h'', f'') \end{aligned}$$

where $f(\mathbf{k})$ is odd in \mathbf{k} , $g(k_x, k_y, k_z)$ is odd in k_z and even in k_x and k_y , and $h(k_x, k_y, k_z)$ is odd in k_y and even in k_x and k_z . Eventually, we will find solutions to $\Delta_-(\mathbf{k}) = 0$ where one of the k 's is zero (in agreement with the particular case of lowest order in k basis functions (2.7)), so we set $f(\mathbf{k}) = 0$ now.

Using (2.4), (2.6) and (2.25-2.27) one finds

$$\begin{aligned} \Delta_-^2 &= |\eta_1|^2(g''^2 + h''^2) + |\eta_2|^2(g'^2 + h'^2) \\ &\quad - 2|\eta_1||\eta_2|\sqrt{h''^2g'^2 + g''^2h'^2 + h''^2h'^2}. \end{aligned} \quad (2.28)$$

Case 1: $k_y = 0$: g'' vanishes and

$$\Delta_-^2 = (|\eta_1|h'' - |\eta_2|\sqrt{g'^2 + h'^2})^2. \quad (2.29)$$

Nodes are found where $\Delta_- = 0$, or where the function

$$\phi_1(k_x, k_z) = h^2(k_z, k_x, 0) - \frac{|\eta_2|^2}{|\eta_1|^2}(g^2(0, k_z, k_x) + h^2(0, k_z, k_x)) \quad (2.30)$$

vanishes.

Case 2: $k_z = 0$: h' vanishes and

$$\Delta_-^2 = (|\eta_2|g' - |\eta_1|\sqrt{g''^2 + h''^2})^2. \quad (2.31)$$

Nodes are found where $\Delta_- = 0$, or where the function

$$\phi_2(k_x, k_y) = \frac{|\eta_2|^2}{|\eta_1|^2}g^2(k_y, 0, k_x) - (g^2(0, k_x, k_y) + h^2(0, k_x, k_y)) \quad (2.32)$$

vanishes.

We have

$$\begin{aligned} \phi_1(k_x, 0) &= h^2(0, k_x, 0) - \frac{|\eta_2|^2}{|\eta_1|^2}g^2(0, 0, k_x) \\ \phi_1(0, k_z) &= -\frac{|\eta_2|^2}{|\eta_1|^2}h^2(0, k_z, 0) < 0 \\ \phi_2(k_x, 0) &= \frac{|\eta_2|^2}{|\eta_1|^2}g^2(0, 0, k_x) - h^2(0, k_x, 0) \\ &= -\phi_1(k_x, 0) \\ \phi_2(0, k_y) &= -g^2(0, 0, k_y) < 0 \end{aligned}$$

If $\phi_1(k_x, 0) > 0$, then $\phi_1(k_x, k_z)$ changes sign, *i.e.*, there is a node of Δ_- in the $k_y = 0$ plane somewhere between the positions $(k_x, 0, 0)$ and $(0, 0, k_z)$. Symmetry requires that there be (at least) four nodes on the Fermi surface. If $\phi_1(k_x, 0) < 0$, then $\phi_2(k_x, k_y)$ changes sign, *i.e.*, there are four nodes in the $k_z = 0$ plane.

Thus we have proved that, in general, the triplet phase with order parameter components $(0, i|\eta_2|, |\eta_1|)$ has four nodes in either the plane $k_y = 0$ or $k_z = 0$ at the positions $[\pm\alpha, 0, \pm\beta]$ or $[\pm\alpha, \pm\beta, 0]$; where α and β depend on the particular form of the basis functions. These nodes are “approximate”, in the sense that they are a consequence of symmetry and follow from the most general basis functions for the T representation. These nodes are also “rigorous”, since the state $(0, i|\eta_2|, |\eta_1|)$ couples to no secondary superconducting order parameters [12].

Chapter 3

Impurity induced density of states and residual transport in nonunitary superconductors

3.1 Abstract

We obtain general expressions for the residual density of states, electrical conductivity and thermal conductivity for non-unitary superconductors due to impurity scattering. We apply the results to the so-called 'B phase' of $\text{PrOs}_4\text{Sb}_{12}$, which we describe using a non-unitary gap function derived from symmetry considerations. The conductivity tensor has inequivalent diagonal components due to off-axis nodal positions which may be detectable in experiments.

3.2 Introduction

Non-unitary pairing in superfluids was first described by Leggett [62], but the A_1 phase of ^3He is the only well-established example of this, so far. However, recently non-unitary pairing was observed in the heavy fermion superconductor $\text{PrOs}_4\text{Sb}_{12}$ by Aoki *et al* [31]. A physically significant consequence of non-unitary pairing is a lifting of the degeneracy of the superconducting energy gap, so that two different energy gap branches, both of which are anisotropic, are observable. Multi-gap behaviour has been observed in $\text{PrOs}_4\text{Sb}_{12}$ [47–50, 63–65] but so far this has mainly been attributed to multi-band superconductivity, and gap splitting due to non-unitary pairing has received little consideration, in spite of numerous citations of Aoki *et al.*'s results.

Superconductivity in $\text{PrOs}_4\text{Sb}_{12}$ is believed to be unconventional [25, 29–37]. The paired electrons are in a spin triplet configuration [36], and the superconducting state has broken time reversal symmetry and is non-unitary [31]. Low temperature power law behaviour, indicative of the presence of nodes in the gap function, has been observed in thermodynamic and transport measurements [29, 30, 32, 35, 37], but some experiments have found the gap function to be nodeless [38–40, 49]. Other experiments observed two superconducting phases, possibly with different symmetries [30–32, 41–46], suggesting a multi-component superconducting order parameter. These two phases are known as the “A phase” and the “B phase”. If it exists, the A phase occupies only a small region of the phase diagram just below $H_{c2}(T)$. Thus, most measurements, including those cited above, have probed the B phase.

The three dimensional representation T_u of the point group T_h best describes superconductivity in $\text{PrOs}_4\text{Sb}_{12}$ [12, 66]. This representation yields several superconducting phases, of which four are accessible from the normal state by a second order phase transition. We have previously identified the states $D_2(C_2) \times \mathcal{K}$ and $D_2(E)$,

with order parameter components $(0, 0, |\eta_1|)$ and $(0, i|\eta_2|, |\eta_1|)$, as the A phase and B phase, respectively [12, 66]. Here, $D_2(C_2)$ is the symmetry group with elements $\{E, C_2^x, U(\pi)C_2^y, U(\pi)C_2^z\}$ while $D_2(E) = \{E, C_2^x\mathcal{K}, U_1(\pi)C_2^y\mathcal{K}, U_1(\pi)C_2^z\}$ [12]. The corresponding gap functions are unitary for the A phase, with two point nodes in the $[00\pm 1]$ directions, and nonunitary for the B phase, with four nodes on unusual points on the Fermi surface, $[0, \pm\alpha, \pm\beta]$.

Low temperature transport is an effective probe for the symmetry of the gap function [19, 67–70]. Impurities induce and scatter quasiparticles at the nodes and the conductance remains finite even in the limit of zero frequency and temperature. Usually, two limiting cases of impurity scattering are considered, the “Born limit” (weak scattering) and the “unitary limit” (strong scattering). The unitary limit is associated with non-magnetic substitutions of magnetic ions in heavy fermion superconductors [71–74]. The self-energy due to isotropic impurity scattering is obtained from the T-matrix [71, 74], $\Sigma(k, \omega) = (n_i/\pi N_n)T(k, k, \omega)$, where n_i is the impurity concentration, N_n is the density of states in the normal state, and the T-matrix is the self-consistent solution to $T(\omega) = V + VG_0(\omega)T(\omega)$, where V is the impurity potential, $G_0(\omega) = (1/\pi N_n)\sum_{\mathbf{k}}G(\mathbf{k}, \omega)$ and $G(\mathbf{k}, \omega)$ is the electronic Green’s function in the superconducting state. The self-energy is then $\Sigma(\omega) = (n_i/\pi N_n)G_0(\omega)/[c^2 - G_0^2(\omega)]$, where c is related to the phase shift, $c = \cot \delta_0$. In unitary limit $c \rightarrow 0$, while $c \rightarrow \infty$ in the Born limit. The main result of this approach is a renormalisation of the frequency $\omega \rightarrow \omega - i\Gamma(\omega)$ due to impurity scattering. We will use this result to find impurity induced residual density of states and transport coefficients.

The outline of this chapter is as follows: in Sec. 3.3 we define the gap function, the mean field Green’s functions and spectral functions. In Secs. 3.4, 3.5 and 3.6 we derive general expressions for the impurity induced quasiparticle density of states, the electrical conductivity and the thermal conductivity in a nonunitary superconducting

state. In Sec. 3.7 we apply our results to the nonunitary B phase in $\text{PrOs}_4\text{Sb}_{12}$, and we summarise our results in Sec. 3.8.

3.3 Mean Field Results

In the following we state the main results of the mean field treatment of an effective pairing Hamiltonian (see Ref. [7] for details).

The gap function is a 2×2 matrix in pseudospin space. For triplet pairing it can be parametrised in terms of an odd pseudovectorial function $\mathbf{d}(\mathbf{k})$ as

$$\tilde{\Delta}_{\mathbf{k}} = i[\tilde{\boldsymbol{\sigma}} \cdot \mathbf{d}_{\mathbf{k}}]\tilde{\sigma}_y = \begin{pmatrix} -d_x(\mathbf{k}) + id_y(\mathbf{k}) & d_z(\mathbf{k}) \\ d_z(\mathbf{k}) & d_x(\mathbf{k}) + id_y(\mathbf{k}) \end{pmatrix}. \quad (3.1)$$

When $\tilde{\Delta}_{\mathbf{k}}\tilde{\Delta}_{\mathbf{k}}^\dagger$ is proportional to the unit matrix, the pairing is said to be “unitary”. Non-unitary pairing occurs only in the triplet channel and only when $\mathbf{q}_{\mathbf{k}} \equiv i\mathbf{d}_{\mathbf{k}} \times \mathbf{d}_{\mathbf{k}}^* \neq 0$. Non-unitary states necessarily have broken time reversal symmetry. However, note that, for example, pairing of the form $\mathbf{d}_{\mathbf{k}} = (k_x + ik_y)\hat{z}$ (proposed for Sr_2RuO_4) breaks time reversal symmetry but is unitary. The quasiparticle energies are

$$E_{\mathbf{k}\pm} = [\varepsilon_{\mathbf{k}}^2 + \Delta_{\mathbf{k}\pm}^2]^{1/2} \quad (3.2)$$

where

$$\Delta_{\mathbf{k}\pm} = [|\mathbf{d}_{\mathbf{k}}|^2 \pm |\mathbf{q}_{\mathbf{k}}|]^{1/2}. \quad (3.3)$$

Thus, non-unitary pairing lifts the gap degeneracy.

For triplet pairing, the normal and anomalous quasiparticle Green’s functions are [7, 75]

$$\tilde{G}(\mathbf{k}, i\omega_n) = \frac{-[\omega_n^2 + \varepsilon_{\mathbf{k}}^2 + |\mathbf{d}_{\mathbf{k}}|^2]\tilde{\sigma}_0 + \mathbf{q}_{\mathbf{k}} \cdot \tilde{\boldsymbol{\sigma}}}{[\omega_n^2 + E_{\mathbf{k}-}^2][\omega_n^2 + E_{\mathbf{k}+}^2]} [i\omega_n + \varepsilon_{\mathbf{k}}] \quad (3.4)$$

$$\tilde{F}(\mathbf{k}, i\omega_n) = \frac{[\omega_n^2 + \varepsilon_{\mathbf{k}}^2 + |\mathbf{d}_{\mathbf{k}}|^2]\mathbf{d}_{\mathbf{k}} - i\mathbf{q}_{\mathbf{k}} \times \mathbf{d}_{\mathbf{k}}}{[\omega_n^2 + E_{\mathbf{k}-}^2][\omega_n^2 + E_{\mathbf{k}+}^2]} \cdot [i\tilde{\boldsymbol{\sigma}}\tilde{\sigma}_y] \quad (3.5)$$

It is useful to expand these expressions as

$$\begin{aligned} \tilde{G}(\mathbf{k}, \omega) = & \frac{\tilde{\sigma}_0}{2} \left[\frac{u_{\mathbf{k}-}^2}{\omega - E_{\mathbf{k}-} + i\delta} + \frac{v_{\mathbf{k}-}^2}{\omega + E_{\mathbf{k}-} + i\delta} \right. \\ & \left. + \frac{u_{\mathbf{k}+}^2}{\omega - E_{\mathbf{k}+} + i\delta} + \frac{v_{\mathbf{k}+}^2}{\omega + E_{\mathbf{k}+} + i\delta} \right] - \frac{\mathbf{q}_{\mathbf{k}} \cdot \tilde{\boldsymbol{\sigma}}}{2|\mathbf{q}_{\mathbf{k}}|} \\ & \times \left[\frac{u_{\mathbf{k}-}^2}{\omega - E_{\mathbf{k}-} + i\delta} + \frac{v_{\mathbf{k}-}^2}{\omega + E_{\mathbf{k}-} + i\delta} \right. \\ & \left. - \frac{u_{\mathbf{k}+}^2}{\omega - E_{\mathbf{k}+} + i\delta} - \frac{v_{\mathbf{k}+}^2}{\omega + E_{\mathbf{k}+} + i\delta} \right] \end{aligned} \quad (3.6)$$

$$\begin{aligned} \tilde{F}(\mathbf{k}, \omega) = & -\frac{\tilde{\sigma}_0}{2} \left[\frac{\tilde{\Delta}_{\mathbf{k}}}{\Delta_{\mathbf{k}-}} \left[\frac{u_{\mathbf{k}-}v_{\mathbf{k}-}}{\omega - E_{\mathbf{k}-} + i\delta} - \frac{u_{\mathbf{k}-}v_{\mathbf{k}-}}{\omega + E_{\mathbf{k}-} + i\delta} \right] \right. \\ & \left. + \frac{\tilde{\Delta}_{\mathbf{k}}}{\Delta_{\mathbf{k}+}} \left[\frac{u_{\mathbf{k}+}v_{\mathbf{k}+}}{\omega - E_{\mathbf{k}+} + i\delta} - \frac{u_{\mathbf{k}+}v_{\mathbf{k}+}}{\omega + E_{\mathbf{k}+} + i\delta} \right] \right] + \frac{\mathbf{q}_{\mathbf{k}} \cdot \tilde{\boldsymbol{\sigma}}}{2|\mathbf{q}_{\mathbf{k}}|} \\ & \times \left[\frac{\tilde{\Delta}_{\mathbf{k}}}{\Delta_{\mathbf{k}-}} \left[\frac{u_{\mathbf{k}-}v_{\mathbf{k}-}}{\omega - E_{\mathbf{k}-} + i\delta} - \frac{u_{\mathbf{k}-}v_{\mathbf{k}-}}{\omega + E_{\mathbf{k}-} + i\delta} \right] \right. \\ & \left. - \frac{\tilde{\Delta}_{\mathbf{k}}}{\Delta_{\mathbf{k}+}} \left[\frac{u_{\mathbf{k}+}v_{\mathbf{k}+}}{\omega - E_{\mathbf{k}+} + i\delta} - \frac{u_{\mathbf{k}+}v_{\mathbf{k}+}}{\omega + E_{\mathbf{k}+} + i\delta} \right] \right] \end{aligned} \quad (3.7)$$

where

$$\begin{aligned} u_{\mathbf{k}\pm}^2 &= \frac{1}{2} \left[1 + \frac{\varepsilon_{\mathbf{k}}}{E_{\mathbf{k}\pm}} \right], \quad v_{\mathbf{k}\pm}^2 = \frac{1}{2} \left[1 - \frac{\varepsilon_{\mathbf{k}}}{E_{\mathbf{k}\pm}} \right] \\ u_{\mathbf{k}\pm}v_{\mathbf{k}\pm} &= \frac{\Delta_{\mathbf{k}\pm}}{2E_{\mathbf{k}\pm}}, \quad u_{\mathbf{k}\pm}^2 + v_{\mathbf{k}\pm}^2 = 1 \end{aligned} \quad (3.8)$$

are the extended coherence factors for this particular state. Note that the following identity has been used in deriving the above expressions

$$\begin{aligned} i(\mathbf{q}_{\mathbf{k}} \times \mathbf{d}_{\mathbf{k}}) \cdot \tilde{\boldsymbol{\sigma}} &= (\mathbf{q}_{\mathbf{k}} \cdot \tilde{\boldsymbol{\sigma}})(\mathbf{d}_{\mathbf{k}} \cdot \tilde{\boldsymbol{\sigma}}) - \mathbf{q}_{\mathbf{k}} \cdot \mathbf{d}_{\mathbf{k}} \\ &= (\mathbf{q}_{\mathbf{k}} \cdot \tilde{\boldsymbol{\sigma}})(\mathbf{d}_{\mathbf{k}} \cdot \tilde{\boldsymbol{\sigma}}) \end{aligned} \quad (3.9)$$

where $\mathbf{q}_{\mathbf{k}} \cdot \mathbf{d}_{\mathbf{k}} = 0$ because $\mathbf{q}_{\mathbf{k}} \perp \mathbf{d}_{\mathbf{k}}$. The self-energy can be included by replacing $i\omega_n$ with $i\omega_n - \Sigma(i\omega_n)$. The retarded self-energy is $\Sigma_{ret}(\omega) = \Sigma(i\omega_n \rightarrow \omega + i\delta) = -i\Gamma(\omega)$ where the real part is assumed to be frequency independent and absorbed in the chemical potential.

The spectral function $\tilde{A}^G(\mathbf{k}, \omega)$ (and similarly $\tilde{A}^F(\mathbf{k}, \omega)$) is defined by

$$\tilde{G}(\mathbf{k}, i\omega_n) = \int_{-\infty}^{+\infty} d\omega \frac{\tilde{A}^G(\mathbf{k}, \omega)}{i\omega_n - \omega}. \quad (3.10)$$

Usually, the spectral function is just $-\frac{1}{\pi} \Im \tilde{G}^{\text{ret}}(\mathbf{k}, \omega)$, but in this case, because the Green's function has a complex numerator, the spectral function must be extracted more carefully. Using (3.6) and (3.7), one finds

$$\begin{aligned} \tilde{A}^G(\mathbf{k}, \omega) = & \frac{\Gamma(\omega)}{2\pi} \tilde{\sigma}_0 \left[\frac{u_{\mathbf{k}-}^2}{(\omega - E_{\mathbf{k}-})^2 + \Gamma^2(\omega)} + \frac{v_{\mathbf{k}-}^2}{(\omega + E_{\mathbf{k}-})^2 + \Gamma^2(\omega)} \right. \\ & \left. + \frac{u_{\mathbf{k}+}^2}{(\omega - E_{\mathbf{k}+})^2 + \Gamma^2(\omega)} + \frac{v_{\mathbf{k}+}^2}{(\omega + E_{\mathbf{k}+})^2 + \Gamma^2(\omega)} \right] - \frac{\Gamma(\omega)}{2\pi} \frac{\mathbf{q}_{\mathbf{k}} \cdot \tilde{\boldsymbol{\sigma}}}{|\mathbf{q}_{\mathbf{k}}|} \\ & \times \left[\frac{u_{\mathbf{k}-}^2}{(\omega - E_{\mathbf{k}-})^2 + \Gamma^2(\omega)} + \frac{v_{\mathbf{k}-}^2}{(\omega + E_{\mathbf{k}-})^2 + \Gamma^2(\omega)} \right. \\ & \left. - \frac{u_{\mathbf{k}+}^2}{(\omega - E_{\mathbf{k}+})^2 + \Gamma^2(\omega)} - \frac{v_{\mathbf{k}+}^2}{(\omega + E_{\mathbf{k}+})^2 + \Gamma^2(\omega)} \right] \end{aligned} \quad (3.11)$$

$$\begin{aligned} \tilde{A}^F(\mathbf{k}, \omega) = & \frac{\Gamma(\omega)}{2\pi} \tilde{\sigma}_0 \left[\frac{\tilde{\Delta}_{\mathbf{k}}}{\Delta_{\mathbf{k}-}} \left[\frac{u_{\mathbf{k}-} v_{\mathbf{k}-}}{(\omega + E_{\mathbf{k}-})^2 + \Gamma^2(\omega)} - \frac{u_{\mathbf{k}-} v_{\mathbf{k}-}}{(\omega - E_{\mathbf{k}-})^2 + \Gamma^2(\omega)} \right] \right. \\ & \left. + \frac{\tilde{\Delta}_{\mathbf{k}}}{\Delta_{\mathbf{k}+}} \left[\frac{u_{\mathbf{k}+} v_{\mathbf{k}+}}{(\omega + E_{\mathbf{k}+})^2 + \Gamma^2(\omega)} - \frac{u_{\mathbf{k}+} v_{\mathbf{k}+}}{(\omega - E_{\mathbf{k}+})^2 + \Gamma^2(\omega)} \right] \right] - \frac{\Gamma(\omega)}{2\pi} \frac{\mathbf{q}_{\mathbf{k}} \cdot \tilde{\boldsymbol{\sigma}}}{|\mathbf{q}_{\mathbf{k}}|} \\ & \times \left[\frac{\tilde{\Delta}_{\mathbf{k}}}{\Delta_{\mathbf{k}-}} \left[\frac{u_{\mathbf{k}-} v_{\mathbf{k}-}}{(\omega + E_{\mathbf{k}-})^2 + \Gamma^2(\omega)} - \frac{u_{\mathbf{k}-} v_{\mathbf{k}-}}{(\omega - E_{\mathbf{k}-})^2 + \Gamma^2(\omega)} \right] \right. \\ & \left. + \frac{\tilde{\Delta}_{\mathbf{k}}}{\Delta_{\mathbf{k}+}} \left[\frac{u_{\mathbf{k}+} v_{\mathbf{k}+}}{(\omega - E_{\mathbf{k}+})^2 + \Gamma^2(\omega)} - \frac{u_{\mathbf{k}+} v_{\mathbf{k}+}}{(\omega + E_{\mathbf{k}+})^2 + \Gamma^2(\omega)} \right] \right] \end{aligned} \quad (3.12)$$

with the spectral functions in hand, we can proceed to calculate the density of states and the transport coefficients.

3.4 Density of states

The quasiparticles density of states can be defined in terms of the spectral function as

$$N(\omega) = \sum_{\mathbf{k}} \text{Tr}[\tilde{A}^G(\mathbf{k}, \omega)] \quad (3.13)$$

using (3.11) we find the general expression for the density of states in a nonunitary superconductor,

$$N(\omega) = \sum_{\mathbf{k}, \pm} [u_{\mathbf{k}\pm}^2 \delta(\omega - E_{\mathbf{k}\pm}) + v_{\mathbf{k}\pm}^2 \delta(\omega + E_{\mathbf{k}\pm})] \quad (3.14)$$

in the absence of impurities. For small ω , in the vicinity of the gap node, we have $v_{\mathbf{k}\pm} \approx 0$, $u_{\mathbf{k}\pm} \approx 1$, and (3.14) is reduced to [7]

$$N(\omega) \approx \sum_{\mathbf{k}, \pm} \delta(\omega - E_{\mathbf{k}\pm}). \quad (3.15)$$

When the impurities are included the density of states becomes

$$N(\omega) \approx \frac{\Gamma(\omega)}{\pi} \sum_{\mathbf{k}, \pm} \left[\frac{1}{(\omega - E_{\mathbf{k}\pm})^2 + \Gamma^2(\omega)} \right]. \quad (3.16)$$

It is clear from (3.16) that the residual density of states depends on the impurity concentration through the self-energy $\Gamma(0)$.

3.5 Electrical conductivity

The dc electrical conductivity is defined by the Kubo formula [23]

$$\tilde{\sigma} = - \lim_{\Omega \rightarrow 0} \frac{\Im \tilde{\Pi}_{ret}(\Omega)}{\Omega} \quad (3.17)$$

where

$$\tilde{\Pi}(\mathbf{q}, i\Omega_n) = - \int_0^\beta d\tau e^{i\Omega_n \tau} \langle T_\tau \mathbf{j}_\mathbf{q}(\tau) \mathbf{j}_{-\mathbf{q}}(0) \rangle \quad (3.18)$$

is the current-current correlation function. The electrical current is defined by

$$\mathbf{j}(\mathbf{r}, \tau) = \frac{ie}{2m^*} [\psi_s^\dagger(\mathbf{r}, \tau) \nabla \psi_s(\mathbf{r}, \tau) - \nabla \psi_s^\dagger(\mathbf{r}, \tau) \psi_s(\mathbf{r}, \tau)] \quad (3.19)$$

where m^* is the effective mass. In second quantization form we get

$$\mathbf{j}(\mathbf{q}, \tau) = -\frac{e}{m^*} \sum_{\mathbf{k}, s} \left[\mathbf{k} + \frac{\mathbf{q}}{2} \right] c_{\mathbf{k}+\mathbf{q}, s}^\dagger(\tau) c_{\mathbf{k}, s}(\tau). \quad (3.20)$$

Evaluating the time order bracket, we get

$$\langle T_\tau \mathbf{j}_q(\tau) \mathbf{j}_{-q}(0) \rangle = \left\langle T_\tau c_{\mathbf{k}+\mathbf{q}, s}^\dagger(\tau) c_{\mathbf{k}, s}(\tau) c_{\mathbf{k}'-\mathbf{q}, s'}^\dagger(0) c_{\mathbf{k}', s'}(0) \right\rangle \quad (3.21)$$

$$= - \left\langle T_\tau c_{\mathbf{k}, s}(\tau) c_{\mathbf{k}'-\mathbf{q}, s'}^\dagger(0) \right\rangle \left\langle T_\tau c_{\mathbf{k}', s'}(0) c_{\mathbf{k}+\mathbf{q}, s}^\dagger(\tau) \right\rangle \\ + \left\langle T_\tau c_{\mathbf{k}', s'}(0) c_{\mathbf{k}, s}(\tau) \right\rangle \left\langle T_\tau c_{\mathbf{k}+\mathbf{q}, s}^\dagger(\tau) c_{\mathbf{k}'-\mathbf{q}, s'}^\dagger(0) \right\rangle \quad (3.22)$$

so,

$$\langle T_\tau \mathbf{j}_q(\tau) \mathbf{j}_{-q}(0) \rangle = - \delta_{\mathbf{k}', \mathbf{k}+\mathbf{q}} G_{ss'}(\mathbf{k}, \tau) G_{s's}(\mathbf{k} + \mathbf{q}, -\tau) + \delta_{\mathbf{k}', -\mathbf{k}} F_{s's}(\mathbf{k}, -\tau) \\ \times F_{ss'}^\dagger(\mathbf{k} + \mathbf{q}, \tau) \quad (3.23)$$

Fourier transform in time, the current-current correlation function becomes

$$\tilde{\Pi}(\mathbf{q}, i\Omega_n) = -\frac{e^2}{m^{*2}} \sum_{\mathbf{k}, \mathbf{k}'} \sum_{s, s'} \frac{1}{\beta} \sum_{i\omega_n} \left[-\delta_{\mathbf{k}', \mathbf{k}+\mathbf{q}} [\mathbf{k} + \mathbf{q}/2] [\mathbf{k}' - \mathbf{q}/2] \right. \\ \times G_{ss'}(\mathbf{k}, i\omega_n) G_{s's}(\mathbf{k} + \mathbf{q}, i\omega_n + i\Omega_n) + \delta_{\mathbf{k}', -\mathbf{k}} [\mathbf{k} + \mathbf{q}/2] [\mathbf{k}' - \mathbf{q}/2] \\ \left. \times F_{s's}(\mathbf{k}, i\omega_n) F_{ss'}^\dagger(\mathbf{k} + \mathbf{q}, i\omega_n + i\Omega_n) \right] \quad (3.24)$$

The current-current correlation function in the bare bubble approximation is therefore

$$\tilde{\Pi}(\mathbf{q}, i\Omega_n) = \frac{e^2}{m^{*2}} \sum_{\mathbf{k}} \left[\mathbf{k} + \frac{\mathbf{q}}{2} \right]^2 \frac{1}{\beta} \sum_{i\omega_n} \text{Tr} [\tilde{G}(\mathbf{k}, i\omega_n) \tilde{G}(\mathbf{k} + \mathbf{q}, i\omega_n + i\Omega_n) \\ + \tilde{F}(\mathbf{k}, i\omega_n) \tilde{F}^\dagger(\mathbf{k} + \mathbf{q}, i\omega_n + i\Omega_n)]. \quad (3.25)$$

The conductivity vanishes when the self-energy is absent, and the contribution from the anomalous part vanishes even when the self-energy is included. In the limit $\mathbf{q} \rightarrow 0$

the correlation function is

$$\begin{aligned} \tilde{\Pi}(i\Omega_n) = & e^2 \sum_{\mathbf{k}} v_F v_F \frac{1}{\beta} \sum_{i\omega_n} \text{Tr}[\tilde{G}(\mathbf{k}, i\omega_n) \tilde{G}(\mathbf{k}, i\omega_n + i\Omega_n) \\ & + \tilde{F}(\mathbf{k}, i\omega_n) \tilde{F}^\dagger(\mathbf{k}, i\omega_n + i\Omega_n)]. \end{aligned} \quad (3.26)$$

To evaluate this correlation function we follow the approach of Refs. [23] and [19] and rewrite the Green's function in terms of the spectral function (3.11) and sum over Matsubara frequencies.

$$\tilde{G}(\mathbf{k}, i\omega_n) = \int_{-\infty}^{\infty} d\omega' \frac{\tilde{A}_{\mathbf{k}}^G(\omega')}{i\omega_n - \omega'}, \quad \tilde{G}(\mathbf{k}, i\omega_n + i\Omega_n) = \int_{-\infty}^{\infty} d\omega'' \frac{\tilde{A}_{\mathbf{k}}^G(\omega'')}{i\omega_n + i\Omega_n - \omega''} \quad (3.27)$$

$$\tilde{\Pi}(i\Omega_n) = e^2 \sum_{\mathbf{k}} v_F v_F \int_{-\infty}^{\infty} \int_{-\infty}^{\infty} d\omega' d\omega'' \text{Tr}[\tilde{A}_{\mathbf{k}}^G(\omega') \tilde{A}_{\mathbf{k}}^G(\omega'') + \tilde{A}_{\mathbf{k}}^F(\omega') \tilde{A}_{\mathbf{k}}^F(\omega'')] S \quad (3.28)$$

$$S = \frac{1}{\beta} \sum_{i\omega_n} \frac{1}{[i\omega_n - \omega'][i\omega_n + i\Omega_n - \omega'']} \quad (3.29)$$

summing over Matsubara frequency yields (see Appendix),

$$S = \frac{n_F(\omega') - n_F(\omega'')}{\omega' - \omega'' + i\Omega_n} \quad (3.30)$$

$$S_{ret} = \frac{n_F(\omega') - n_F(\omega'')}{\omega' - \omega'' + \Omega + i\delta} \quad (3.31)$$

This eventually leads to

$$\begin{aligned} \Im \tilde{\Pi}_{ret}(\Omega) = & -\pi e^2 \sum_{\mathbf{k}} v_F v_F \int_{-\infty}^{\infty} d\omega' \text{Tr}[\tilde{A}_{\mathbf{k}}^G(\omega') \tilde{A}_{\mathbf{k}}^G(\omega' + \Omega) + \tilde{A}_{\mathbf{k}}^F(\omega') \tilde{A}_{\mathbf{k}}^F(\omega' + \Omega)] \\ & \times [n_F(\omega') - n_F(\omega' + \Omega)]. \end{aligned} \quad (3.32)$$

Then the dc electrical conductivity (3.17) is

$$\begin{aligned} \tilde{\sigma} = & \pi e^2 \sum_{\mathbf{k}} v_F v_F \int_{-\infty}^{\infty} d\omega' \text{Tr}[\tilde{A}_{\mathbf{k}}^G(\omega') \tilde{A}_{\mathbf{k}}^G(\omega') + \tilde{A}_{\mathbf{k}}^F(\omega') \tilde{A}_{\mathbf{k}}^F(\omega')] \\ & \times \left[-\frac{\partial n_F(\omega')}{\partial \omega'} \right]. \end{aligned} \quad (3.33)$$

In the limit $T \rightarrow 0$ we have $-\frac{\partial n_F(\omega')}{\partial \omega'} = \delta(\omega')$, and the conductivity is

$$\tilde{\sigma} = \pi e^2 \sum_{\mathbf{k}} v_F v_F \text{Tr}[\tilde{A}_{\mathbf{k}}^G(0)\tilde{A}_{\mathbf{k}}^G(0) + \tilde{A}_{\mathbf{k}}^F(0)\tilde{A}_{\mathbf{k}}^F(0)]. \quad (3.34)$$

from Eq. (3.12) we see that $\tilde{A}_{\mathbf{k}}^F(0) = 0$, so the second term in the trace will vanish.

Using (3.11) we finally obtain the conductivity for a non-unitary superconductor,

$$\tilde{\sigma} = \frac{e^2 \Gamma_0^2}{\pi} \sum_{\mathbf{k}} v_F v_F \left[\frac{1}{(\Gamma_0^2 + E_{\mathbf{k}-}^2)^2} + \frac{1}{(\Gamma_0^2 + E_{\mathbf{k}+}^2)^2} \right] \quad (3.35)$$

where $\Gamma_0 = \Gamma(\omega = 0)$.

3.6 Thermal conductivity

The dc thermal conductivity is defined by the Kubo formula [19]

$$\frac{\tilde{\kappa}}{T} = -\frac{1}{T^2} \lim_{\Omega \rightarrow 0} \frac{\Im \tilde{\Pi}_{ret}(\Omega)}{\Omega}. \quad (3.36)$$

The heat current is

$$\mathbf{j}(\mathbf{r}, \tau) = -\frac{1}{2m^*} \sum_s \left[\frac{\partial \psi_s^\dagger(\mathbf{r}, \tau)}{\partial \tau} \nabla \psi_s(\mathbf{r}, \tau) + \nabla \psi_s^\dagger(\mathbf{r}, \tau) \frac{\partial \psi_s(\mathbf{r}, \tau)}{\partial \tau} \right] \quad (3.37)$$

which can be written in second quantization form as

$$\mathbf{j}(\mathbf{r}, \tau) = -\frac{1}{2m^*} \sum_{\mathbf{k}, \mathbf{k}', s} \left[i\mathbf{k} \frac{\partial c_{\mathbf{k}', s}^\dagger(\tau)}{\partial \tau} c_{\mathbf{k}, s}(\tau) e^{i(\mathbf{k}-\mathbf{k}') \cdot \mathbf{r}} - i\mathbf{k}' c_{\mathbf{k}', s}^\dagger(\tau) \frac{\partial c_{\mathbf{k}, s}(\tau)}{\partial \tau} e^{i(\mathbf{k}-\mathbf{k}') \cdot \mathbf{r}} \right] \quad (3.38)$$

where

$$\psi_s(\mathbf{r}, \tau) = \sum_{\mathbf{k}} c_{\mathbf{k}, s}(\tau) e^{i\mathbf{k} \cdot \mathbf{r}} \quad (3.39)$$

has been used. Fourier transforming in space, we get

$$\begin{aligned} \mathbf{j}_q(\tau) &= -\frac{1}{2m^*} \sum_{\mathbf{k}, \mathbf{k}', s} \left[i\mathbf{k} \frac{\partial c_{\mathbf{k}', s}^\dagger(\tau)}{\partial \tau} c_{\mathbf{k}, s}(\tau) \delta(\mathbf{k} - \mathbf{k}' - \mathbf{q}) - i\mathbf{k}' c_{\mathbf{k}', s}^\dagger(\tau) \frac{\partial c_{\mathbf{k}, s}(\tau)}{\partial \tau} \delta(\mathbf{k} - \mathbf{k}' - \mathbf{q}) \right] \\ &= -\frac{1}{2m^*} \sum_{\mathbf{k}, s} \left[i[\mathbf{k} + \mathbf{q}] \frac{\partial c_{\mathbf{k}, s}^\dagger(\tau)}{\partial \tau} c_{\mathbf{k}+\mathbf{q}, s}(\tau) - i\mathbf{k} c_{\mathbf{k}, s}^\dagger(\tau) \frac{\partial c_{\mathbf{k}+\mathbf{q}, s}(\tau)}{\partial \tau} \right]. \end{aligned} \quad (3.40)$$

This form is similar to (4.17) in Ref. [19] except that we have neglected the term proportional to the gap velocity, which we assume to be much smaller than the Fermi velocity. The time order bracket can be solved as follows,

$$\begin{aligned}
& \langle T_\tau j_q(\tau) j_{-q}(\tau') \rangle = \\
& \frac{1}{4m_*^2} \sum_{\mathbf{k}, \mathbf{k}', s, s'} \left[-[\mathbf{k} + \mathbf{q}][\mathbf{k}' - \mathbf{q}] \left\langle T_\tau \frac{\partial c_{\mathbf{k}, s}^\dagger(\tau)}{\partial \tau} c_{\mathbf{k} + \mathbf{q}, s}(\tau) \frac{\partial c_{\mathbf{k}', s'}^\dagger(\tau')}{\partial \tau'} c_{\mathbf{k}' - \mathbf{q}, s'}(\tau') \right\rangle \right. \\
& \left. + [\mathbf{k} + \mathbf{q}]\mathbf{k}' \left\langle T_\tau \frac{\partial c_{\mathbf{k}, s}^\dagger(\tau)}{\partial \tau} c_{\mathbf{k} + \mathbf{q}, s}(\tau) c_{\mathbf{k}', s'}^\dagger(\tau') \frac{\partial c_{\mathbf{k}' - \mathbf{q}, s'}(\tau')}{\partial \tau'} \right\rangle \right] + \mathbf{k}[\mathbf{k}' - \mathbf{q}] \\
& \times \left\langle T_\tau c_{\mathbf{k}, s}^\dagger(\tau) \frac{\partial c_{\mathbf{k} + \mathbf{q}, s}(\tau)}{\partial \tau} \frac{\partial c_{\mathbf{k}', s'}^\dagger(\tau')}{\partial \tau'} c_{\mathbf{k}' - \mathbf{q}, s'}(\tau') \right\rangle - \mathbf{k}\mathbf{k}' \\
& \times \left\langle T_\tau c_{\mathbf{k}, s}^\dagger(\tau) \frac{\partial c_{\mathbf{k} + \mathbf{q}, s}(\tau)}{\partial \tau} c_{\mathbf{k}', s'}^\dagger(\tau') \frac{\partial c_{\mathbf{k}' - \mathbf{q}, s'}(\tau')}{\partial \tau'} \right\rangle \quad (3.41)
\end{aligned}$$

$$\begin{aligned}
& \left\langle T_\tau \frac{\partial c_{\mathbf{k}, s}^\dagger(\tau)}{\partial \tau} c_{\mathbf{k} + \mathbf{q}, s}(\tau) \frac{\partial c_{\mathbf{k}', s'}^\dagger(\tau')}{\partial \tau'} c_{\mathbf{k}' - \mathbf{q}, s'}(\tau') \right\rangle = \\
& - \left\langle T_\tau c_{\mathbf{k} + \mathbf{q}, s}(\tau) \frac{\partial c_{\mathbf{k}', s'}^\dagger(\tau')}{\partial \tau'} \right\rangle \left\langle T_\tau c_{\mathbf{k}' - \mathbf{q}, s'}(\tau') \frac{\partial c_{\mathbf{k}, s}^\dagger(\tau)}{\partial \tau} \right\rangle \\
& + \langle T_\tau c_{\mathbf{k}' - \mathbf{q}, s'}(\tau') c_{\mathbf{k} + \mathbf{q}, s}(\tau) \rangle \left\langle T_\tau \frac{\partial c_{\mathbf{k}, s}^\dagger(\tau)}{\partial \tau} \frac{\partial c_{\mathbf{k}', s'}^\dagger(\tau')}{\partial \tau'} \right\rangle \quad (3.42)
\end{aligned}$$

$$\begin{aligned}
& \left\langle T_\tau c_{\mathbf{k} + \mathbf{q}, s}(\tau) \frac{\partial c_{\mathbf{k}', s'}^\dagger(\tau')}{\partial \tau'} \right\rangle = \\
& \Theta(\tau - \tau') \left\langle c_{\mathbf{k} + \mathbf{q}, s}(\tau) \frac{\partial c_{\mathbf{k}', s'}^\dagger(\tau')}{\partial \tau'} \right\rangle - \Theta(\tau' - \tau) \left\langle \frac{\partial c_{\mathbf{k}', s'}^\dagger(\tau')}{\partial \tau'} c_{\mathbf{k} + \mathbf{q}, s}(\tau) \right\rangle \quad (3.43)
\end{aligned}$$

adding to the right hand side the zero term

$$0 = \delta(\tau - \tau') \left\langle \left[c_{\mathbf{k}', s'}^\dagger(\tau'), c_{\mathbf{k} + \mathbf{q}, s}(\tau) \right] \right\rangle \quad (3.44)$$

$$= \delta(\tau - \tau') \left\langle c_{\mathbf{k}', s'}^\dagger(\tau') c_{\mathbf{k} + \mathbf{q}, s}(\tau) \right\rangle - \delta(\tau - \tau') \left\langle c_{\mathbf{k} + \mathbf{q}, s}(\tau) c_{\mathbf{k}', s'}^\dagger(\tau') \right\rangle \quad (3.45)$$

$$= -\frac{\partial \Theta(\tau - \tau')}{\partial \tau'} \left\langle c_{\mathbf{k}', s'}^\dagger(\tau') c_{\mathbf{k} + \mathbf{q}, s}(\tau) \right\rangle + \frac{\partial \Theta(\tau - \tau')}{\partial \tau'} \left\langle c_{\mathbf{k} + \mathbf{q}, s}(\tau) c_{\mathbf{k}', s'}^\dagger(\tau') \right\rangle \quad (3.46)$$

so Eq. (3.43) becomes

$$\left\langle T_{\tau} c_{\mathbf{k}+\mathbf{q},s}(\tau) \frac{\partial c_{\mathbf{k}',s'}^{\dagger}(\tau')}{\partial \tau'} \right\rangle = \frac{\partial}{\partial \tau'} \left\langle c_{\mathbf{k}+\mathbf{q},s}(\tau) c_{\mathbf{k}',s'}^{\dagger}(\tau') \right\rangle \quad (3.47)$$

similarly, one can prove that all derivatives can be taken out of the averages, so Eq. (3.42) can be written as

$$\begin{aligned} & \left\langle T_{\tau} \frac{\partial c_{\mathbf{k},s}^{\dagger}(\tau)}{\partial \tau} c_{\mathbf{k}+\mathbf{q},s}(\tau) \frac{\partial c_{\mathbf{k}',s'}^{\dagger}(\tau')}{\partial \tau'} c_{\mathbf{k}'-\mathbf{q},s'}(\tau') \right\rangle = \\ & -\frac{\partial}{\partial \tau'} \left\langle T_{\tau} c_{\mathbf{k}+\mathbf{q},s}(\tau) c_{\mathbf{k}',s'}^{\dagger}(\tau') \right\rangle \frac{\partial}{\partial \tau} \left\langle T_{\tau} c_{\mathbf{k}'-\mathbf{q},s'}(\tau') c_{\mathbf{k},s}^{\dagger}(\tau) \right\rangle \\ & + \left\langle T_{\tau} c_{\mathbf{k}'-\mathbf{q},s'}(\tau') c_{\mathbf{k}+\mathbf{q},s}(\tau) \right\rangle \frac{\partial}{\partial \tau} \frac{\partial}{\partial \tau'} \left\langle T_{\tau} c_{\mathbf{k},s}^{\dagger}(\tau) c_{\mathbf{k}',s'}^{\dagger}(\tau') \right\rangle \end{aligned} \quad (3.48)$$

and in terms of the Green's functions, Eq. (3.48) becomes

$$\begin{aligned} & \left\langle T_{\tau} \frac{\partial c_{\mathbf{k},s}^{\dagger}(\tau)}{\partial \tau} c_{\mathbf{k}+\mathbf{q},s}(\tau) \frac{\partial c_{\mathbf{k}',s'}^{\dagger}(\tau')}{\partial \tau'} c_{\mathbf{k}'-\mathbf{q},s'}(\tau') \right\rangle = \\ & -\delta(\mathbf{k} + \mathbf{q} - \mathbf{k}') \frac{\partial}{\partial \tau'} G_{ss'}(\mathbf{k} + \mathbf{q}, \tau, \tau') \frac{\partial}{\partial \tau} G_{s's}(\mathbf{k}, \tau', \tau) \\ & + \delta(\mathbf{k}' + \mathbf{k}) F_{s's}(\mathbf{k} + \mathbf{q}, \tau', \tau) \frac{\partial}{\partial \tau} \frac{\partial}{\partial \tau'} F_{ss'}^{\dagger}(\mathbf{k}, \tau, \tau') \end{aligned} \quad (3.49)$$

using the following derivatives

$$\frac{\partial}{\partial \tau'} G_{ss'}(\mathbf{k} + \mathbf{q}, \tau, \tau') = -\frac{\partial}{\partial(\tau - \tau')} G_{ss'}(\mathbf{k} + \mathbf{q}, \tau - \tau') = -\frac{\partial}{\partial \tau} G_{ss'}(\mathbf{k} + \mathbf{q}, \tau) \quad (3.50)$$

$$\frac{\partial}{\partial \tau} G_{s's}(\mathbf{k}, \tau', \tau) = \frac{\partial}{\partial(\tau - \tau')} G_{s's}(\mathbf{k}, \tau' - \tau) = \frac{\partial}{\partial \tau} G_{s's}(\mathbf{k}, -\tau) \quad (3.51)$$

$$\frac{\partial}{\partial \tau} \frac{\partial}{\partial \tau'} = -\frac{\partial^2}{\partial(\tau - \tau')^2} = -\frac{\partial^2}{\partial \tau^2} \quad (3.52)$$

then Eq. (3.49) will have the following form

$$\begin{aligned} & \left\langle T_{\tau} \frac{\partial c_{\mathbf{k},s}^{\dagger}(\tau)}{\partial \tau} c_{\mathbf{k}+\mathbf{q},s}(\tau) \frac{\partial c_{\mathbf{k}',s'}^{\dagger}(\tau')}{\partial \tau'} c_{\mathbf{k}'-\mathbf{q},s'}(\tau') \right\rangle = \\ & \delta(\mathbf{k} + \mathbf{q} - \mathbf{k}') \frac{\partial}{\partial \tau} G_{ss'}(\mathbf{k} + \mathbf{q}, \tau) \frac{\partial}{\partial \tau} G_{s's}(\mathbf{k}, -\tau) \\ & -\delta(\mathbf{k}' + \mathbf{k}) F_{s's}(\mathbf{k} + \mathbf{q}, -\tau) \frac{\partial^2}{\partial \tau^2} F_{ss'}^{\dagger}(\mathbf{k}, \tau) \end{aligned} \quad (3.53)$$

similarly, we can work out the other brackets in Eq. (3.41), the results are

$$\begin{aligned} & \left\langle T_\tau \frac{\partial c_{\mathbf{k},s}^\dagger(\tau)}{\partial \tau} c_{\mathbf{k}+\mathbf{q},s}(\tau) c_{\mathbf{k}',s'}^\dagger(\tau') \frac{\partial c_{\mathbf{k}'-\mathbf{q},s'}(\tau')}{\partial \tau'} \right\rangle = \\ & \delta(\mathbf{k} + \mathbf{q} - \mathbf{k}') G_{ss'}(\mathbf{k} + \mathbf{q}, \tau) \frac{\partial^2}{\partial \tau^2} G_{s's}(\mathbf{k}, -\tau) \\ & - \delta(\mathbf{k}' + \mathbf{k}) \frac{\partial}{\partial \tau} F_{s's}(\mathbf{k} + \mathbf{q}, -\tau) \frac{\partial}{\partial \tau} F_{ss'}^\dagger(\mathbf{k}, \tau) \end{aligned} \quad (3.54)$$

$$\begin{aligned} & \left\langle T_\tau c_{\mathbf{k},s}^\dagger(\tau) \frac{\partial c_{\mathbf{k}+\mathbf{q},s}(\tau)}{\partial \tau} \frac{\partial c_{\mathbf{k}',s'}^\dagger(\tau')}{\partial \tau'} c_{\mathbf{k}'-\mathbf{q},s'}(\tau') \right\rangle = \\ & \delta(\mathbf{k} + \mathbf{q} - \mathbf{k}') \frac{\partial^2}{\partial \tau^2} G_{ss'}(\mathbf{k} + \mathbf{q}, \tau) G_{s's}(\mathbf{k}, -\tau) \\ & - \delta(\mathbf{k}' + \mathbf{k}) \frac{\partial}{\partial \tau} F_{s's}(\mathbf{k} + \mathbf{q}, -\tau) \frac{\partial}{\partial \tau} F_{ss'}^\dagger(\mathbf{k}, \tau) \end{aligned} \quad (3.55)$$

$$\begin{aligned} & \left\langle T_\tau c_{\mathbf{k},s}^\dagger(\tau) \frac{\partial c_{\mathbf{k}+\mathbf{q},s}(\tau)}{\partial \tau} c_{\mathbf{k}',s'}^\dagger(\tau') \frac{\partial c_{\mathbf{k}'-\mathbf{q},s'}(\tau')}{\partial \tau'} \right\rangle = \\ & \delta(\mathbf{k} + \mathbf{q} - \mathbf{k}') \frac{\partial}{\partial \tau} G_{ss'}(\mathbf{k} + \mathbf{q}, \tau) \frac{\partial}{\partial \tau} G_{s's}(\mathbf{k}, -\tau) \\ & - \delta(\mathbf{k}' + \mathbf{k}) \frac{\partial^2}{\partial \tau^2} F_{s's}(\mathbf{k} + \mathbf{q}, -\tau) F_{ss'}^\dagger(\mathbf{k}, \tau) \end{aligned} \quad (3.56)$$

inserting into Eq. (3.41) and Fourier transforming in time we get

$$\begin{aligned} & \int_0^\beta d\tau e^{i\Omega_n \tau} \langle T_\tau \mathbf{j}_\mathbf{q}(\tau) \mathbf{j}_{-\mathbf{q}}(\tau') \rangle = \\ & \frac{1}{4m^*2} \sum_{\mathbf{k},s,s'} \frac{1}{\beta} \sum_{i\omega'_n} \left[[-2\mathbf{k}[\mathbf{k} + \mathbf{q}]i\omega'_n[-i\omega'_n - i\Omega_n] + \mathbf{k}^2[-i\omega'_n - i\Omega_n]^2 + [\mathbf{k} + \mathbf{q}]^2[i\omega'_n]^2] \right. \\ & \times G_{ss'}(\mathbf{k} + \mathbf{q}, i\omega'_n + i\Omega_n) G_{s's}(\mathbf{k}, -i\omega'_n) + [2\mathbf{k}[\mathbf{k} + \mathbf{q}]i\omega'_n[-i\omega'_n - i\Omega_n] \\ & \left. - \mathbf{k}^2[i\omega'_n]^2 + [\mathbf{k} + \mathbf{q}]^2[-\omega'_n - i\Omega_n]^2] F_{s's}(\mathbf{k} + \mathbf{q}, -i\omega'_n) F_{ss'}^\dagger(\mathbf{k}, i\omega'_n + i\Omega_n) \right] \end{aligned} \quad (3.57)$$

taking the limit $\mathbf{q} \rightarrow 0$ we get

$$\begin{aligned} & \int_0^\beta d\tau e^{i\Omega_n \tau} \langle T_\tau \mathbf{j}_\mathbf{q}(\tau) \mathbf{j}_{-\mathbf{q}}(\tau') \rangle = \sum_{\mathbf{k},s,s'} \left[\frac{\mathbf{k}}{m^*} \right]^2 \frac{1}{\beta} \sum_{i\omega_n} \left[i\omega_n + \frac{i\Omega_n}{2} \right]^2 \\ & \times \left[G_{ss'}(\mathbf{k}, i\omega_n + i\Omega_n) G_{s's}(\mathbf{k}, -i\omega_n) - F_{s's}(\mathbf{k}, -i\omega_n) F_{ss'}^\dagger(\mathbf{k}, i\omega_n + i\Omega_n) \right] \end{aligned} \quad (3.58)$$

The current-current correlation function is then

$$\begin{aligned} \tilde{\Pi}(i\Omega_n) = & \frac{1}{\beta} \sum_{\mathbf{k}, i\omega_n} \mathbf{v}_F \mathbf{v}_F \left[i\omega_n + \frac{i\Omega_n}{2} \right]^2 \text{Tr} [\tilde{G}_{\mathbf{k}}(i\omega_n + i\Omega_n) \tilde{G}_{\mathbf{k}}(-i\omega_n) \\ & - \tilde{F}_{\mathbf{k}}(-i\omega_n) \tilde{F}_{\mathbf{k}}^\dagger(i\omega_n + i\Omega_n)] \end{aligned} \quad (3.59)$$

As in the electrical conductivity, the anomalous part does not contribute to the thermal conductivity. Again, the correlation function is expressed in terms of the spectral function as

$$\tilde{\Pi}(i\Omega_n) = \sum_{\mathbf{k}} \mathbf{v}_F \mathbf{v}_F \int_{-\infty}^{\infty} d\omega' \int_{-\infty}^{\infty} d\omega'' \text{Tr} [\tilde{A}_{\mathbf{k}}^G(\omega') \tilde{A}_{\mathbf{k}}^G(\omega'')] S \quad (3.60)$$

where

$$S = \frac{1}{\beta} \sum_{i\omega_n} \frac{i\omega_n + i\Omega_n/2}{[i\omega_n + i\Omega_n - \omega'][-i\omega_n - \omega'']} \quad (3.61)$$

this summation can be easily evaluated (see Appendix), the result is

$$S = \frac{[\omega' - i\Omega_n/2]^2 n_F(\omega') - [\omega'' - i\Omega_n/2]^2 n_F(-\omega'')}{\omega' + \omega'' - i\Omega_n} \quad (3.62)$$

and the retarded S will be

$$S_{ret} = \frac{[\omega' - \Omega/2]^2 n_F(\omega') - [\omega'' - \Omega/2]^2 n_F(-\omega'')}{\omega' + \omega'' - \Omega - i\delta} \quad (3.63)$$

inserting into Eq. (3.60) and taking the imaginary part we get

$$\begin{aligned} \Im \tilde{\Pi}_{ret}(\Omega) = & \sum_{\mathbf{k}} \mathbf{v}_F \mathbf{v}_F \int_{-\infty}^{\infty} d\omega' \text{Tr} [\tilde{A}_{\mathbf{k}}^G(\omega' + \Omega) \tilde{A}_{\mathbf{k}}^G(-\omega')] \left[\omega' + \frac{\Omega}{2} \right]^2 \\ & [n_F(\omega' + \Omega) - n_F(\omega')]. \end{aligned} \quad (3.64)$$

Substituting this into the Kubo formula (3.36) and evaluating in the limit $\Omega \rightarrow 0$ and $T \rightarrow 0$, we find

$$\frac{\tilde{\kappa}}{T} = \sum_{\mathbf{k}} \mathbf{v}_F \mathbf{v}_F \lim_{T \rightarrow 0} \int_{-\infty}^{\infty} d\omega' \text{Tr} [\tilde{A}_{\mathbf{k}}^G(\omega') \tilde{A}_{\mathbf{k}}^G(-\omega')] \omega'^2 \left[-\frac{\partial n_F(\omega')}{\partial \omega'} \right] \quad (3.65)$$

at low temperatures the integrand peaks at zero frequency, Taylor expanding at $\omega' = 0$ and noting that

$$\int_{-\infty}^{\infty} d\omega' \omega'^2 \left[-\frac{\partial n_F(\omega')}{\partial \omega'} \right] = \frac{\pi^2}{3} k_B^2 T^2 \quad (3.66)$$

we get

$$\frac{\tilde{\kappa}}{T} = \frac{\pi^2}{3} k_B^2 \sum_{\mathbf{k}} v_F v_F \text{Tr}[\tilde{A}_{\mathbf{k}}^G(0) \tilde{A}_{\mathbf{k}}^G(0)]. \quad (3.67)$$

Comparing (3.34) and (3.67) we can see that the Wiedemann-Franz law $\frac{\kappa}{\sigma T} = \frac{\pi k_B^2}{3e^2}$ is satisfied. Explicitly, the thermal conductivity is

$$\frac{\tilde{\kappa}}{T} = \frac{k_B^2}{3} \Gamma_0^2 \sum_{\mathbf{k}} v_F v_F \left[\frac{1}{(\Gamma_0^2 + E_{\mathbf{k}-}^2)^2} + \frac{1}{(\Gamma_0^2 + E_{\mathbf{k}+}^2)^2} \right]. \quad (3.68)$$

3.7 Application to $\text{PrOs}_4\text{Sb}_{12}$

As discussed in the Introduction, we assume that the gap function for the A phase is

$$\Delta_{\mathbf{k}} = |\eta_1| [a^2 k_y^2 + b^2 k_x^2]^{1/2}, \quad (3.69)$$

where a and b are undetermined constants, while for the B phase it has the form

$$\begin{aligned} \Delta_{\mathbf{k}\pm} = & \left[[|\eta_1|^2 b^2 + |\eta_2|^2 a^2] k_x^2 + |\eta_1|^2 a^2 k_y^2 + |\eta_2|^2 b^2 k_z^2 \right. \\ & \left. \pm 2|\eta_1||\eta_2||k_x| \sqrt{a^2 b^2 k_x^2 + a^4 k_y^2 + b^4 k_z^2} \right]^{1/2}. \end{aligned} \quad (3.70)$$

which is non-degenerate [66]. The gap function in the A phase is unitary and has two cusp point nodes in the $[00\pm 1]$ directions. The lower branch of the B phase gap function has four point nodes which are in the $k_y = 0$ plane at the positions $\sqrt{|\eta_1|^2 b^2 - |\eta_2|^2 a^2} k_x = \pm |\eta_2| b k_x$ if $|\eta_1|^2 b^2 > |\eta_2|^2 a^2$; else they are in the $k_z = 0$ plane. We will assume the former in our calculations. Since we are interested in the very low temperature regime, we will consider only the B phase.

The gap function of the B phase in the vicinity of nodes can be linearised as

$$\Delta_{\mathbf{k}} \approx v \sqrt{k_{\parallel}^2 + k_y'^2} \quad (3.71)$$

where $v = \sqrt{|\eta_1|^2 b^2 - |\eta_2|^2 a^2}$, $k_y' = \frac{a}{b} k_y$ and

$$k_{\parallel} = \frac{\sqrt{|\eta_1|^2 b^2 - |\eta_2|^2 a^2}}{|\eta_1| b} k_x \pm \frac{|\eta_2| a}{|\eta_1| b} k_z. \quad (3.72)$$

k_{\parallel} and k_{\perp} (used below) are momenta parallel and perpendicular to the Fermi surface at the node. The upper branch, which is degenerate with the lower branch on the line $k_x = 0$ between each pair of nodes, is properly included with this linearisation of the gap function. Therefore, we relabel the two branches of the gap function as shown in Fig. 3.1. Thus for any function we have

$$f(E_+) + f(E_-) = f(E_1) + f(E_2). \quad (3.73)$$

Each branch 1 and 2 has two cusp point nodes and the contribution to the excitation spectrum from each branch is equal. With this picture in mind, we now calculate the density of states and the transport coefficients.

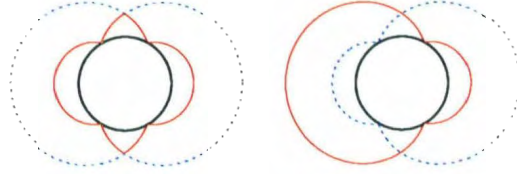


Figure 3.1: Gap function for the B phase of $\text{PrOs}_4\text{Sb}_{12}$ drawn in the k_x - k_z plane over a spherical Fermi surface (bold black). Left: the '+' branch is shown in blue (dashed) and the '-' branch in red (solid). Right: the '1' branch is shown in blue (dashed) and the '2' branch in red (solid).

3.7.1 Density of states

The density of states was calculated previously in Ref. [66] in the absence of impurities; here we will include the effect of impurities starting from (3.16). Linearising the gap function as described above, we find

$$N(\omega) = \frac{\Gamma(\omega)}{\pi} 2 \sum_{j=1}^2 \int \frac{d^3k}{(2\pi)^3} \frac{1}{(\omega - E_{\mathbf{k}})^2 + \Gamma^2(\omega)} \quad (3.74)$$

where there is a factor of 2 because there are two branches of the gap function and the sum is over the two nodes in each branch. To perform the integration we change variables to $p^2 = v^2(k_{\parallel}^2 + k_{\perp}^2) + v_F^2 k_{\perp}^2 \approx E_{\mathbf{k}}^2$,

$$N(\omega) = \frac{2\Gamma(\omega)}{\pi^3} \frac{b}{a} \frac{1}{[|\eta_1|^2 b^2 - |\eta_2|^2 a^2] v_F} \int_0^{p_0} \frac{dp p^2}{(\omega - p)^2 + \Gamma^2(\omega)} \quad (3.75)$$

and introduce a cutoff p_0 . Performing the integration we arrive at the result

$$\begin{aligned} N(\omega) = & \frac{2}{\pi^3} \frac{b}{a} \frac{1}{[|\eta_1|^2 b^2 - |\eta_2|^2 a^2] v_F} \left[[\omega^2 - \Gamma^2(\omega)] \right. \\ & \left. \left[\tan^{-1} \left(\frac{p_0 - \omega}{\Gamma(\omega)} \right) + \tan^{-1} \left(\frac{\omega}{\Gamma(\omega)} \right) \right] \right. \\ & \left. + \omega \Gamma(\omega) \ln \left(\frac{[p_0 - \omega]^2 + \Gamma^2(\omega)}{\omega^2 + \Gamma^2(\omega)} \right) - \omega \Gamma(\omega) \right. \\ & \left. + p_0 \Gamma(\omega) \right]. \end{aligned} \quad (3.76)$$

Setting $\Gamma(\omega) = 0$ we obtain our previous result [66]

$$N(\omega) = \frac{b}{a} \frac{2\omega^2}{\pi^2 v_F [|\eta_1|^2 b^2 - |\eta_2|^2 a^2]}, \quad (3.77)$$

which has a quadratic dependence on frequency as expected for point nodes. In the limit $\omega \rightarrow 0$ (3.76) becomes

$$N(0) = \frac{2}{\pi^3} \frac{b}{a} \frac{\Gamma_0^2}{[|\eta_1|^2 b^2 - |\eta_2|^2 a^2] v_F} \left[\tan^{-1} \left(-\frac{p_0}{\Gamma_0} \right) + \frac{p_0}{\Gamma_0} \right]. \quad (3.78)$$

This is the zero energy density of states induced by impurities. The cut-off is normally taken to be the size of the Brillouin zone [19] but it may be more physical to use the

reciprocal of the range of the single impurity potential [70], $p_0 \propto \lambda^{-1}$. In terms of the ratio (p_0/Γ_0) the two limits are

$$\frac{p_0}{\Gamma_0} \gg 1 \text{ (unitary)} \quad (3.79)$$

$$\frac{p_0}{\Gamma_0} \ll 1 \text{ (Born)} \quad (3.80)$$

In the unitary limit the density of states is

$$N(0) = \frac{2}{\pi^3} \frac{b}{a} \frac{p_0 \Gamma_0^u}{[|\eta_1|^2 b^2 - |\eta_2|^2 a^2] v_F} \quad (3.81)$$

where u refers to unitary scattering. If Γ_c is the critical scattering rate at which the superconductor becomes normal, then we can write (3.81) as

$$\frac{N(0)}{N_n} = \frac{\Gamma_0^u}{\Gamma_c^u} = \frac{n_{imp}}{n_{imp}^c}. \quad (3.82)$$

In the Born limit, the density of states vanishes as Γ_0^2 .

The presence of residual density of states, in general, gives a contribution linear in temperature to the specific heat and the nuclear spin relaxation rate at low temperature. The prefactor dependence on impurity doping may be helpful in identifying the symmetry of the order parameter. The specific heat is [7]

$$C(T) = \frac{2}{T} \int_0^\infty d\omega \omega^2 N(\omega) \left[-\frac{\partial f}{\partial \omega} \right]. \quad (3.83)$$

At low temperature this yields

$$\frac{(C(T)/T)}{(C(T)/T)_n} = \frac{\Gamma_0^u}{\Gamma_c^u} \quad (3.84)$$

and the nuclear spin relaxation rate is [7]

$$\begin{aligned} \frac{(1/T_1)_T}{(1/T_1)_n} &= 2 \frac{T}{T_c} \int_0^\infty d\omega N(\omega) N(\omega - \omega_0) \left[-\frac{\partial f}{\partial \omega} \right] \\ \frac{(1/TT_1)_T}{(1/TT_1)_n} &= \frac{\Gamma_0^{u^2}}{\Gamma_c^{u^2}}. \end{aligned} \quad (3.85)$$

3.7.2 Electrical and thermal conductivities

Beginning with (3.35) and making use of (3.73), we divide the integration into four parts, each centred about one node in the gap function. The factor $v_F v_F$ is evaluated at each node; the sum over nodes yields

$$\sum_{j=1}^4 v_F v_F = 4v_F^2 \begin{pmatrix} \frac{|\eta_2|^2 a^2}{|\eta_1|^2 b^2} & 0 & 0 \\ 0 & 0 & 0 \\ 0 & 0 & \frac{|\eta_1|^2 b^2 - |\eta_2|^2 a^2}{|\eta_1|^2 b^2} \end{pmatrix} \quad (3.86)$$

The remaining integration is the same for each part. Performing the same change of variables as in the density of states calculation, we find

$$\tilde{\sigma} = \frac{e^2 \Gamma_0^2 b}{2\pi^3 a [|\eta_1|^2 b^2 - |\eta_2|^2 a^2]} v_F \int_0^{p_0} \frac{dp p^2}{[p^2 + \Gamma_0^2]^2} \quad (3.87)$$

and completing the integration we get

$$\begin{aligned} \tilde{\sigma} &= \frac{e^2}{\pi^3} v_F \Gamma_0 \left[\tan^{-1} \left(\frac{p_0}{\Gamma_0} \right) - \frac{(p_0/\Gamma_0)}{1 + (p_0/\Gamma_0)^2} \right] \\ &\times \begin{pmatrix} \frac{a|\eta_2|^2}{b|\eta_1|^2 [b^2 |\eta_1|^2 - a^2 |\eta_2|^2]} & 0 & 0 \\ 0 & 0 & 0 \\ 0 & 0 & \frac{1}{ab|\eta_1|^2} \end{pmatrix} \end{aligned} \quad (3.88)$$

This is the impurity induced DC electrical conductivity for the B phase of $\text{PrOs}_4\text{Sb}_{12}$.

The thermal conductivity can be easily obtained by using the Wiedemann-Franz law.

In the unitary limit ($\frac{p_0}{\Gamma_0} \gg 1$), the term which includes $\tan^{-1} \left(\frac{p_0}{\Gamma_0} \right) = \frac{\pi}{2}$ will dominate, the conductivities become

$$\tilde{\sigma} = \frac{e^2}{2\pi^2} v_F \Gamma_0^u \begin{pmatrix} \frac{a|\eta_2|^2}{b|\eta_1|^2 [b^2 |\eta_1|^2 - a^2 |\eta_2|^2]} & 0 & 0 \\ 0 & 0 & 0 \\ 0 & 0 & \frac{1}{ab|\eta_1|^2} \end{pmatrix} \quad (3.89)$$

and

$$\frac{\tilde{\kappa}}{T} = \frac{k_B^2}{6\pi} v_F \Gamma_0^u \begin{pmatrix} \frac{a|\eta_2|^2}{b|\eta_1|^2[b^2|\eta_1|^2 - a^2|\eta_2|^2]} & 0 & 0 \\ 0 & 0 & 0 \\ 0 & 0 & \frac{1}{ab|\eta_1|^2} \end{pmatrix}. \quad (3.90)$$

Thus the conductivities in the B phase of $\text{PrOs}_4\text{Sb}_{12}$ are non-universal (dependent on impurity concentration) for unitary scattering but vanish in the Born limit. The conductivity tensor has two inequivalent components, σ_{xx} and σ_{zz} due to the off-axis nodal positions *and* the choice of a particular domain of superconducting phase. This domain is represented by order parameter components $(0, i|\eta_2|, |\eta_1|)$. If all three domains are present then all diagonal components of the conductivity tensor will be equal. The σ_{xx} component is proportional to the parameter $|\eta_2|$ which is absent in the unitary A phase. Therefore, measurement of residual conductivities in a domain-pinned set-up, such as the one used in directional dependent thermal conductivity measurements [30] could determine the direction of nodes. Of all the possible SC states in tetrahedral systems, $D_2(E)$, with OP components $(0, i|\eta_2|, |\eta_1|)$, is the only one with off-axis nodes [12, 66].

3.7.3 Discussion

There have been several studies on Ru and La doped samples [34, 50, 76–78], with the surprising result that Ru substitution leads to a doping-dependent residual density of states and resistivity [34, 76], while La substitution does not [50]. In $\text{PrOs}_4\text{Sb}_{12}$, it is speculated that quadrupolar fluctuations of the Pr ions play a role similar to the magnetic fluctuations of Ce and U ions in other heavy fermion superconductors, thus substitution of the Pr ions by La would be expected to produce unitary scatterers. However, in contrast to Eq. 3.85, there is no dependence on doping on NQR relaxation rate beyond the La concentration $x = 0.05$.

Both $\text{Pr}_{1-x}\text{La}_x\text{Os}_4\text{Sb}_{12}$ and $\text{Pr}(\text{Os}_{1-x}\text{Ru}_x)_4\text{Sb}_{12}$ are superconducting for the entire range of x , and both become s -wave superconductors at some intermediate value of x . In the Ru doped series, T_c has a minimum at $x = 0.6$, with a leveling off of the specific heat at the same value. This suggests that a phase transition between triplet and singlet superconductivity occurs at $x \approx 0.6$, with possibly a region of co-existence of these two phases [79]. A 0.4% change in lattice constant occurs between $\text{PrOs}_4\text{Sb}_{12}$ and $\text{PrRu}_4\text{Sb}_{12}$ [76], and effects due to quadrupolar fluctuations appear to be absent in $\text{PrRu}_4\text{Sb}_{12}$. In the La doped series, T_c decreases linearly along the entire range of x , while the specific heat levels off at $x \approx 0.3$.

According to (3.81) and (3.89), the dependence of the residual density of states and resistivity on Ru doping suggests that the scattering from Ru ions is unitary. Unitary scattering due to the substitution of Os by Ru may be explained by noting that quadrupolar fluctuations of the Pr ions are charge density fluctuations and will couple to, and possibly be enhanced by, quadrupolar lattice vibration modes. The change in lattice constant that accompanies Ru doping will alter the quadrupole moment of those modes. In addition, Ru substitution has a strong effect on the low-lying crystal electric field (CEF) levels of the Pr ions which eventually removes quadrupole fluctuations [78]. La substitution produces a much smaller change in lattice constant and has a much weaker effect on the Pr CEF levels. Nevertheless, it is still difficult to explain why there is no dependence at all on the La concentration.

3.8 Summary and Conclusions

It is evident from (3.16), (3.35) and (3.68) that the main effect of a non-unitary superconducting state is a lifting of the gap degeneracy, and that this would be observed as multi-gap behaviour similar to what could be expected for multi-band supercon-

ductivity. There are, however, some differences which we outline here. We base the following discussion on the unitary state $D_2(C_2) \times \mathcal{K}$ and the non-unitary state $D_2(E)$, with order parameter components $(0, 0, |\eta_1|)$ and $(0, i|\eta_2|, |\eta_1|)$ respectively. There are many other states, but all the rest are either nodeless, or else they have a C_3 symmetry element which has been positively ruled out by experiment [33].

In a multi-band superconductor with a single T_c the symmetry of the superconducting order parameter should either be the same on both bands, or possibly, superconductivity on one band is a secondary order parameter to superconductivity on the other. The alternative, which is the simultaneous appearance of two different order parameters, would be unprecedented. This means that the symmetries of superconducting states on the different bands should either be the same, or have a group-subgroup relation. For example, in MgB_2 , the archetypal multi-band superconductor, s-wave superconductivity is observed as a full gap for both bands. The best candidates for nodal superconductivity in the triplet channel in $\text{PrOs}_4\text{Sb}_{12}$ are the unitary state $D_2(C_2) \times \mathcal{K}$ and the non-unitary state $D_2(E)$, and neither of these has secondary order parameters [12]. Therefore multi-band superconductivity entails nodes at the same places for both gaps, unless that part of the Fermi surface is missing. On the other hand, the non-unitary superconducting state has nodes in the lower branch and a fully gapped upper branch. This difference may help to distinguish these two possibilities.

To summarise, we have found general expressions for the residual density of states and electrical and thermal conductivities due to impurity scattering, and we have applied the results to the non-unitary B phase of $\text{PrOs}_4\text{Sb}_{12}$. The nodal positions of the non-unitary state $D_2(E)$ are unique among all the superconducting states for crystals with tetrahedral symmetry [12, 66], in that they are not found on a symmetry axis. Inequivalent diagonal components of the conductivity tensor would

be an unmistakable signature of such a state.

3.9 Appendix: Derivation of Green's functions for a nonunitary superconducting state

The Green's functions for a nonunitary spin-triplet superconducting state will be derived here. The many-body Hamiltonian for a system of interacting electrons at the Fermi surface in the presence of a weak attractive potential is

$$H = \sum_{\mathbf{k},s} \varepsilon(\mathbf{k}) c_{\mathbf{k},s}^\dagger c_{\mathbf{k},s} + \frac{1}{2} \sum_{\mathbf{k},\mathbf{k}',s_1,s_2,s_3,s_4} V_{s_1 s_2 s_3 s_4}(\mathbf{k}, \mathbf{k}') c_{-\mathbf{k},s_1}^\dagger c_{\mathbf{k},s_2}^\dagger c_{\mathbf{k}',s_3} c_{-\mathbf{k}',s_4} \quad (3.91)$$

let

$$t_1 = c_{-\mathbf{k},s_1}^\dagger c_{\mathbf{k},s_2}^\dagger - \langle c_{-\mathbf{k},s_1}^\dagger c_{\mathbf{k},s_2}^\dagger \rangle \quad (3.92)$$

$$t_2 = c_{\mathbf{k}',s_3} c_{-\mathbf{k}',s_4} - \langle c_{\mathbf{k}',s_3} c_{-\mathbf{k}',s_4} \rangle \quad (3.93)$$

then

$$\begin{aligned} c_{-\mathbf{k},s_1}^\dagger c_{\mathbf{k},s_2}^\dagger c_{\mathbf{k}',s_3} c_{-\mathbf{k}',s_4} &= [t_1 + \langle c_{-\mathbf{k},s_1}^\dagger c_{\mathbf{k},s_2}^\dagger \rangle] [t_2 + \langle c_{\mathbf{k}',s_3} c_{-\mathbf{k}',s_4} \rangle] \\ &= t_1 \langle c_{\mathbf{k}',s_3} c_{-\mathbf{k}',s_4} \rangle + t_2 \langle c_{-\mathbf{k},s_1}^\dagger c_{\mathbf{k},s_2}^\dagger \rangle \\ &\quad + \langle c_{-\mathbf{k},s_1}^\dagger c_{\mathbf{k},s_2}^\dagger \rangle \langle c_{\mathbf{k}',s_3} c_{-\mathbf{k}',s_4} \rangle + t_1 t_2 \\ &= c_{-\mathbf{k},s_1}^\dagger c_{\mathbf{k},s_2}^\dagger \langle c_{\mathbf{k}',s_3} c_{-\mathbf{k}',s_4} \rangle + c_{\mathbf{k}',s_3} c_{-\mathbf{k}',s_4} \langle c_{-\mathbf{k},s_1}^\dagger c_{\mathbf{k},s_2}^\dagger \rangle \\ &\quad - \langle c_{-\mathbf{k},s_1}^\dagger c_{\mathbf{k},s_2}^\dagger \rangle \langle c_{\mathbf{k}',s_3} c_{-\mathbf{k}',s_4} \rangle + t_1 t_2 \end{aligned} \quad (3.94)$$

substituting this into the Hamiltonian we get

$$\begin{aligned} H &= \sum_{\mathbf{k},s} \varepsilon(\mathbf{k}) c_{\mathbf{k},s}^\dagger c_{\mathbf{k},s} + \frac{1}{2} \sum_{\mathbf{k},\mathbf{k}',s_1,s_2,s_3,s_4} V_{s_1 s_2 s_3 s_4}(\mathbf{k}, \mathbf{k}') \langle c_{\mathbf{k}',s_3} c_{-\mathbf{k}',s_4} \rangle c_{-\mathbf{k},s_1}^\dagger c_{\mathbf{k},s_2}^\dagger \\ &\quad + \frac{1}{2} \sum_{\mathbf{k},\mathbf{k}',s_1,s_2,s_3,s_4} V_{s_1 s_2 s_3 s_4}(\mathbf{k}, \mathbf{k}') \langle c_{-\mathbf{k},s_1}^\dagger c_{\mathbf{k},s_2}^\dagger \rangle c_{\mathbf{k}',s_3} c_{-\mathbf{k}',s_4} \end{aligned} \quad (3.95)$$

recalling that the mean fields or the primary gap equations are given by,

$$\Delta_{ss'}(\mathbf{k}) = - \sum_{\mathbf{k}', s_3, s_4} V_{s's_3s_4}(\mathbf{k}, \mathbf{k}') \langle c_{\mathbf{k}', s_3} c_{-\mathbf{k}', s_4} \rangle \quad (3.96)$$

$$\Delta_{ss'}^*(-\mathbf{k}) = \sum_{\mathbf{k}' s_1 s_2} V_{s_1 s_2 s' s}(\mathbf{k}', \mathbf{k}) \langle c_{-\mathbf{k}', s_1}^\dagger c_{\mathbf{k}', s_2}^\dagger \rangle \quad (3.97)$$

then, the mean field Hamiltonian is

$$\begin{aligned} H &= \sum_{\mathbf{k}, s} \varepsilon(\mathbf{k}) c_{\mathbf{k}, s}^\dagger c_{\mathbf{k}, s} - \frac{1}{2} \sum_{\mathbf{k}, s_1, s_2} \Delta_{s_1 s_2}(\mathbf{k}) c_{-\mathbf{k}, s_1}^\dagger c_{\mathbf{k}, s_2}^\dagger + \frac{1}{2} \sum_{\mathbf{k}, s_3, s_4} \Delta_{s_3 s_4}^*(-\mathbf{k}) c_{\mathbf{k}, s_3} c_{-\mathbf{k}, s_4} \\ &= \sum_{\mathbf{k}, s} \varepsilon(\mathbf{k}) c_{\mathbf{k}, s}^\dagger c_{\mathbf{k}, s} + \frac{1}{2} \sum_{\mathbf{k}, s_1, s_2} [\Delta_{s_1 s_2}(\mathbf{k}) c_{\mathbf{k}, s_1}^\dagger c_{-\mathbf{k}, s_2}^\dagger - \Delta_{s_1 s_2}^*(-\mathbf{k}) c_{-\mathbf{k}, s_1} c_{\mathbf{k}, s_2}] \quad (3.98) \end{aligned}$$

Now, in general, the Green's functions for a superconducting state is defined by

$$G_{ss'}(\mathbf{k}, \mathbf{k}'; \tau) = - \langle T_\tau c_{\mathbf{k}, s}(\tau) c_{\mathbf{k}', s'}^\dagger(0) \rangle \quad (3.99)$$

and it is called normal Green's function, and

$$F_{ss'}(\mathbf{k}, \mathbf{k}'; \tau) = \langle T_\tau c_{\mathbf{k}, s}(\tau) c_{\mathbf{k}', s'}(0) \rangle \quad (3.100)$$

$$F_{ss'}^\dagger(\mathbf{k}, \mathbf{k}'; \tau) = \langle T_\tau c_{\mathbf{k}', s'}^\dagger(\tau) c_{\mathbf{k}, s}^\dagger(0) \rangle \quad (3.101)$$

which is called anomalous Green's functions. let $\mathbf{k} = \mathbf{k}'$ in G , and $\mathbf{k} = -\mathbf{k}'$ in F and F^\dagger , then the equations of motion for the Green's function can be written as

$$\frac{\partial G_{ss'}(\mathbf{k}, \tau)}{\partial \tau} = - \frac{\partial}{\partial \tau} \left[\Theta(\tau) \langle c_{\mathbf{k}, s}(\tau) c_{\mathbf{k}', s'}^\dagger(0) \rangle - \Theta(-\tau) \langle c_{\mathbf{k}, s'}^\dagger(0) c_{\mathbf{k}, s}(\tau) \rangle \right] \quad (3.102)$$

$$= -\delta(\tau) \langle \{ c_{\mathbf{k}, s}(\tau), c_{\mathbf{k}', s'}^\dagger(0) \} \rangle - \langle T_\tau [H, c_{\mathbf{k}, s}](\tau) c_{\mathbf{k}', s'}^\dagger(0) \rangle \quad (3.103)$$

$$\frac{\partial F_{ss'}(\mathbf{k}, \tau)}{\partial \tau} = - \frac{\partial}{\partial \tau} \left[\Theta(\tau) \langle c_{\mathbf{k}, s}(\tau) c_{-\mathbf{k}, s'}(0) \rangle - \Theta(-\tau) \langle c_{-\mathbf{k}, s'}(0) c_{\mathbf{k}, s}(\tau) \rangle \right] \quad (3.104)$$

$$= \delta(\tau) \langle \{ c_{\mathbf{k}, s}(\tau), c_{-\mathbf{k}, s'}(0) \} \rangle + \langle T_\tau [H, c_{\mathbf{k}, s}](\tau) c_{-\mathbf{k}, s'}(0) \rangle \quad (3.105)$$

$$\frac{\partial F_{ss'}^\dagger(\mathbf{k}, \tau)}{\partial \tau} = \delta(\tau) \langle \{ c_{-\mathbf{k}, s'}^\dagger(\tau), c_{\mathbf{k}, s}^\dagger(0) \} \rangle + \langle T_\tau [H, c_{-\mathbf{k}, s'}^\dagger](\tau) c_{\mathbf{k}, s}^\dagger(0) \rangle \quad (3.106)$$

using the following equations

$$\tilde{\Delta}(\mathbf{k}) = -\tilde{\Delta}^T(-\mathbf{k}) \quad (3.107)$$

$$[H, c_{\mathbf{k},s}] = -\varepsilon(\mathbf{k})c_{\mathbf{k},s} - \sum_{s''} \Delta_{ss''}(\mathbf{k})c_{-\mathbf{k},s''} \quad (3.108)$$

$$[H, c_{-\mathbf{k},s'}^\dagger] = \varepsilon(\mathbf{k})c_{-\mathbf{k},s'}^\dagger - \sum_{s''} \Delta_{s''s'}^*(\mathbf{k})c_{\mathbf{k},s''} \quad (3.109)$$

then Eqs. (3.103), (3.105) and (3.106) become,

$$[i\omega_n - \varepsilon(\mathbf{k})]G_{ss'}(\mathbf{k}, i\omega_n) + \sum_{s''} \Delta_{ss''}(\mathbf{k})F_{s's''}^\dagger(\mathbf{k}, i\omega_n) = \delta_{ss'} \quad (3.110)$$

$$[i\omega_n - \varepsilon(\mathbf{k})]F_{ss'}(\mathbf{k}, i\omega_n) - \sum_{s''} \Delta_{ss''}(\mathbf{k})G_{s's''}(-\mathbf{k}, -i\omega_n) = 0 \quad (3.111)$$

$$[i\omega_n + \varepsilon(\mathbf{k})]F_{s's'}^\dagger(\mathbf{k}, i\omega_n) + \sum_{s''} \Delta_{s's''}^\dagger(\mathbf{k})G_{s''s}(\mathbf{k}, i\omega_n) = 0 \quad (3.112)$$

where a Fourier transform in time has been performed. Substituting 3.112 into 3.110 we get

$$[(i\omega_n)^2 - \varepsilon^2(\mathbf{k})]G_{ss'}(\mathbf{k}, i\omega_n) - \sum_{s'',\sigma} \Delta_{ss''}(\mathbf{k})\Delta_{s''\sigma}^\dagger(\mathbf{k})G_{\sigma s'}(\mathbf{k}, i\omega_n) = [i\omega_n + \varepsilon(\mathbf{k})]\delta_{ss'} \quad (3.113)$$

expanding the spin space, we get four different equations which can be solved simultaneously,

$$[(i\omega_n)^2 - \varepsilon^2]G_{\uparrow\downarrow} - \Delta_{\uparrow\uparrow}[\Delta_{\uparrow\uparrow}^\dagger G_{\uparrow\downarrow} + \Delta_{\uparrow\downarrow}^\dagger G_{\downarrow\downarrow}] - \Delta_{\uparrow\downarrow}[\Delta_{\downarrow\uparrow}^\dagger G_{\uparrow\downarrow} + \Delta_{\downarrow\downarrow}^\dagger G_{\downarrow\downarrow}] = 0$$

$$[(i\omega_n)^2 - \varepsilon^2 - |\mathbf{d}|^2 - i(\mathbf{d} \times \mathbf{d}^*)_z]G_{\uparrow\downarrow} - [(\mathbf{d} \times \mathbf{d}^*)_y + i(\mathbf{d} \times \mathbf{d}^*)_x]G_{\downarrow\downarrow} = 0 \quad (3.114)$$

$$[(i\omega_n)^2 - \varepsilon^2]G_{\downarrow\uparrow} - \Delta_{\downarrow\uparrow}[\Delta_{\uparrow\uparrow}^\dagger G_{\uparrow\uparrow} + \Delta_{\uparrow\downarrow}^\dagger G_{\downarrow\uparrow}] - \Delta_{\downarrow\downarrow}[\Delta_{\downarrow\uparrow}^\dagger G_{\uparrow\uparrow} + \Delta_{\downarrow\downarrow}^\dagger G_{\downarrow\uparrow}] = 0$$

$$[(i\omega_n)^2 - \varepsilon^2 - |\mathbf{d}|^2 + i(\mathbf{d} \times \mathbf{d}^*)_z]G_{\uparrow\uparrow} - [-(\mathbf{d} \times \mathbf{d}^*)_y + i(\mathbf{d} \times \mathbf{d}^*)_x]G_{\uparrow\uparrow} = 0 \quad (3.115)$$

$$[(i\omega_n)^2 - \varepsilon^2]G_{\uparrow\uparrow} - \Delta_{\uparrow\uparrow}[\Delta_{\uparrow\uparrow}^\dagger G_{\uparrow\uparrow} + \Delta_{\uparrow\downarrow}^\dagger G_{\uparrow\downarrow}] - \Delta_{\uparrow\downarrow}[\Delta_{\uparrow\uparrow}^\dagger G_{\uparrow\uparrow} + \Delta_{\uparrow\downarrow}^\dagger G_{\uparrow\downarrow}] = [i\omega_n + \varepsilon]$$

$$[(i\omega_n)^2 - \varepsilon^2 - |\mathbf{d}|^2 - i(\mathbf{d} \times \mathbf{d}^*)_z]G_{\uparrow\uparrow} - [(\mathbf{d} \times \mathbf{d}^*)_y + i(\mathbf{d} \times \mathbf{d}^*)_x]G_{\uparrow\uparrow} = [i\omega_n + \varepsilon] \quad (3.116)$$

$$[(i\omega_n)^2 - \varepsilon^2]G_{\downarrow\downarrow} - \Delta_{\downarrow\downarrow}[\Delta_{\downarrow\downarrow}^\dagger G_{\downarrow\downarrow} + \Delta_{\downarrow\uparrow}^\dagger G_{\downarrow\uparrow}] - \Delta_{\downarrow\uparrow}[\Delta_{\downarrow\downarrow}^\dagger G_{\downarrow\downarrow} + \Delta_{\downarrow\uparrow}^\dagger G_{\downarrow\uparrow}] = [i\omega_n + \varepsilon]$$

$$[(i\omega_n)^2 - \varepsilon^2 - |\mathbf{d}|^2 + i(\mathbf{d} \times \mathbf{d}^*)_z]G_{\downarrow\downarrow} - [-(\mathbf{d} \times \mathbf{d}^*)_y + i(\mathbf{d} \times \mathbf{d}^*)_x]G_{\downarrow\downarrow} = [i\omega_n + \varepsilon] \quad (3.117)$$

solving the above equations we get

$$G_{\uparrow\uparrow} = \frac{(i\omega_n)^2 - \varepsilon^2 - |\mathbf{d}|^2 + i(\mathbf{d} \times \mathbf{d}^*)_z}{[(i\omega_n)^2 - E_-^2][(i\omega_n)^2 - E_+^2]} [i\omega_n + \varepsilon] \quad (3.118)$$

$$G_{\uparrow\downarrow} = \frac{-(\mathbf{d} \times \mathbf{d}^*)_y + i(\mathbf{d} \times \mathbf{d}^*)_x}{[(i\omega_n)^2 - E_-^2][(i\omega_n)^2 - E_+^2]} [i\omega_n + \varepsilon] \quad (3.119)$$

$$G_{\downarrow\uparrow} = \frac{(\mathbf{d} \times \mathbf{d}^*)_y + i(\mathbf{d} \times \mathbf{d}^*)_x}{[(i\omega_n)^2 - E_-^2][(i\omega_n)^2 - E_+^2]} [i\omega_n + \varepsilon] \quad (3.120)$$

$$G_{\downarrow\downarrow} = \frac{(i\omega_n)^2 - \varepsilon^2 - |\mathbf{d}|^2 - i(\mathbf{d} \times \mathbf{d}^*)_z}{[(i\omega_n)^2 - E_-^2][(i\omega_n)^2 - E_+^2]} [i\omega_n + \varepsilon] \quad (3.121)$$

or

$$\tilde{G}(\mathbf{k}, i\omega_n) = \frac{[(i\omega_n)^2 - \varepsilon_{\mathbf{k}}^2 - |\mathbf{d}_{\mathbf{k}}|^2] \tilde{\sigma}_0 + \mathbf{q}_{\mathbf{k}} \cdot \tilde{\boldsymbol{\sigma}}}{[(i\omega_n)^2 - E_{\mathbf{k}-}^2][(i\omega_n)^2 - E_{\mathbf{k}+}^2]} [i\omega_n + \varepsilon_{\mathbf{k}}] \quad (3.122)$$

similarly, we can solve for the components of $\tilde{F}(\mathbf{k}, i\omega_n)$, starting from 3.111, the expansion in spin space yields,

$$[i\omega_n - \varepsilon(\mathbf{k})]F_{\uparrow\uparrow}(\mathbf{k}, i\omega_n) - \Delta_{\uparrow\uparrow}(\mathbf{k})G_{\uparrow\uparrow}(-\mathbf{k}, -i\omega_n) - \Delta_{\uparrow\downarrow}(\mathbf{k})G_{\uparrow\downarrow}(-\mathbf{k}, -i\omega_n) = 0 \quad (3.123)$$

and this gives

$$F_{\uparrow\uparrow} = -\frac{[(i\omega_n)^2 - \varepsilon_{\mathbf{k}}^2 - |\mathbf{d}_{\mathbf{k}}|^2][i(\mathbf{d}_{\mathbf{k}} \cdot \tilde{\boldsymbol{\sigma}})\tilde{\sigma}_y]_{\uparrow\uparrow} + [i(\mathbf{q}_{\mathbf{k}} \times \mathbf{d}_{\mathbf{k}}) \cdot \tilde{\boldsymbol{\sigma}}\tilde{\sigma}_y]_{\uparrow\uparrow}}{[(i\omega_n)^2 - E_{\mathbf{k}-}^2][(i\omega_n)^2 - E_{\mathbf{k}+}^2]} \quad (3.124)$$

the other components can be derived by the same way, the results are

$$[i\omega_n - \varepsilon(\mathbf{k})]F_{\downarrow\downarrow}(\mathbf{k}, i\omega_n) - \Delta_{\downarrow\downarrow}(\mathbf{k})G_{\downarrow\downarrow}(-\mathbf{k}, -i\omega_n) - \Delta_{\uparrow\uparrow}(\mathbf{k})G_{\uparrow\uparrow}(-\mathbf{k}, -i\omega_n) = 0 \quad (3.125)$$

$$F_{\downarrow\downarrow} = -\frac{[(i\omega_n)^2 - \varepsilon_{\mathbf{k}}^2 - |\mathbf{d}_{\mathbf{k}}|^2][i(\mathbf{d}_{\mathbf{k}} \cdot \tilde{\boldsymbol{\sigma}})\tilde{\sigma}_y]_{\downarrow\downarrow} + [i(\mathbf{q}_{\mathbf{k}} \times \mathbf{d}_{\mathbf{k}}) \cdot \tilde{\boldsymbol{\sigma}}\tilde{\sigma}_y]_{\downarrow\downarrow}}{[(i\omega_n)^2 - E_{\mathbf{k}-}^2][(i\omega_n)^2 - E_{\mathbf{k}+}^2]} \quad (3.126)$$

$$[i\omega_n - \varepsilon(\mathbf{k})]F_{\uparrow\downarrow}(\mathbf{k}, i\omega_n) - \Delta_{\uparrow\uparrow}(\mathbf{k})G_{\downarrow\uparrow}(-\mathbf{k}, -i\omega_n) - \Delta_{\uparrow\downarrow}(\mathbf{k})G_{\downarrow\downarrow}(-\mathbf{k}, -i\omega_n) = 0 \quad (3.127)$$

$$F_{\uparrow\downarrow} = -\frac{[(i\omega_n)^2 - \varepsilon_{\mathbf{k}}^2 - |\mathbf{d}_{\mathbf{k}}|^2][i(\mathbf{d}_{\mathbf{k}} \cdot \tilde{\boldsymbol{\sigma}})\tilde{\sigma}_y]_{\uparrow\downarrow} + [i(\mathbf{q}_{\mathbf{k}} \times \mathbf{d}_{\mathbf{k}}) \cdot \tilde{\boldsymbol{\sigma}}\tilde{\sigma}_y]_{\uparrow\downarrow}}{[(i\omega_n)^2 - E_{\mathbf{k}-}^2][(i\omega_n)^2 - E_{\mathbf{k}+}^2]} \quad (3.128)$$

$$[i\omega_n - \varepsilon(\mathbf{k})]F_{\downarrow\uparrow}(\mathbf{k}, i\omega_n) - \Delta_{\downarrow\uparrow}(\mathbf{k})G_{\uparrow\uparrow}(-\mathbf{k}, -i\omega_n) - \Delta_{\downarrow\downarrow}(\mathbf{k})G_{\uparrow\downarrow}(-\mathbf{k}, -i\omega_n) = 0 \quad (3.129)$$

$$F_{\downarrow\uparrow} = -\frac{[(i\omega_n)^2 - \varepsilon_{\mathbf{k}}^2 - |\mathbf{d}_{\mathbf{k}}|^2][i(\mathbf{d}_{\mathbf{k}} \cdot \tilde{\boldsymbol{\sigma}})\tilde{\sigma}_y]_{\downarrow\uparrow} + [i(\mathbf{q}_{\mathbf{k}} \times \mathbf{d}_{\mathbf{k}}) \cdot \tilde{\boldsymbol{\sigma}}\tilde{\sigma}_y]_{\downarrow\uparrow}}{[(i\omega_n)^2 - E_{\mathbf{k}-}^2][(i\omega_n)^2 - E_{\mathbf{k}+}^2]} = F_{\uparrow\downarrow} \quad (3.130)$$

and finally, this can be taken to the following matrix form in spin space,

$$\tilde{F}(\mathbf{k}, i\omega_n) = -\frac{[(i\omega_n)^2 - \varepsilon_{\mathbf{k}}^2 - |\mathbf{d}_{\mathbf{k}}|^2][i(\mathbf{d}_{\mathbf{k}} \cdot \tilde{\boldsymbol{\sigma}})\tilde{\sigma}_y] + i(\mathbf{q}_{\mathbf{k}} \times \mathbf{d}_{\mathbf{k}}) \cdot \tilde{\boldsymbol{\sigma}}\tilde{\sigma}_y}{[(i\omega_n)^2 - E_{\mathbf{k}-}^2][(i\omega_n)^2 - E_{\mathbf{k}+}^2]} \quad (3.131)$$

Chapter 4

Field angle-dependent thermal conductivity in nodal superconductors

4.1 Abstract

We apply a semi-classical method to the problem of field angle-dependent oscillations of the density of states and thermal conductivity for nodal superconductors and apply our results to the superconductor $\text{PrOs}_4\text{Sb}_{12}$. The oscillatory contributions to the thermal conductivity for all possible point node configurations for a superconductor with T_h symmetry are calculated. It is found that experimental results are best accounted for by nodes in the off-axis directions $[\pm \sin \phi_0, 0, \pm \cos \phi_0]$, which are associated with the time-reversal breaking, triplet paired phase $D_2(E)$.

4.2 Introduction

The low temperature thermodynamic properties of unconventional superconductors are governed by nodal quasiparticles. In the presence of a small magnetic field $H_{c1} \leq H \ll H_{c2}$, it was shown by Volovik [5] that the dominant contribution to the density of states (DOS) for superconductors with line nodes comes from delocalized quasiparticles, in contrast to *s*-wave superconductors in which the DOS is dominated by quasiparticles localised inside vortex cores [5, 80]. Volovik argued that the delocalised states experience a semi-classical adjustment to their energy due to the magnetic field which is expressed as a Doppler shift $\omega \rightarrow \omega - \mathbf{v}_s(\mathbf{r}) \cdot \mathbf{k}$, where $\mathbf{v}_s(\mathbf{r}) = \frac{1}{2mr} \hat{\beta}$ is the superfluid velocity and β is the winding angle around a single vortex. As a result, contributions proportional to the magnetic field have been predicted to appear in thermodynamic and transport properties of line node superconductors [5, 59, 81–87].

Magnetic contributions that appear because of the Doppler shift will strongly depend on the orientation of the magnetic field with respect to the nodes. Consequently, oscillations in the DOS and related quantities have been predicted for superconductors with line nodes in a rotating magnetic field [82, 88–99], and have been observed experimentally in in-plane thermal conductivity in $\text{YBa}_2\text{Cu}_3\text{O}_7$ [100, 101]. Similar results have been found for other unconventional superconductors [30, 102–107], including $\text{YNi}_2\text{B}_2\text{C}$ [107] and $\text{PrOs}_4\text{Sb}_{12}$ [30], which are reported to have point nodes instead of line nodes. Oscillations in the field-angle dependent specific heat have also been observed in several unconventional superconductors [63, 108–114].

Volovik's proof that, in superconductors with line nodes, delocalised quasiparticles have a greater contribution to the low-energy DOS than vortex localised quasiparticles does not extend to superconductors with point nodes. However, we are

interested in finding the oscillatory component of the DOS in a rotating magnetic field, for which the semi-classical method (the Doppler shift of the quasiparticles energy), applied to delocalised quasi-particles, may be valid. For delocalised states, oscillations are obtained just by Doppler-shifting the quasiparticle energies. For localised states, the amplitude of oscillations may be found by calculating separately the DOS for the case when the field points in the direction of the nodes and the case when the field is perpendicular to the nodes and subtracting the results for the two cases. The former case corresponds to the s -wave result, which gives the contribution from localised quasi-particles as $N_{s\text{-loc.}} \sim N_F \xi^2 / R^2 \sim N_F H / H_{c2}$, where ξ is the coherence length and R is the inter-vortex spacing. This sets a lower bound on the DOS contributions from localised quasi-particles in superconductors with line nodes or point nodes. The upper bound of the DOS contribution from localised quasiparticles in superconductors with nodes is found when the field is parallel to the nodes. Volovik found that for superconductors with line nodes, the localised quasiparticles contribute $N_{\text{line-loc.}} \sim N_F \sqrt{H/H_{c2}} / \log \sqrt{H_{c2}/H}$ which he found to be less than the delocalised contribution $N_{\text{line-deloc.}} \sim N_F \sqrt{H/H_{c2}}$. The oscillatory contribution for the delocalised states is contained within $N_{\text{line-deloc.}}$ while the oscillation amplitude for the localised states is $\sim N_{\text{line-loc.}} - N_{s\text{-loc.}} \approx N_{\text{line-loc.}}$. Thus the DOS oscillations in a line node superconductor are dominated by the delocalised contribution, and the semi-classical treatment is valid. For a point node superconductor, one finds that the delocalised contribution is $N_{\text{point-deloc.}} \sim N_{\text{point-loc.}} \sim N_{s\text{-loc.}}$. Again, the oscillatory contribution for delocalised states is contained within $N_{\text{point-deloc.}}$ while the oscillation amplitude for the localised states is found by comparing $N_{\text{point-loc.}}$ to $N_{s\text{-loc.}}$. This suggests that while both localised and delocalised states contribute to the DOS in point node superconductors, the oscillatory component is dominated by the delocalised states. We will assume that this is the case, but a more thorough in-

investigation of the role of vortex localised quasiparticles in point node superconductors is warranted.

Field dependent thermal conductivity measurements are usually performed in one of two experimental configurations. In layered compounds in which the *c*-axis conductivity is low, such as in $\text{YBa}_2\text{Cu}_3\text{O}_7$, the in-plane conductivity is usually measured with the *B*-field rotating in the same plane. Then one in-plane component of the current will be parallel to vortices produced by the *B*-field while the other in-plane component of the current is perpendicular to the vortices. This introduces complications when calculating the different components of the current averaged over the vortex lattice, since a different kind of averaging procedure should be used depending on whether the heat current is parallel or perpendicular to the vortices [84]. As a consequence, for a field rotating in the *xy* plane, in-plane components of the conductivity will oscillate with a period of twice the field angle even when there are no nodes at all, and this oscillation will dominate any nodal contribution [106, 115]. Thus, whenever possible, the preferred set-up is to measure the heat currents perpendicular to the rotating *B*-field [106].

In the superconductor $\text{PrOs}_4\text{Sb}_{12}$, the pairing symmetry is widely thought to be unconventional [25, 29–37], with spin triplet pairing [36] and broken time reversal symmetry [31]. Power law behavior has been observed in many thermodynamic and transport measurements at low temperature [29, 30, 32, 35, 37], which suggests the existence of nodes in the gap function; however a nodeless gap function has been observed in some experiments [38–40, 49]. Oscillations of the thermal conductivity in a rotating magnetic field are another indication that there are nodes in the gap function [30]. In previous works [12, 66], we have attempted to determine the symmetry of the superconducting state in $\text{PrOs}_4\text{Sb}_{12}$ using available experimental results. Among the various possible choices, we selected the spin triplet paired states belonging to the

three dimensional irreducible representation T_u of the point group T_h with symmetry $D_2(C_2) \times \mathcal{K}$ and order parameter components $(0, 0, 1)$ and $D_2(E)$ with components $(i|\eta_2|, 0, |\eta_1|)$. We label these phases 'A' and 'B' respectively. The A phase is unitary, and has two cusp point nodes in the directions $\pm[0, 0, 1]$, while the B phase is nonunitary and has four cusp point nodes in the directions $[\pm \sin \phi_0, 0, \pm \cos \phi_0]$, where ϕ_0 is an angle determined from phenomenological parameters [66]. We will consider these and all other symmetry-allowed phases with point nodes.

In this chapter we calculate the DOS and residual transport under an applied magnetic field. We consider both the clean and dirty limits, in which the impurity scattering rate is much smaller or greater than the Doppler shift, respectively. For the purpose of comparison, we begin by stating in Section 4.3 results for the residual DOS and thermal conductivity for the d -wave (line node) superconductors. Section 4.4 is devoted to point nodes applied to $\text{PrOs}_4\text{Sb}_{12}$. In Section 4.5 we compare our results to experiment. Concluding remarks are made in Section 4.6.

4.3 Density of States and thermal conductivity for superconductors with line nodes

In this section we consider a d -wave superconductor (such as $\text{YBa}_2\text{Cu}_3\text{O}_7$) with line nodes along the directions $k_x = \pm k_y$ and a magnetic field applied in the $k_x k_y$ -plane at an angle ϵ with respect to the x axis. In the vicinity of a node, the gap function takes the form $\Delta(\mathbf{k}) \approx v_g k_2$, where k_2 points perpendicular to the node in the xy -plane and $v_g = \left. \frac{\partial \Delta(\mathbf{k})}{\partial k} \right|_{\text{node}}$ is the gap velocity. The quasiparticle energy is $E(\mathbf{k}) = \sqrt{\epsilon^2(\mathbf{k}) + \Delta^2(\mathbf{k})} \approx \sqrt{v_F^2 k_1^2 + v_g^2 k_2^2}$, where k_1 points in the direction of the node. Thus

in the vicinity of a node, the Green's function takes the form [67]

$$G(\mathbf{k}, i\tilde{\omega}_n, \mathbf{r}) = \frac{i\tilde{\omega}_n + \alpha_j(\mathbf{r}) + v_F k_1}{(i\tilde{\omega}_n + \alpha_j(\mathbf{r}))^2 + v_F^2 k_1^2 + v_g^2 k_2^2} \quad (4.1)$$

where $i\tilde{\omega}_n = i\omega_n + i\Gamma_0$, $\alpha_j(\mathbf{r}) = \mathbf{v}_s(\mathbf{r}) \cdot \mathbf{k}_{Fj}$ is the Doppler shift at the j th node and $\Gamma_0 = -\Im \Sigma_{ret}(\omega = 0)$ is the scattering rate at zero energy. The self-energy Σ is derived from the T-matrix formalism for impurity scattering and is the solution to the self-consistent equation [71, 82]

$$\Sigma(i\omega_n) = \frac{\Gamma G_0(i\tilde{\omega}_n, \mathbf{r})}{c^2 - G_0^2(i\tilde{\omega}_n, \mathbf{r})} \quad (4.2)$$

where $\Gamma = \frac{n_i}{\pi N_F}$ (n_i is the impurity concentration), c is related to the phase shift δ_0 , $c = \cot \delta_0$ and

$$G_0(i\tilde{\omega}_n, \mathbf{r}) = \frac{1}{\pi N_F} \sum_{\mathbf{k}} G(\mathbf{k}, i\tilde{\omega}_n, \mathbf{r}). \quad (4.3)$$

N_F is the density of states at the Fermi surface.

In the limits of unitary scattering ($c = 0$) and zero energy ($\omega \rightarrow 0$), Eq. 4.2 becomes

$$\Sigma_{ret}(0) = -\frac{\Gamma}{G_0(0, \mathbf{r})} \quad (4.4)$$

Solving for $G_0(0, \mathbf{r})$, we get

$$G_0(0, \mathbf{r}) = \frac{1}{\pi N_F} \frac{1}{(2\pi)^2 v_F v_g} \sum_{j=1}^4 \int_0^{2\pi} d\theta \int_0^{p_0} dp p \times \frac{-\alpha_j(\mathbf{r}) + i\Gamma_0 + p \cos \theta}{(-\alpha_j(\mathbf{r}) + i\Gamma_0)^2 - p^2}, \quad (4.5)$$

which leads to the following result

$$G_0(0, \mathbf{r}) = -\frac{1}{2\pi^2 N_F v_F v_g} \sum_{j=1}^4 [-\alpha_j(\mathbf{r}) + i\Gamma_0] \ln \left(\frac{p_0}{i\alpha_j(\mathbf{r}) + \Gamma_0} \right). \quad (4.6)$$

Separating the real and imaginary parts we get

$$G_0(0, \mathbf{r}) = -\frac{1}{2\pi^2 N_F v_F v_g} \sum_{j=1}^4 [-\alpha_j(\mathbf{r}) + i\Gamma_0] \left[\ln \left(\sqrt{\frac{p_0^2}{\alpha_j^2(\mathbf{r}) + \Gamma_0^2}} \right) - i \tan^{-1} \left(\frac{\alpha_j(\mathbf{r})}{\Gamma_0} \right) \right]. \quad (4.7)$$

This yields a self-consistent equation for the scattering rate [84, 116]

$$\Gamma_0^2 = \pi^2 N_F v_F v_g \Gamma \left[\ln \left(\frac{p_0^2}{\sqrt{(\alpha_1^2(\mathbf{r}) + \Gamma_0^2)(\alpha_2^2(\mathbf{r}) + \Gamma_0^2)}} \right) + \frac{\alpha_1(\mathbf{r})}{\Gamma_0} \tan^{-1} \left(\frac{\alpha_1(\mathbf{r})}{\Gamma_0} \right) + \frac{\alpha_2(\mathbf{r})}{\Gamma_0} \tan^{-1} \left(\frac{\alpha_2(\mathbf{r})}{\Gamma_0} \right) \right]^{-1}. \quad (4.8)$$

where p_0 is a cutoff and $\alpha_{1,2}(\mathbf{r})$ are the Doppler shifts at two opposite nodes and can be written as

$$\alpha_1(\mathbf{r}) = \frac{k_F}{2m\tau} \sin \beta \sin(\pi/4 - \epsilon) \quad (4.9)$$

$$\alpha_2(\mathbf{r}) = \frac{k_F}{2m\tau} \sin \beta \cos(\pi/4 - \epsilon) \quad (4.10)$$

and τ is the distance from the centre of the vortex core and ϵ is the angle of the magnetic field relative to the x -axis.

4.3.1 Density of States

The DOS is given by

$$-N(\omega, \mathbf{r}) = \frac{1}{\pi} \int \frac{d^3k}{(2\pi)^3} \Im G_{\text{ret}}(\mathbf{k}, \omega, \mathbf{r}) \quad (4.11)$$

where the integral over \mathbf{k} is evaluated as the sum of four separate volume integrations centred about each node [19]. Then the DOS at the Fermi energy is

$$N(0, \mathbf{r}) = \frac{\Gamma_0}{\pi^2 v_F v_g} \left[\ln \left(\frac{p_0^2}{\sqrt{(\alpha_1^2(\mathbf{r}) + \Gamma_0^2)(\alpha_2^2(\mathbf{r}) + \Gamma_0^2)}} \right) + \frac{\alpha_1(\mathbf{r})}{\Gamma_0} \tan^{-1} \left(\frac{\alpha_1(\mathbf{r})}{\Gamma_0} \right) + \frac{\alpha_2(\mathbf{r})}{\Gamma_0} \tan^{-1} \left(\frac{\alpha_2(\mathbf{r})}{\Gamma_0} \right) \right] \quad (4.12)$$

In the clean limit $(\Gamma_0/|\alpha_j(\mathbf{r})|) \rightarrow 0$ and

$$N(0, \mathbf{r}) \approx \frac{|\alpha_1(\mathbf{r})| + |\alpha_2(\mathbf{r})|}{2\pi v_F v_g} \quad (4.13)$$

$$= \frac{k_F}{2m\tau} |\sin \beta| \frac{\max[|\sin \epsilon|, |\cos \epsilon|]}{2\sqrt{2}\pi v_F v_g} \quad (4.14)$$

This result necessarily has the same form as the finite frequency DOS $N(\omega) \sim |\omega|$ of superconductor with line nodes. Averaging over the vortex unit cell we obtain the result as in Ref. [88]

$$\langle N(0, \mathbf{r}) \rangle_H = \frac{1}{\pi R^2} \int_{\xi_0}^R dr r \int_0^{2\pi} d\beta N(0, \mathbf{r}) \quad (4.15)$$

$$\sim N_F \frac{\xi_0}{R} \max[|\sin \epsilon|, |\cos \epsilon|] \quad (4.16)$$

where $\frac{\xi_0}{R} \sim \sqrt{\frac{H}{H_{c2}}}$. Evidently there are four-fold oscillations in the DOS as a function of the field angle ϵ .

In the dirty limit $|\alpha_j(\mathbf{r})|/\Gamma_0 \ll 1$ we find

$$N(0, \mathbf{r}) = \frac{\Gamma_0}{\pi^2 v_F v_g} \left[2 \ln \left(\frac{p_0}{\Gamma_0} \right) + \frac{\alpha_1^2(\mathbf{r}) + \alpha_2^2(\mathbf{r})}{\Gamma_0^2} \right] \quad (4.17)$$

The first term is just the impurity induced DOS $N(0)$ [19], so

$$\delta N(0, \mathbf{r}) = N(0, \mathbf{r}) - N(0) = \frac{1}{4\pi^2 r^2} \frac{v_F}{v_g \Gamma_0} \sin^2 \beta \quad (4.18)$$

and the average DOS is [83]

$$\langle \delta N(0, \mathbf{r}) \rangle_H \sim N_F \frac{\Delta_0}{\Gamma_0} \frac{H}{H_{c2}} \ln \left(\frac{H_{c2}}{H} \right). \quad (4.19)$$

where $\Delta_0 = \frac{v_F}{\xi_0} \sim N_F v_F v_g$. In this case, impurities remove the field directional dependence of the DOS.

4.3.2 Thermal conductivity

The thermal conductivity tensor is defined by the Kubo formula [19]. In the limit $T \rightarrow 0$ it is expressed in terms of the imaginary part of the Green's function as [19, 117]

$$\frac{\tilde{\kappa}(0, \mathbf{r})}{T} = \frac{k_B^2}{3} \sum_{\mathbf{k}} \mathbf{v}_F \mathbf{v}_F \text{Tr}[\Im \tilde{G}_{ret}(0, \mathbf{r}) \Im \tilde{G}_{ret}(0, \mathbf{r})], \quad (4.20)$$

where k_B is the Boltzmann constant and \mathbf{v}_F is the Fermi velocity in the direction of \mathbf{k} . By again dividing the integration over \mathbf{k} into regions centred over each node, this eventually leads to

$$\begin{aligned} \frac{\tilde{\kappa}(0, \mathbf{r})}{T} = & \frac{k_B^2 \sum_{j=1}^4 \mathbf{v}_F \mathbf{v}_F}{3 (2\pi)^2 v_F v_g} \int_0^{2\pi} d\theta \int_0^{p_0} dp p \\ & \times \frac{2\Gamma_0^2}{[(\alpha_j(\mathbf{r}) + p)^2 + \Gamma_0^2]^2} \end{aligned} \quad (4.21)$$

where the integration variable is $p = \sqrt{v_F^2 k_1^2 + v_g^2 k_2^2}$. Performing the integration yields

$$\frac{\tilde{\kappa}(0, \mathbf{r})}{T} = \frac{k_B^2}{3} \frac{\sum_{j=1}^4 \mathbf{v}_F \mathbf{v}_F}{\pi v_F v_g} \left(1 + \frac{\alpha_j(\mathbf{r})}{\Gamma_0} \left[\tan^{-1} \left(\frac{\alpha_j(\mathbf{r})}{\Gamma_0} \right) - \frac{\pi}{2} \right] \right) \quad (4.22)$$

where now \mathbf{v}_F is evaluated at each node. Summing over nodes yields

$$\begin{aligned} \frac{\tilde{\kappa}(0, \mathbf{r})}{T} = & \frac{k_B^2}{3} \frac{1}{\pi v_F v_g} \left[(\mathbf{v}_F \mathbf{v}_F)_1 + (\mathbf{v}_F \mathbf{v}_F)_2 + (\mathbf{v}_F \mathbf{v}_F)_1 \frac{\alpha_1(\mathbf{r})}{\Gamma_0} \tan^{-1} \left(\frac{\alpha_1(\mathbf{r})}{\Gamma_0} \right) \right. \\ & \left. + (\mathbf{v}_F \mathbf{v}_F)_2 \frac{\alpha_2(\mathbf{r})}{\Gamma_0} \tan^{-1} \left(\frac{\alpha_2(\mathbf{r})}{\Gamma_0} \right) \right] \end{aligned} \quad (4.23)$$

noting that

$$(\mathbf{v}_F \mathbf{v}_F)_1 + (\mathbf{v}_F \mathbf{v}_F)_2 = v_F^2 \begin{pmatrix} 1 & 0 \\ 0 & 1 \end{pmatrix}. \quad (4.24)$$

then

$$\begin{aligned} \frac{\delta \tilde{\kappa}(0, \mathbf{r})}{T} = & \frac{\tilde{\kappa}(0, \mathbf{r}) - \tilde{\kappa}(0, 0)}{T} = \\ & \frac{k_B^2 v_F}{6\pi v_g} \begin{pmatrix} \frac{\alpha_1}{\Gamma_0} \tan^{-1} \left(\frac{\alpha_1}{\Gamma_0} \right) + \frac{\alpha_2}{\Gamma_0} \tan^{-1} \left(\frac{\alpha_2}{\Gamma_0} \right) & \frac{\alpha_1}{\Gamma_0} \tan^{-1} \left(\frac{\alpha_1}{\Gamma_0} \right) - \frac{\alpha_2}{\Gamma_0} \tan^{-1} \left(\frac{\alpha_2}{\Gamma_0} \right) \\ \frac{\alpha_1}{\Gamma_0} \tan^{-1} \left(\frac{\alpha_1}{\Gamma_0} \right) - \frac{\alpha_2}{\Gamma_0} \tan^{-1} \left(\frac{\alpha_2}{\Gamma_0} \right) & \frac{\alpha_1}{\Gamma_0} \tan^{-1} \left(\frac{\alpha_1}{\Gamma_0} \right) + \frac{\alpha_2}{\Gamma_0} \tan^{-1} \left(\frac{\alpha_2}{\Gamma_0} \right) \end{pmatrix} \end{aligned} \quad (4.25)$$

In the clean limit $\alpha_j(\mathbf{r}) \gg \Gamma_0$, the thermal conductivity is

$$\frac{\delta\tilde{\kappa}(0, \mathbf{r})}{T} = \frac{k_B^2 v_F}{12 v_g} \begin{pmatrix} \frac{|\alpha_1|+|\alpha_2|}{\Gamma_0} & \frac{|\alpha_1|-|\alpha_2|}{\Gamma_0} \\ \frac{|\alpha_1|-|\alpha_2|}{\Gamma_0} & \frac{|\alpha_1|+|\alpha_2|}{\Gamma_0} \end{pmatrix} \quad (4.26)$$

The average over the vortex unit cell is

$$\begin{aligned} \left\langle \frac{\delta\tilde{\kappa}(0, \mathbf{r})}{T} \right\rangle_H &\sim k_B^2 \frac{v_F \Delta_0}{v_g \Gamma_0} \sqrt{\frac{H}{H_{c2}}} \\ &\times \begin{pmatrix} \frac{1}{\sqrt{2}} \max[|\sin \epsilon|, |\cos \epsilon|] & |\sin(\pi/4 - \epsilon)| - |\cos(\pi/4 - \epsilon)| \\ |\sin(\pi/4 - \epsilon)| - |\cos(\pi/4 - \epsilon)| & \frac{1}{\sqrt{2}} \max[|\sin \epsilon|, |\cos \epsilon|] \end{pmatrix}. \end{aligned} \quad (4.27)$$

In the dirty limit $\alpha_j(\mathbf{r}) \ll \Gamma_0$ we find

$$\frac{\delta\tilde{\kappa}(0, \mathbf{r})}{T} = \frac{k_B^2 v_F}{6\pi v_g} \begin{pmatrix} \frac{\alpha_1^2 + \alpha_2^2}{\Gamma_0^2} & \frac{\alpha_1^2 - \alpha_2^2}{\Gamma_0^2} \\ \frac{\alpha_1^2 - \alpha_2^2}{\Gamma_0^2} & \frac{\alpha_1^2 + \alpha_2^2}{\Gamma_0^2} \end{pmatrix} \quad (4.28)$$

The average over the vortex unit cell is

$$\left\langle \frac{\delta\tilde{\kappa}(0, \mathbf{r})}{T} \right\rangle_H \sim k_B^2 \frac{v_F \Delta_0^2}{v_g \Gamma_0^2} \frac{H}{H_{c2}} \ln\left(\frac{H_{c2}}{H}\right) \begin{pmatrix} 1 & -\sin 2\epsilon \\ -\sin 2\epsilon & 1 \end{pmatrix}. \quad (4.29)$$

Thus as in the DOS, impurities remove oscillations due to nodes in the diagonal components of the thermal conductivity.

4.4 Density of states and thermal conductivity for a point node superconductor

We will first assume that there are an arbitrary number of *linear* (*i.e.* vanishing linearly with momentum) point nodes in the gap function, and that the gap velocities

v_g are equal and isotropic around each node. We begin by finding a self-consistent equation for the scattering rate Γ_0 analogous to Eq. 4.8. For point nodes, Eq. 4.3 is

$$G_0(0, \mathbf{r}) = \frac{1}{\pi N_F} \frac{\sum_{\text{nodes}}}{(2\pi)^3 v_F v_g^2} \int_0^{2\pi} d\phi \int_0^\pi d\theta \sin \theta \int_0^{p_0} dp p^2 \times \frac{-\alpha_j(\mathbf{r}) + i\Gamma_0 + p \cos \theta}{(-\alpha_j(\mathbf{r}) + i\Gamma_0)^2 - p^2} \quad (4.30)$$

where the integration variable is $p = \sqrt{v_F^2 k_1^2 + v_g^2 (k_2^2 + k_3^2)}$ and k_1 is parallel to the node while $k_{2,3}$ are perpendicular to the node. In Eq. 4.30, we have again divided the volume of integration into parts each centred around a node. The integrations yield

$$G_0(0, \mathbf{r}) = \frac{-i}{\pi N_F} \frac{\sum_{\text{nodes}}}{2\pi^2 v_F v_g^2} (\Gamma_0 + i\alpha_j(\mathbf{r}))^2 \left[\frac{p_0}{\Gamma_0 + i\alpha_j(\mathbf{r})} - \tan^{-1} \left(\frac{p_0}{\Gamma_0 + i\alpha_j(\mathbf{r})} \right) \right] \quad (4.31)$$

separating the real and imaginary parts of the arctan

$$\begin{aligned} \tan^{-1} \left(\frac{p_0}{\Gamma_0 + i\alpha_j(\mathbf{r})} \right) &= \tan^{-1} \left(\frac{p_0 \Gamma_0 - i p_0 \alpha_j(\mathbf{r})}{\Gamma_0^2 + \alpha_j^2(\mathbf{r})} \right) \\ &= \tan^{-1} (x_0 + iy_0) = \tan^{-1} z \end{aligned} \quad (4.32)$$

using

$$\tan^{-1} z = \frac{i}{2} [\ln(1 - iz) - \ln(1 + iz)] \quad (4.33)$$

$$= \frac{i}{2} [\ln(1 + y_0 - ix_0) - \ln(1 - y_0 + ix_0)] \quad (4.34)$$

we get

$$\begin{aligned} \tan^{-1} z &= \frac{1}{2} \left[\tan^{-1} \left(\frac{x_0}{1 + y_0} \right) + \left(\frac{x_0}{1 - y_0} \right) \right. \\ &\quad \left. + \frac{i}{2} \ln \left(\frac{x_0^2 + [1 + y_0]^2}{x_0^2 + [1 - y_0]^2} \right) \right] \end{aligned} \quad (4.35)$$

substituting for $x_0 = \frac{p_0 \Gamma_0}{\Gamma_0^2 + \alpha_j^2(\mathbf{r})}$, $y_0 = -\frac{p_0 \alpha_j(\mathbf{r})}{\Gamma_0^2 + \alpha_j^2(\mathbf{r})}$ the logarithm will vanish, and we will end up with

$$\tan^{-1} \left(\frac{p_0}{\Gamma_0 + i \alpha_j(\mathbf{r})} \right) = \frac{1}{2} \left[\tan^{-1} \left(\frac{p_0 \Gamma_0}{\Gamma_0^2 + p_0 \alpha_j(\mathbf{r})} \right) + \tan^{-1} \left(\frac{p_0 \Gamma_0}{\Gamma_0^2 - p_0 \alpha_j(\mathbf{r})} \right) \right] \quad (4.36)$$

$$= \frac{1}{2} \left[\tan^{-1} \left(\frac{[p_0/\Gamma_0]}{1 + [p_0/\Gamma_0][\alpha_j(\mathbf{r})/\Gamma_0]} \right) + \tan^{-1} \left(\frac{[p_0/\Gamma_0]}{1 - [p_0/\Gamma_0][\alpha_j(\mathbf{r})/\Gamma_0]} \right) \right] \quad (4.37)$$

using the following identity

$$\tan^{-1} \left(\frac{u+v}{1-uv} \right) = \tan^{-1} u + \tan^{-1} v \quad (4.38)$$

the cutoff $p_0 \gg \alpha_j(\mathbf{r})$, so we can add $\alpha_j(\mathbf{r})/\Gamma_0$ to the numerator of the arctan's argument as

$$\begin{aligned} \tan^{-1} \left(\frac{[p_0/\Gamma_0]}{1 - [p_0/\Gamma_0][\alpha_j(\mathbf{r})/\Gamma_0]} \right) &= \tan^{-1} \left(\frac{[p_0/\Gamma_0] + [\alpha_j(\mathbf{r})/\Gamma_0]}{1 - [p_0/\Gamma_0][\alpha_j(\mathbf{r})/\Gamma_0]} \right) \\ &= \tan^{-1} \left(\frac{p_0}{\Gamma_0} \right) + \tan^{-1} \left(\frac{\alpha_j(\mathbf{r})}{\Gamma_0} \right) \end{aligned} \quad (4.39)$$

also

$$\begin{aligned} \tan^{-1} \left(\frac{[p_0/\Gamma_0]}{1 + [p_0/\Gamma_0][\alpha_j(\mathbf{r})/\Gamma_0]} \right) &= \tan^{-1} \left(\frac{[p_0/\Gamma_0] - [\alpha_j(\mathbf{r})/\Gamma_0]}{1 - [p_0/\Gamma_0][\alpha_j(\mathbf{r})/\Gamma_0]} \right) \\ &= \tan^{-1} \left(\frac{p_0}{\Gamma_0} \right) - \tan^{-1} \left(\frac{\alpha_j(\mathbf{r})}{\Gamma_0} \right) \end{aligned} \quad (4.40)$$

so

$$\tan^{-1} \left(\frac{p_0}{\Gamma_0 + i \alpha_j(\mathbf{r})} \right) = \frac{1}{2} [2 \tan^{-1} \left(\frac{p_0}{\Gamma_0} \right)] = \tan^{-1} \left(\frac{p_0}{\Gamma_0} \right) \quad (4.41)$$

Note that this result is valid for both the clean and dirty limits. Substituting this into the Green's function in 4.31 we get

$$G_0(0, \mathbf{r}) = \frac{-i}{N_F 2\pi^3 v_F v_g^2} \sum_{\text{nodes}} \left[(\Gamma_0 + i\alpha_j(\mathbf{r})) p_0 - \frac{\pi}{2} (\Gamma_0 + i\alpha_j(\mathbf{r}))^2 \right] \quad (4.42)$$

Now we assume that there are four nodes which occur in pairs on opposite sides of the Fermi surface. Partners in each pair produce equal and opposite Doppler shifts. Summing over nodes we find

$$\begin{aligned} G_0(0, \mathbf{r}) &= \frac{-i}{N_F 2\pi^3 v_F v_g^2} \left[4p_0 \Gamma_0 + \pi(\alpha_1^2(\mathbf{r}) + \alpha_2^2(\mathbf{r}) - 2\Gamma_0^2) \right] \\ &\equiv \frac{\Gamma}{i\Gamma_0} \end{aligned} \quad (4.43)$$

This result can easily be generalised to include more pairs of nodes. Equating the imaginary parts of (4.43) yields the self-consistent equation for the scattering rate Γ_0 ,

$$\Gamma_0 = \frac{\pi^3}{2} \frac{N_F v_F v_g^2 \Gamma}{p_0 \Gamma_0 - \frac{\pi}{2} \Gamma_0^2 + \frac{\pi}{4} (\alpha_1^2(\mathbf{r}) + \alpha_2^2(\mathbf{r}))} \quad (4.44)$$

This equation describes how the scattering rate due to impurities is modified in the presence of Doppler shifted quasiparticles.

As in Section 4.3, we will assume that the magnetic field is parallel to the xy -plane with an angle ϵ from the x axis,

$$\mathbf{H} = H(\cos \epsilon \hat{x} + \sin \epsilon \hat{y}) \quad (4.45)$$

The supercurrent is

$$\mathbf{v}_s(\mathbf{r}) = \frac{1}{2mr} (-\sin \epsilon \cos \beta \hat{x} + \cos \epsilon \cos \beta \hat{y} + \sin \beta \hat{z}). \quad (4.46)$$

For now we will assume that all pairs of nodes are in the $k_x k_y$ -plane at the positions

$$\mathbf{k}_{F1} = \pm k_F (\cos \phi_0 \hat{x} - \sin \phi_0 \hat{y}) \quad (4.47)$$

$$\mathbf{k}_{F2} = \pm k_F (\cos \phi_0 \hat{x} + \sin \phi_0 \hat{y}) \quad (4.48)$$

The angle ϕ_0 is zero in the A phase of $\text{PrOs}_4\text{Sb}_{12}$ (and the gap function is doubly degenerate) and $\phi_0 \neq 0$ in the B phase. This corresponds to the choice of the domain $(1, 0, 0)$ of the A phase and the domain $(|\eta_1|, i|\eta_2|, 0)$ of the B phase. In each phase, two other domains are possible and these will be discussed in the next section.

The Doppler shifts are

$$\begin{aligned}\alpha_1(\mathbf{r}) &= \pm \mathbf{v}_s \cdot \mathbf{k}_{F1} \\ &= \pm \frac{k_F}{2m\tau} \cos \beta [-\sin \phi_0 \cos \epsilon - \cos \phi_0 \sin \epsilon]\end{aligned}\quad (4.49)$$

$$\begin{aligned}\alpha_2(\mathbf{r}) &= \pm \mathbf{v}_s \cdot \mathbf{k}_{F2} \\ &= \pm \frac{k_F}{2m\tau} \cos \beta [\sin \phi_0 \cos \epsilon - \cos \phi_0 \sin \epsilon]\end{aligned}\quad (4.50)$$

The following averages over the vortex unit cell will be useful:

$$\begin{aligned}\langle \alpha_1^2(\mathbf{r}) + \alpha_2^2(\mathbf{r}) \rangle_H &\sim \frac{v_F^2}{R^2} \ln \left(\frac{R}{\xi_0} \right) [\cos^2 \phi_0 \sin^2 \epsilon + \sin^2 \phi_0 \cos^2 \epsilon] \\ \langle \alpha_1^2(\mathbf{r}) - \alpha_2^2(\mathbf{r}) \rangle_H &\sim \frac{v_F^2}{R^2} \ln \left(\frac{R}{\xi_0} \right) \sin 2\phi_0 \sin 2\epsilon\end{aligned}\quad (4.51)$$

4.4.1 Density of states

The DOS is given by Eq. 4.11. Using (4.3) and (4.43) we find

$$\begin{aligned}N(0, \mathbf{r}) &= \frac{2\Gamma_0^2}{\pi^3 v_F v_g^2} \left[\frac{p_0}{\Gamma_0} - \tan^{-1} \left(\frac{p_0}{\Gamma_0} \right) \right. \\ &\quad \left. + \frac{\alpha_1^2(\mathbf{r}) + \alpha_2^2(\mathbf{r})}{2\Gamma_0^2} \tan^{-1} \left(\frac{p_0}{\Gamma_0} \right) \right]\end{aligned}\quad (4.52)$$

which in zero magnetic field we retain our previous result for the impurity induced density of states [117], then the magnetic contribution is

$$\delta N(0, \mathbf{r}) \approx \frac{\alpha_1^2(\mathbf{r}) + \alpha_2^2(\mathbf{r})}{2\pi^2 v_F v_g^2}\quad (4.53)$$

which takes the same form as the low frequency DOS, $N(\omega) \sim \omega^2$ for superconductors with point nodes. Taking the average over the vortex unit cell, we get

$$\frac{\langle \delta N(0, \mathbf{r}) \rangle_H}{N_F} \sim \frac{H}{H_{c2}} \ln \left(\frac{H_{c2}}{H} \right) [\cos^2 \phi_0 \sin^2 \epsilon + \sin^2 \phi_0 \cos^2 \epsilon] \quad (4.54)$$

Thus we find that the DOS oscillates with rotating magnetic field as $\cos 2\epsilon$ and it is universal *i.e.* it is independent of the scattering rate.

4.4.2 Thermal Conductivity

Beginning with Eq. 4.20 we divide the volume of integration into parts centred around each node,

$$\begin{aligned} \frac{\tilde{\kappa}(0, \mathbf{r})}{T} &= \frac{k_B^2}{3} \frac{\sum_{j=1}^4 \mathbf{v}_F \mathbf{v}_F}{(2\pi)^3 v_F v_g^2} \int_0^{2\pi} d\phi \int_0^\pi d\theta \sin \theta \\ &\int_0^{p_0} dp p^2 \frac{\Gamma_0^2}{[(\alpha_j(\mathbf{r}) + p)^2 + \Gamma_0^2]^2} \end{aligned} \quad (4.55)$$

where the integration variable is again $p = \sqrt{v_F^2 k_1^2 + v_g^2 (k_2^2 + k_3^2)}$. The integrations yield

$$\begin{aligned} \frac{\tilde{\kappa}(0, \mathbf{r})}{T} &= \frac{k_B^2}{12\pi^2} \frac{\sum_{j=1}^4 \mathbf{v}_F \mathbf{v}_F}{v_F v_g^2} \left[\frac{\Gamma_0^2 + \alpha_j^2(\mathbf{r})}{\Gamma_0} \right] \\ &\times \left[\frac{\pi}{2} - \tan^{-1} \frac{\alpha_j(\mathbf{r})}{\Gamma_0} - \frac{\alpha_j(\mathbf{r}) \Gamma_0}{\alpha_j^2(\mathbf{r}) + \Gamma_0^2} \right] \end{aligned} \quad (4.56)$$

where again our previously derived expression for the residual conductivity in zero magnetic field [117] is recovered. The matrix $\mathbf{v}_F \mathbf{v}_F$ for one node is equal to the contribution for the node on the opposite side of the Fermi surface, but $\alpha_j(\mathbf{r})$ changes sign at opposite nodes, therefore terms which are odd in $\alpha_j(\mathbf{r})$ will vanish. The sum over nodes yields (keeping only the magnetic part)

$$\frac{\delta \tilde{\kappa}(0, \mathbf{r})}{T} = \frac{k_B^2}{12\pi v_F v_g^2 \Gamma_0} [\alpha_1^2(\mathbf{r}) (\mathbf{v}_F \mathbf{v}_F)_1 + \alpha_2^2(\mathbf{r}) (\mathbf{v}_F \mathbf{v}_F)_2] \quad (4.57)$$

$$= \frac{k_B^2 v_F}{12\pi v_g^2 \Gamma_0} \begin{pmatrix} (\alpha_1^2 + \alpha_2^2) \cos^2 \phi_0 & \frac{1}{2}(\alpha_2^2 - \alpha_1^2) \sin 2\phi_0 & 0 \\ \frac{1}{2}(\alpha_2^2 - \alpha_1^2) \sin 2\phi_0 & (\alpha_1^2 + \alpha_2^2) \sin^2 \phi_0 & 0 \\ 0 & 0 & 0 \end{pmatrix}$$

Finally we perform the average over the vortex unit cell,

$$\begin{aligned} \left\langle \frac{\delta \tilde{\kappa}(0, \mathbf{r})}{T} \right\rangle_H &\sim k_B^2 \frac{v_F \Delta_0^2}{v_g^2 \Gamma_0} \frac{H}{H_{c2}} \ln \left(\frac{H_{c2}}{H} \right) \\ &\times \begin{pmatrix} \cos^2 \phi_0 [\cos^2 \phi_0 \sin^2 \epsilon + \sin^2 \phi_0 \cos^2 \epsilon] & -\frac{1}{4} \sin 2\phi_0 \sin 2\epsilon & 0 \\ -\frac{1}{4} \sin 2\phi_0 \sin 2\epsilon & \sin^2 \phi_0 [\cos^2 \phi_0 \sin^2 \epsilon + \sin^2 \phi_0 \cos^2 \epsilon] & 0 \\ 0 & 0 & 0 \end{pmatrix} \end{aligned} \quad (4.58)$$

where $\Delta_0^2 = \frac{v_F^2}{\xi_0^2} \sim N_F v_F v_g^2$. The A phase of $\text{PrOs}_4\text{Sb}_{12}$ corresponds to $\phi_0 = 0$, and the only component of the thermal conductivity which is non-vanishing is $\kappa_{xx} \sim \sin^2 \epsilon$.

Other domains

The phase $D_2(E)$ has two other nodal configurations [61], which may be found by applying the operation C_3 on the components $(|\eta_1|, i|\eta_2|, 0)$ or directly on the gap function. The second domain we consider is when the nodes are in the $k_x k_z$ -plane. Then the B phase has order parameter components $(i|\eta_2|, 0, |\eta_1|)$ and the A phase has components $(0, 0, 1)$. Then the positions of the nodes are

$$\mathbf{k}_{F1} = \pm k_F (-\sin \phi_0 \hat{x} + \cos \phi_0 \hat{z}) \quad (4.59)$$

$$\mathbf{k}_{F2} = \pm k_F (\sin \phi_0 \hat{x} + \cos \phi_0 \hat{z}) \quad (4.60)$$

and the Doppler shifts are

$$\alpha_1(\mathbf{r}) = \pm \frac{k_F}{2m\tau} [\sin \phi_0 \sin \epsilon \cos \beta + \cos \phi_0 \sin \beta] \quad (4.61)$$

$$\alpha_2(\mathbf{r}) = \pm \frac{k_F}{2m\tau} [-\sin \phi_0 \sin \epsilon \cos \beta + \cos \phi_0 \sin \beta] \quad (4.62)$$

In the average over the vortex unit cell $\langle \alpha_1^2(\mathbf{r}) - \alpha_2^2(\mathbf{r}) \rangle$ vanishes, and

$$\langle \alpha_1^2(\mathbf{r}) + \alpha_2^2(\mathbf{r}) \rangle_H \sim \frac{v_F^2}{R^2} \ln \left(\frac{R}{\xi_0} \right) [\sin^2 \phi_0 \sin^2 \epsilon + \cos^2 \phi_0]. \quad (4.63)$$

The B phase thermal conductivity is

$$\begin{aligned} \left\langle \frac{\delta \tilde{\kappa}(0, \mathbf{r})}{T} \right\rangle_H &\sim k_B^2 \frac{v_F \Delta_0^2}{v_g^2 \Gamma_0} \frac{H}{H_{c2}} \ln \left(\frac{H_{c2}}{H} \right) [\sin^2 \phi_0 \sin^2 \epsilon + \cos^2 \phi_0] \\ &\times \begin{pmatrix} \sin^2 \phi_0 & 0 & 0 \\ 0 & 0 & 0 \\ 0 & 0 & \cos^2 \phi_0 \end{pmatrix} \end{aligned} \quad (4.64)$$

and the A phase thermal conductivity is $\kappa_{zz} \sim \text{constant}$.

In the third domain the nodes are found in the $k_y k_z$ -plane

$$\mathbf{k}_{F1} = \pm k_F (\cos \phi_0 \hat{y} - \sin \phi_0 \hat{z}) \quad (4.65)$$

$$\mathbf{k}_{F2} = \pm k_F (\cos \phi_0 \hat{y} + \sin \phi_0 \hat{z}) \quad (4.66)$$

averaging over the vortex unit cell, again $\alpha_1^2(\mathbf{r}) - \alpha_2^2(\mathbf{r})$ will vanish, and we get for $\alpha_1^2(\mathbf{r}) + \alpha_2^2(\mathbf{r})$

$$\langle \alpha_1^2(\mathbf{r}) + \alpha_2^2(\mathbf{r}) \rangle_H \sim \frac{v_F^2}{R^2} \ln \left(\frac{H_{c2}}{H} \right) [\sin^2 \phi_0 + \cos^2 \phi_0 \cos^2 \epsilon] \quad (4.67)$$

The B phase thermal conductivity is

$$\begin{aligned} \left\langle \frac{\delta \tilde{\kappa}(0, \mathbf{r})}{T} \right\rangle_H &\sim k_B^2 \frac{v_F \Delta_0^2}{v_g^2 \Gamma_0} \frac{H}{H_{c2}} \ln \left(\frac{H_{c2}}{H} \right) [\sin^2 \phi_0 + \cos^2 \phi_0 \cos^2 \epsilon] \\ &\times \begin{pmatrix} 0 & 0 & 0 \\ 0 & \cos^2 \phi_0 & 0 \\ 0 & 0 & \sin^2 \phi_0 \end{pmatrix} \end{aligned} \quad (4.68)$$

and for the A phase it is $\kappa_{yy} \sim \cos 2\epsilon$.

Domain averaging

In real situations, one may expect that either a single domain will form either because of sample shape or applied strains or fields, or that all three domains will be present. If all three domains are present then detailed knowledge of the domain structure is required to calculate the conductivity. Lacking that, we consider two limiting cases: *i*) serial domains and *ii*) parallel domains. When the domains are in series the conductivity is $\tilde{\kappa} = (\tilde{\kappa}_1^{-1} + \tilde{\kappa}_2^{-1} + \tilde{\kappa}_3^{-1})^{-1}$ which vanishes in all components. When the domains are in parallel the three conductivities are simply added:

$$\tilde{\kappa} \sim \begin{pmatrix} \sin^2 \epsilon (1 - \frac{3}{4} \sin^2 2\phi_0) + \frac{1}{2} \sin^2 2\phi_0 & -\frac{1}{4} \sin^2 \phi_0 \sin 2\epsilon & 0 \\ -\frac{1}{4} \sin^2 2\phi_0 \sin 2\epsilon & \cos^2 \epsilon (1 - \frac{3}{4} \sin^2 2\phi_0) + \frac{1}{2} \sin^2 2\phi_0 & 0 \\ 0 & 0 & 1 - \sin^2 \phi_0 \cos^2 \phi_0 \end{pmatrix} \quad (4.69)$$

which reduces to the A phase result ($\phi_0 = 0$)

$$\tilde{\kappa} \sim \begin{pmatrix} \sin^2 \epsilon & 0 & 0 \\ 0 & \cos^2 \epsilon & 0 \\ 0 & 0 & 1 \end{pmatrix} \quad (4.70)$$

Other nodal configurations

According to Table I of Ref. [12,118] there are other nodal configurations corresponding to other superconducting phases which should be considered. For **eight point nodes in the [111] directions**, the thermal conductivity is

$$\tilde{\kappa} \sim \begin{pmatrix} 2 & -\sin 2\epsilon & 0 \\ -\sin 2\epsilon & 2 & 0 \\ 0 & 0 & 2 \end{pmatrix} \quad (4.71)$$

The thermal conductivity for **two point nodes in the [111] directions** is

$$\tilde{\kappa} \sim \left(1 - \frac{\sin 2\epsilon}{2}\right) \begin{pmatrix} 1 & 1 & 1 \\ 1 & 1 & 1 \\ 1 & 1 & 1 \end{pmatrix}. \quad (4.72)$$

Such a phase has four domains; the domain averaged conductivity is given by (4.71).

The thermal conductivity for **six point nodes in the [100] directions** is given by (4.70).

The thermal conductivity for **six point nodes in the [100] directions and two point nodes in the [111] directions** is given by the sum of (4.70) and (4.72). Such a phase has four domains; the domain averaged conductivity is given by the sum of (4.70) and (4.71).

Eqs. 4.58, 4.64 and 4.68-4.72 are summarised in Table 4.1.

4.5 Discussion

So far there has only been one report of thermal conductivity in a rotating magnetic field, namely the results by Izawa *et al.* [30], who measured κ_{zz} and found four-fold oscillations near H_{c2} and two-fold oscillations at a lower field. We do not obtain four-fold oscillations for any of the point node configurations we considered and so we conclude that the formalism we have used is inapplicable in large magnetic fields. One possible source of error is that we have omitted contributions from quasi-particle states localised in vortex cores, and that these states may dominate the oscillatory contribution to the density of states as the field increases and the vortices become closer together. Another possibility is higher order in α (the Doppler shift) contributions become important as the field is increased. We do not obtain four-fold oscillations simply because we did not retain contributions to the density of states and

Nodes	κ_{xx}	κ_{yy}	κ_{xy}	$\kappa_{xz,yz}$	κ_{zz}
4 nodes $[\cos \phi_0, \pm \sin \phi_0, 0]$	c	c	s	0	0
4 nodes $[\pm \sin \phi_0, 0, \cos \phi_0]$	c	0	0	0	c
4 nodes $[0, \cos \phi_0, \pm \sin \phi_0]$	0	c	0	0	c
domain average $[\cos \phi_0, \pm \sin \phi_0, 0]$	c	c	s	0	1
2 nodes $[1, 0, 0]$	c	0	0	0	0
2 nodes $[0, 1, 0]$	0	c	0	0	0
2 nodes $[0, 0, 1]$	0	0	0	0	1
domain average/ 6 nodes $[1, 0, 0]$	c	c	0	0	1
2 nodes $[1, 1, 1]$	s	s	s	s	s
domain average/ 8 nodes $[1, 1, 1]$	1	1	s	0	1
6 nodes $[1, 0, 0]$ and 2 nodes $[1, 1, 1]$	c+s	c+s	s	s	s
domain average	c	c	s	0	1

Table 4.1: Oscillatory contributions to the thermal conductivity with a field rotating in the xy plane for various nodal configurations. ‘s’ stands for $\sin 2\epsilon$, ‘c’ stands for $\cos 2\epsilon$, ‘1’ stands for no oscillations and ‘0’ means that the component vanishes. ϵ is the angle of the field with respect to the x axis.

thermal conductivity for powers of α higher than two. In any case, unlike $d_{x^2-y^2}$ line node superconductors, the four-fold oscillations reported in Ref. [30] are not related in any simple way to the nodal structure of $\text{PrOs}_4\text{Sb}_{12}$. In particular, the four-fold oscillations should *not* be interpreted as arising from four point nodes on the $k_x k_y$ equator.

Our results may be applicable to the lower field measurements in which two-fold oscillations are found. Fig. 2b) of Ref. [30] clearly shows two-fold oscillations of the form $\kappa_{zz} \sim \cos 2\epsilon$ and *not* $\sin 2\epsilon$. This indicates that the most likely superconducting

phase of $\text{PrOs}_4\text{Sb}_{12}$ is $D_2(E)$ which belongs to the three dimensional order parameter T_u and that a single domain with order parameter components $(0, |\eta_1|, i|\eta_2|)$ or $(i|\eta_2|, 0, |\eta_1|)$ was measured in Ref. [30]. We note that this phase agrees with various properties observed in other experiments, including triplet pairing [36], broken time reversal symmetry [31] and broken C_3 symmetry [33, 58].

In all of our calculations we performed the vortex average as a simple areal average over a plane perpendicular to a vortex, which is appropriate when the heat current is parallel to the magnetic field. For currents in other directions a different averaging procedure should be used, which results in a more complicated field dependence of the oscillation amplitudes than what we have shown here. The correct procedure is an average of κ over paths through the vortex lattice, which is in fact more involved than the series average $\langle \kappa^{-1} \rangle^{-1}$ described in Ref. [84]. Moreover, the vortex averaging procedure for a given in-plane component of the conductivity will vary with the field angle, producing oscillations $\sim \cos 2\epsilon$ which are unrelated to nodes and which will dominate over any nodal contributions [106, 115]. Thus observations of oscillations $\sim \cos 2\epsilon$ in κ_{xx} , κ_{yy} or in off-diagonal components of κ measured with an in-plane current should not be interpreted as evidence of nodes. These additional oscillations will mix into all components of the thermal conductivity via the vortex averaging procedure (which in general does involve averaging κ^{-1}) but we expect their contribution to κ_{zz} to be small compared to the oscillations originating from nodes.

4.6 Summary and conclusions

We have reviewed previous works concerning field-angle dependent DOS and thermal conductivity for line node superconductors using a semi-classical method, and applied the same method to point node superconductors. This method neglects vor-

tex localised quasi-particles and retains only the contribution from extended, nodal quasiparticles to the density of states. Clearly there are limitations to this approach; in particular it cannot be expected to produce an accurate estimate of the total low-energy density of states in point node superconductors. However it may be a reasonable way to estimate the field-angle dependent oscillatory component of the density of states and related quantities for fields $H_{c1} \leq H \ll H_{c2}$. We find that in point node superconductors there is no difference between the clean and dirty limits, unlike in line node superconductors in which the different limits produce significantly different expressions for the oscillatory part of the thermal conductivity. Considering all possible configurations of point nodes in a tetrahedral superconductor, we find that the superconducting phase $D_2(E)$, which we previously proposed based on other experimental evidence, best accounts for field-angle dependent oscillations in the thermal conductivity of $\text{PrOs}_4\text{Sb}_{12}$.

Acknowledgements

We thank Ilya Vekhter for helpful discussions. We gratefully acknowledge the hospitality of the University of Waterloo, where this work was completed.

Chapter 5

Concluding remarks

In this thesis, superconductivity in the heavy fermion superconductor $\text{PrOs}_4\text{Sb}_{12}$ has been studied. In this system, the point group is T_h (tetrahedral), which has one-dimensional, two-dimensional and three-dimensional irreducible representations in two channels: spin-singlet (even parity) and spin triplet (odd parity). Among all possible superconducting states in a tetrahedral system, we have found the superconducting state that best matches experiments on $\text{PrOs}_4\text{Sb}_{12}$. This state has a three component order parameter with spin-triplet pairing and is nonunitary. Two possible scenarios for the superconducting phase transitions have been identified. In one scenario, the superconducting phase with order parameter components $(|\eta_1|, i|\eta_2|, 0)$ (B phase) can be reached from the normal phase via an intermediate superconducting phase with order parameter components $(|\eta_1|, 0, 0)$ (A phase). The other scenario is when the A phase is absent from the phase diagram. Since the superconducting state $(|\eta_1|, i|\eta_2|, 0)$ is nonunitary, the energy gap is non-degenerate, and the lower gap has point nodes, but the upper gap is nodeless. The nodes in the lower gap are located in the directions $[\pm\alpha, \pm\beta, 0]$.

Consequently, a nonunitary superconducting state has been studied, and general

expressions for the impurity induced density of states and transport properties have been obtained. We have applied the results to the B phase of $\text{PrOs}_4\text{Sb}_{12}$. In the Born limit of weak scattering all quantities vanish, but in the unitary limit (strong scattering) we obtain nonuniversal (impurity scattering dependent) density of states and conductivities. The conductivity tensors have a diagonal off-axis components due to the off-axis positions of nodes at the Fermi surface. Differences between a nonunitary superconducting state and multiband superconductivity, to which multi-gap behavior has also been attributed by some experimentalists, have been reviewed and discussed.

We have also used semi-classical methods to study the effect of applying a magnetic field on this system. First we have reviewed the magnetic field dependent density of states and thermal conductivity for the case of superconductors with lines of nodes in the gap function. We have considered the two limiting cases: the clean and dirty limits. The delocalized quasiparticles, which are generated at the nodes, will be Doppler shifted by the supercurrent flow around vortices, and will dominate over the contribution of the quasiparticles localized inside the vortex cores in the density of states. As a result, in the clean limit, oscillations are expected to be present in all thermodynamic and transport measurements. These oscillations will depend on the direction of the magnetic field relative to the nodes, in which a maximum (minimum) will show up when the field is pointed in the antinodal (nodal) direction, respectively. The period of oscillations, in this case, reflects the symmetry of the order parameter, and determines the the number and location of nodes on the Fermi surface. On the other hand, in the dirty limit, the density of states becomes insensitive to the direction of the magnetic field and no oscillations will be present. However, for point-node superconductors, we have predicted universal expressions for the density of states and thermal conductivity which are valid for both limits. In contrast to line node

superconductors, the oscillations in this case are not washed out by impurities, nor are they related to the number nor the position of point nodes in the gap function. However, they do reflect the symmetry of the order parameter, which in the case of $\text{PrOs}_4\text{Sb}_{12}$ leads again to the superconducting state with $D_2(E)$ symmetry, and order parameter components $(|\eta_1|, i|\eta_2|, 0)$ which has four point nodes in the directions $[\pm\alpha, \pm\beta, 0]$.

In summary, we have studied the superconductivity in the heavy fermion system $\text{PrOs}_4\text{Sb}_{12}$. Using symmetry considerations, we have been able to determine the most probable superconducting state that best describes experiments on $\text{PrOs}_4\text{Sb}_{12}$. Calculations of thermodynamic and transport properties have been performed using this superconducting state and have been compared to experiment. We conclude that our proposed superconducting state with order parameter components $(|\eta_1|, i|\eta_2|, 0)$ and $D_2(E)$ symmetry best describes superconductivity in the superconductor $\text{PrOs}_4\text{Sb}_{12}$.

Bibliography

- [1] J. Bardeen, L. N. Cooper, and J. R. Schrieffer, *Phys. Rev.* **108**, 1175 (1957).
- [2] H. Fröhlich, *Phys. Rev.* **79**, 845 (1950).
- [3] G. Eliashberg, *Sov. Phys. JETP* **11**, 696 (1960).
- [4] J. G. Bednorz and K. A. Müller, *Z. Phys. B* **64**, 189 (1986).
- [5] G. E. Volovik, *JETP Lett.* **58**, 469 (1993).
- [6] T. Tsuneto, *Superconductivity and Superfluidity* (Cambridge University Press, 2nd edition, Cambridge, U. K.) (1998).
- [7] M. Sigrist, and K. Ueda, *Rev. Mod. Phys.*, **63**, 239 (1991).
- [8] A. P. Mackenzie and Y. Maeno, *Rev. Mod. Phys.* **75**, 657 (2003).
- [9] M. Tinkham, *Introduction to superconductivity* (McGraw-Hill Book Co., New York) (1996).
- [10] G. E. Volovik and L. P. Gor'kov, *Sov. Phys. JETP* **61**, 843 (1985); Yu. M. Gufan, *JETP* **80**, 485 (1995).
- [11] M. Tinkham, *Group theory and quantum mechanics*, (McGraw-Hill Book Co., New York) (1964).

- [12] I. A. Sergienko and S. H. Curnoe, *Phys. Rev. B*, **70**, 144522 (2004); see Ref. [15].
- [13] T. R. Abu Alrub and S. H. Curnoe, arXiv: 0804.2658
- [14] S. H. Curnoe, T. R. Abu Alrub, I. A. Sergienko and I. Vekhter, *J. Magn. Magn. Mater.* **310**, 605 (2007).
- [15] There is an error in Table I of Ref. [12]. The triplet-paired phase with symmetry $D_2(E)$ was reported to be nodeless. However, it does in fact have four point nodes (approximate and rigorous) at the positions $[\pm\alpha, \pm\beta, 0]$. This result can be proved rigorously as a strict consequence of symmetry (see Sec. 2.8). This error lead to our claim [14] that the nodes lift away from the Fermi surface to form deep dips in the gap function at the A-B transition.
- [16] L. C. Hebel and C. P. Slichter, *Phys. Rev.* **107**, 901 (1957).
- [17] R. E. Glover and M. Tinkham, *Phys. Rev.* **104**, 844 (1956).
- [18] V. Z. Kresin and S. A. Wolf, *Fundamentals of superconductivity*, (Plenum Press, New York) (1990).
- [19] A. C. Durst and P. A. Lee, *Phys. Rev. B* **62**, 1270 (2000).
- [20] A. A. Abrikosov, *Sov. Phys. JETP* **5**, 1174 (1957).
- [21] J. F. Annet, *Superconductivity, Superfluids and Condensates*, (Oxford University Press Inc., New York) (2004).
- [22] R. Kubo, *J. Phys. Soc. Japan* **12**, 570, (1957). R. Kubo, M. Yokota, and S. Nakajima, *J. Phys. Soc. Japan* **12**, 1203 (1957).
- [23] G. D. Mahan, *Many-Particle Physics* (Plenum Press, 3rd edition, New York) (2000).

- [24] M. B. Maple, P. -C. Ho, V. S. Zapf, N. A. Frederick, E. D. Bauer, W. M. Yuhasz, F. M. Woodward and J. W. Lynn, *J. Phys. Soc. Jpn.* **71**, 23 (2002).
- [25] M. B. Maple, E. D. Bauer, V. S. Zapf, E. J. Freeman, N. A. Frederick and R. P. Dickey, *Acta. Phys. Pol.* **32**, 3291 (2001).
- [26] D. J. Braun and W. Jeitschko, *J. Less-Common Met.* **72**, 147 (1980).
- [27] This figure was done by S. H. Curnoe.
- [28] H. Sugawara *et al.*, *Phys. Rev. B* **66**, 220504, (2002).
- [29] E. D. Bauer, N. A. Frederick, P.-C. Ho, V. S. Zapf, and M. B. Maple, *Phys. Rev. B* **65**, 100506(R) (2002).
- [30] K. Izawa, Y. Nakajima, J. Goryo, Y. Matsuda, S. Osaki, H. Sugawara, H. Sato, P. Thalmeier, and K. Maki, *Phys. Rev. Lett.* **90**, 117001 (2003).
- [31] Y. Aoki, A. Tsuchiya, T. Kanayama, S. R. Saha, H. Sugawara, H. Sato, W. Higemoto, A. Koda, K. Ohishi, K. Nishiyama, and R. Kadono, *Phys. Rev. Lett.* **91**, 067003 (2003).
- [32] E. E. M. Chia, M. B. Salamon, H. Sugawara, and H. Sato, *Phys. Rev. Lett.* **91**, 247003 (2003).
- [33] A. D. Huxley, M.-A. Measson, K. Izawa, C. D. Dewhurst, R. Cubitt, B. Grenier, H. Sugawara, J. Flouquet, Y. Matsuda and H. Sato, *Phys. Rev. Lett.* **93**, 187005 (2004).
- [34] M. Nishiyama, T. Kato, H. Sugawara, D. Kikuchi, H. Sato, H. Harima, and G.-q. Zheng, *J. Phys. Soc. Jpn.* **74**, 1938 (2005).

- [35] N. A. Frederick, T. A. Sayles and M. B. Maple, *Phys. Rev. B* **71**, 064508 (2005).
- [36] W. Higemoto, S. R. Saha, A. Koda, K. Ohishi, R. Kadono, Y. Aoki, H. Sugawara and H. Sato, *Phys. Rev. B* **75**, 020510(R) (2007).
- [37] K. Katayama, S. Kawasaki, M. Nishiyama, H. Sugawara, D. Kikuchi, H. Sato, and G.-q. Zheng, *J. Phys. Soc. Jpn.* **76**, 023701 (2007).
- [38] D. E. MacLaughlin, J. E. Sonier, R. H. Heffner, O. O. Bernal, B.-L. Young, M. S. Rose, G. D. Morris, E. D. Bauer, T. D. Do and M. B. Maple, *Phys. Rev. Lett.* **89**, 157001 (2002).
- [39] H. Suderow, S. Viera, J. D. Strand, S. Bud'ko and P. C. Canfield, *Phys. Rev. B* **69**, 060504 (2004).
- [40] H. Kotegawa, M. Yogi, Y. Imamura, Y. Kawasaki, G.-q. Zheng, Y. Kitaoka, S. Ohsaki, H. Sugawara, Y. Aoki, and H. Sato, *Phys. Rev. Lett.* **90**, 027001 (2003).
- [41] Y. Aoki, T. Namiki, S. Ohsaki, S. R. Saha, H. Sugawara and H. Sato, *J. Phys. Soc. Jpn.* **71**, 2098 (2002).
- [42] R. Vollmer, A. Faißt, C. Pfeleiderer, H. v. Löhneysen, E. D. Bauer, P.-C. Ho, V. Zapf, and M. B. Maple, *Phys. Rev. Lett.* **90**, 057001 (2003).
- [43] T. Tayama, T. Sakakibara, H. Sugawara, Y. Aoki and H. Sato, *J. Phys. Soc. Jpn.* **72**, 1516 (2003).
- [44] P.-C. Ho, N. A. Frederick, V. S. Zapf, E. D. Bauer, T. D. Do, M. B. Maple, A. D. Christianson, and A. H. Lacerda, *Phys. Rev. B* **67**, 180508(R) (2003).

- [45] N. Oeschler, P. Gegenwart, F. Weickert, I. Zerec, P. Thalmeier, F. Steglich, E. D. Bauer, N. A. Frederick and M. B. Maple, *Phys. Rev. B* **69**, 235108 (2004).
- [46] K. Grube, S. Drobnik, C. Pfleiderer, H. v. Löhneysen, E. D. Bauer and M. B. Maple, *Phys. Rev. B* **73**, 104503 (2006).
- [47] M.-A. Measson, D. Braithewaite, J. Flouquet, G. Seyfarth, J. P. Brison, E. Lhotel, C. Paulsen, H. Sugawara and H. Sato, *Phys. Rev. B* **70**, 064516 (2004).
- [48] G. Seyfarth, J. P. Brison, M.-A. Measson, J. Flouquet, K. Izawa, Y. Matsuda, H. Sugawara, and H. Sato, *Phys. Rev. Lett.* **95**, 107004 (2005).
- [49] G. Seyfarth, J. P. Brison, M.-A. Méasson, D. Braithewaite, G. Lapertot and J. Flouquet, *Phys. Rev. Lett.* **97**, 236403 (2006).
- [50] M. Yogi, T. Nagai, Y. Imamura, H. Mukuda, Y. Kitaoka, D. Kikuchi, H. Sugawara, Y. Aoki, H. Sato and H. Harima, *J. Phys. Soc. Jpn.* **75**, 124702 (2006).
- [51] J. Goryo, *Phys. Rev. B* **67**, 184511 (2003).
- [52] M. Ichioka, N. Nakai and K. Machida, *J. Phys. Soc. Jpn.* **72**, 1322 (2003).
- [53] K. Miyake, H. Kohno and H. Harima, *J. Phys.: Condens. Matter* **15**, L275 (2003).
- [54] K. Maki, S. Haas, D. Parker, H. Won, K. Izawa and Y. Matsuda, *Europhys. Lett.* **68**, 720 (2004).
- [55] M. Matsumoto and M. Koga, *J. Phys. Jpn.* **73**, 1135 (2004); M. Matsumoto and M. Koga, *J. Phys. Jpn.* **74**, 1686 (2005); M. Koga, M. Matsumoto and H. Shiba, *J. Phys. Soc. Jpn.* **75**, 014709 (2006).

- [56] P. Thalmeier, *Physica B* **378-380**, 261 (2006).
- [57] V. Kuznetsova and V. Barzykin, *Europhys. Lett.* **72** (3), 437 (2005).
- [58] S. Mukherjee and D. F. Agterberg, *Phys. Rev. B* **74**, 174505 (2006).
- [59] Y. S. Barash and A. A. Svidzinsky, *Phys. Rev. B* **53**, 15254 (1996); *ibid* **58**, 6476 (1998); *ibid* *JETP Lett.* **63**, 365 (1996)
- [60] R. Joynt, and L. Taillefer, *Rev. Mod. Phys.* **74**, 235 (2002).
- [61] In Ref. [66] we incorrectly stated that there were 6 domains with 6 different nodal structures associated with $(|\eta_1|, i|\eta_2|, 0)$. There in fact only three different nodal structures.
- [62] A. J. Leggett, *Rev. Mod. Phys.* **47**, 331 (1975).
- [63] T. Sakakibara, A. Yamada, J. Custers, K. Yano, T. Tayama, H. Aoki, and K. Machida, *J. Phys. Soc. Jpn.* **76**, 051004 (2007).
- [64] C. S. Turel, J. Y. T. Wei, W. M. Yuhasz and M. B. Maple, *Physica C*, **463-465**, 32 (2007).
- [65] D. E. MacLaughlin, L. Shu, R. H. Heffner, J. E. Sonier, F. D. Callaghan, G. D. Morris, O. O. Bernal, W. M. Yuhasz, N. A. Frederick and M. B. Maple, *Proceedings of the International Conference on Strongly Correlated Electron Systems, Houston, May 2007* (unpublished).
- [66] T. R. Abu Alrub and S. H. Curnoe, *Phys. Rev. B* **76**, 054514 (2007)
- [67] P. A. Lee, *Phys. Rev. Lett.* **71**, 1887 (1993).

- [68] P. J. Hirschfeld, W. O. Putikka, and D. J. Scalapino, *Phys. Rev. Lett.* **71**, 3705 (1993); P. J. Hirschfeld, W. O. Putikka, and D. J. Scalapino, *Phys. Rev. B* **50**, 10 250 (1994); P. J. Hirschfeld and W. O. Putikka, *Phys. Rev. Lett.* **77**, 3909 (1996).
- [69] M. J. Graf, S-K. Yip, J. A. Sauls, and D. Rainer, *Phys. Rev. B* **53**, 15 147 (1996).
- [70] A. V. Balatsky, A. Rosengren, and B. L. Altshuler, *Phys. Rev. Lett.* **73**, 720 (1994).
- [71] C. J. Pethick and D. Pines, *Phys. Rev. Lett.* **57**, 118 (1986).
- [72] B. Arfi and C. J. Pethick, *Phys. Rev. B* **38**, 2312 (1987).
- [73] S. Schmitt-Rink, K. Miyake, and C. M. Varma, *Phys. Rev. Lett.* **57**, 2575 (1986).
- [74] P. J. Hirschfeld, P. Wölfle and D. Einzel, *Phys. Rev. B* **37**, 83 (1988).
- [75] There is a minus sign in front of the first term in (3.4) which is missing in Ref. [7].
- [76] N. A. Frederick, T. D. Do, P.-C. Ho, N. P. Butch, V. S. Zapf and M. B. Maple, *Phys. Rev. B* **69**, 024523 (2004); N. A. Frederick, T. A. Sayles and M. B. Maple, *Phys. Rev. B* **71**, 064508 (2005).
- [77] C. R. Rotundu, P. Kumar and B. Andraka, *Phys. Rev. B* **73**, 014515 (2006).
- [78] M. B. Maple, N. A. Frederick, P.-C. Ho, W. M. Yuhasz and T. Yanagisawa, *J. Superconductivity and Novel Magnetism* **19**, 299 (2006).

- [79] I. A. Sergienko, Phys. Rev. B **69**, 174502 (2004).
- [80] C. Caroli, P. G. de Gennes, and J. Matricon, Phys. Lett. **9**, 307 (1964).
- [81] Y. S. Barash, A. A. Svidzinsky and V. P. Mineev, JETP Lett. **65**, 638 (1997).
- [82] P. J. Hirschfeld, J. Korean Phys. Soc. **33**, 485 (1998).
- [83] C. Kübert and P. J. Hirschfeld, Solid State Commun. **105**, 459 (1998).
- [84] C. Kübert and P. J. Hirschfeld, Phys. Rev. Lett. **80**, 4963 (1998).
- [85] I. Vekhter, J. P. Carbotte and E. J. Nicol, Phys. Rev. B **59**, 1417 (1999).
- [86] M. Franz, Phys. Rev. Lett. **82**, 1760 (1999).
- [87] I. Vekhter and A. Houghton, Phys. Rev. Lett. **83**, 4626 (1999).
- [88] K. A. Moler, A. Kapitulnik, D. J. Baar, R. Liang, and W. N. Hardy, Phys. Chem. Solids **56**, 1899 (1995).
- [89] K. A. Moler, D. L. Sisson, J. S. Urbach, M. R. Beasley, A. Kapitulnik, D. J. Baar, R. Liang, and W. N. Hardy, Phys. Rev. B **55** 3954 (1997).
- [90] I. Vekhter, P. J. Hirschfeld, J. P. Carbotte and E. J. Nicol, Phys. Rev. B **59**, R9023 (1999).
- [91] I. Vekhter, P. J. Hirschfeld and E. J. Nicol, Phys. Rev. B **64**, 064513 (2001)
- [92] H. Won and K. Maki, Europhys. Lett. **56**, 729 (2001).
- [93] P. Miranović, N. Nakai, M. Ichioka, and K. Machida, Phys. Rev. B **68**, 052501 (2003).
- [94] M. Udagawa, Y. Yanase, and M. Ogata, Phys. Rev. B **70**, 184515 (2004).

- [95] P. Thalmeier, T. Watanabe, K. Izawa, and Y. Matsuda, *Phys. Rev B* **72**, 024539 (2005).
- [96] L. Tewordt and D. Fay, *Phys. Rev. B* **72**, 014502 (2005).
- [97] A. Vorontsov and I. Vekhter, *Phys. Rev. Lett.* **96**, 237001 (2006).
- [98] A. Vorontsov and I. Vekhter *Phys. Rev. B* **75**, 224501 (2007).
- [99] A. Vorontsov and I. Vekhter *Phys. Rev. B* **75**, 224502 (2007).
- [100] H. Aubin, K. Behnia, M. Ribault, R. Gagnon and L. Taillefer, *Phys. Rev. Lett.* **78**, 2624 (1997).
- [101] F. Yu, M. B. Salamon, A. J. Leggett, W. C. Lee, and D. M. Ginsberg, *Phys. Rev. Lett.* **74**, 5136 (1995).
- [102] K. Izawa, H. Takahashi, H. Yamaguchi, Y. Matsuda, M. Suzuki, T. Sasaki, T. Fukase, Y. Yoshida, R. Settai, and Y. Onuki, *Phys. Rev. Lett.* **86**, 2653 (2001).
- [103] K. Izawa, H. Yamaguchi, Yuji Matsuda, H. Shishido, R. Settai, and Y. Onuki, *Phys. Rev. Lett.* **87**, 057002 (2001).
- [104] K. Izawa, H. Yamaguchi, T. Sasaki, and Y. Matsuda, *Phys. Rev. Lett.* **88**, 027002 (2001).
- [105] T. Watanabe, K. Izawa, Y. Kasahara, Y. Haga, Y. Onuki, P. Thalmeier, K. Maki, and Y. Matsuda, *Phys. Rev. B* **70**, 184502 (2004).
- [106] Y. Matsuda, K. Izawa, and I. Vekhter, *J. Phys.: Condens. Matter* **18**, R705 (2006).

- [107] K. Izawa, K. Kamata, Y. Nakajima, Y. Matsuda, T. Watanabe, M. Nohara, H. Takagi, P. Thalmeier, and K. Maki, *Phys. Rev. Lett.* **89**, 137006 (2002).
- [108] T. Park, M. Salamon, E. Choi, H. Kim, and S. Lee, *Phys. Rev. Lett.* **90**, 177001 (2003).
- [109] T. Park, E. Chia, M. Salamon, E. Bauer, I. Vekhter, J. Thompson, E. Choi, H. Kim, S. Lee, and P. Canfield, *Phys. Rev. Lett.* **92**, 237002 (2004).
- [110] K. Deguchi, Z. Q. Mao, H. Yaguchi, and Y. Maeno, *Phys. Rev. Lett.* **92**, 047002 (2004).
- [111] K. Deguchi, Z. Q. Mao, and Y. Maeno, *J. Phys. Soc. Jpn.* **73** 1313 (2004).
- [112] H. Aoki, T. Sakakibara, H. Shishido, R. Settai, Y. Onuki, P. Miranović and K. Machida, *J. Phys.: Condens. Matter* **16**, L13 (2004).
- [113] J. Custers, Y. Namai, T. Tayama, T. Sakakibara, H. Sugawara, Y. Aoki, and H. Sato, *Physica B* **378-380**, 179 (2006).
- [114] J. Custers, A. Yamada, T. Tayama, T. Sakakibara, H. Sugawara, Y. Aoki, H. Sato, Y. Onuki, and K. Machida, *J. Magn. Magn. Mater.* **310**, 700 (2007).
- [115] K. Maki, *Phys. Rev.* **158**, 397 (1967).
- [116] A slight error in Ref. [84] has been corrected here.
- [117] T. R. Abu Alrub and S. H. Curnoe, *Phys. Rev. B* **76**, 184511 (2007).
- [118] An error in Table I of Ref. [12], which stated that there are no nodes in the $(|\eta_1|, i|\eta_2|, 0)$ triplet phase was corrected in Ref. [66].



